Theses and dissertations

1-1-2009

Nonlinear model predictive control of LDPE autoclave reactors

Noel C. Jacob
Ryerson University

NONLINEAR MODEL PREDICTIVE CONTROL OF LDPE AUTOCLAVE REACTORS

by

Noel C. Jacob, B.Eng.

Ryerson University, Toronto, ON, Canada

A thesis presented to

Ryerson University

in partial fulfillment of the requirements

for the degree of

Master of Applied Science

in

Chemical Engineering

Toronto, ON, Canada, 2009

© Noel C. Jacob, 2009

Author's Declaration

I hereby declare that I am the sole author of this thesis. I authorize Ryerson University to lend this thesis to other institutions or individuals for the purpose of scholarly research.

I further authorize Ryerson University to reproduce this thesis by photocopying or by other means, in total or in part, at the request of other institutions or individuals for the purpose of scholarly research.

Borrower's Page

Ryerson University requires the names and signatures of all persons using or photocopying this thesis. Please sign below and provide address and date.

Abstract

Noel C. Jacob, Master of Applied Science, Ryerson University, Toronto, 2009

Polymerization reactors are characterized by highly nonlinear dynamics, multiple operating regions, and significant interaction among the process variables, and are therefore, usually difficult to control efficiently using conventional linear process control strategies. It is generally accepted that nonlinear control strategies are required to adequately handle such processes. In this work, we develop, implement, and evaluate via simulation a nonlinear model predictive control (NMPC) formulation for the control of two classes of commercially relevant low-density polyethylene (LDPE) autoclave reactors, namely, the single, and multi-zone multi-feed LDPE autoclave reactors.

Mathematical models based on rigorous, first-principles mechanistic modeling of the underlying reaction kinetics, previously developed by our research group, were extended to describe the dynamic behavior of the two LDPE autoclave reactors. Unscented Kalman filtering (UKF) based state estimation, not commonly used in chemical engineering applications, was implemented and found to perform quite well. The performance of the proposed NMPC formulation was investigated through a select number of simulation cases on the mathematical 'plant' models. The resulting closed-loop NMPC performance was compared with performance obtained with conventional linear model predictive control (LMPC) and proportional–integral–derivative (PID) controllers. The results of the present study indicate that the closed-loop disturbance rejection and tracking performance delivered by the NMPC algorithm is a significant improvement over the aforementioned controllers.

Contents

List of Figures

List of Tables

Chapter 1

Introduction

Continuous polymerization reactors have long been known to exhibit highly complex and nonlinear dynamical behavior. For example, Schmidt and Ray [73] demonstrated the existence of multiple steady states in continuous isothermal methyl methacrylate (MMA) solution polymerization reactors. Hamer, Akramov, and Ray [26] extended the results of Schmidt and Ray to the nonisothermal case, and showed the presence of multiple steady states and limit cycle oscillations in continuous MMA and vinyl acetate (VA) polymerization systems. Russo and Bequette [71] produced conditions for observing input and output multiplicities in continuous styrene polymerization reactors. Ham and Rhee [25] studied the behavior of LDPE autoclave reactors and found, using an appropriate compartmental mixing model, the possibility of up to nine different steady states. However, linear control methodologies which have traditionally been used for chemical process control are fundamentally incapable of dealing with the highly nonlinear behavior observed in many polymerization systems, oftentimes resulting in poor control performance.

Furthermore, it is well known that the maximization of profitability of most chemical processes demands operation in the vicinity of process constraints. For example, the rate of polymer production, or equivalently monomer conversion, in LDPE autoclave reactors is 'maximized' by operation at high temperatures. However, ethylene decomposes extremely rapidly around 300°C leading to thermal runaway, which is a safety constraint on the operation of the reactor. Other examples of process constraints include environmental regulations, product quality specifications, and input sat-

uration constraints, to name a few. Unfortunately, most conventional linear and nonlinear control algorithms do not account for the presence of constraints, potentially leading to poor performance, and in certain situations, instability.

Over the past two decades, model predictive control (MPC) technology has emerged as a general purpose control strategy for process control. MPC based on linear process models, or linear model predictive control (LMPC), has been extraordinarily successful in the chemical process industries with numerous reported applications, especially in refinery and petrochemical operations, where the degree of process nonlinearity is not 'too severe'. The principal appeal of MPC as a control strategy for chemical processes stems from its ability to explicitly handle process and operational constraints within its framework, leading to more efficient and profitable operation. Despite the success of conventional LMPC, it is not recommended for systems that exhibit a high degree of process nonlinearity, or for systems that are required to operate over a wide region, which is the case for most continuous polymerization reactors. For such systems, it is essential to design control systems that take the nonlinear system dynamics into account over the operating range.

Nonlinear model predictive control (NMPC) is an alternative to conventional LMPC, especially for situations where LMPC performs, or is expected to perform poorly. NMPC inherits many of the advantageous properties of LMPC, such as explicit handling of constraints, and intuitive treatment of multivariable (MIMO) systems. However, instead of a local linear model, the NMPC controller utilizes a *nonlinear* representation of the plant dynamics in the controller framework, making it (at least theoretically) appealing for processes with significant nonlinearity. While this would appear to be only a natural extension of MPC technology, it is clear from the significantly fewer industrial applications that NMPC has *not* had the level of industrial impact that LMPC has had in the process industries [62, 63].

Furthermore, while academic contributions to the theoretical understanding of NMPC have been substantial, relatively little work has been done by way of *application* (both experimental and simulation based) of 'modern' NMPC algorithms for the control of chemical processes, especially with respect to continuous polymerization systems. Thus, the motivation behind the present study is to investigate the performance of NMPC for the control of LDPE autoclave reactors.

1.1 Research Objectives

The goal of this study was to develop and test, through simulations, a nonlinear model predictive control scheme for the control of low-density polyethylene (LDPE) autoclave reactors. The ultimate prize, from an industrial perspective, to be gained from the implementation of advanced process control strategies–such as NMPC–on continuous polymerization reactors is that it permits good control of 'polymer quality' indices in the production (polymerization) stage. In the current highly-competitive industrial environment, good polymer quality control can result in a marked reduction in degree of product variability, and frequency of downstream blending operations due to production of off-spec product, potentially leading to significant cost savings [84]. The indicator of polymer quality chosen in this study is the polymer weight-averaged molecular weight. Industrially, the most frequently used indicator of polymer grade and end-use properties is the melt flow index (MFI) or melt index (MI). However, for a particular polymer type, it is usually possible to develop fairly accurate correlations relating MFI to polymer weight-averaged molecular weight, thus allowing direct conversion between the two quantities. For example, the review papers of Shenoy and Saini [74, 75] list a number of published MFI correlations for polyethylenes, which is of interest in this study.

In this work, we consider two classes of industrially relevant LDPE autoclaves, namely, single-zone (or compact), and multi-zone multi-feed reactors. In both cases we are primarily interested in applying an NMPC formulation for the control of the reactor temperature (in case of the multi-zone reactor, the temperature *profile*), and the polymer weight-averaged molecular weight (controlled outputs). The flowrates of the feed initiator and monomer stream(s) were the control inputs (manipulated variables) selected to drive the controlled outputs to their setpoints. The closed-loop disturbance rejection and setpoint tracking performance of the NMPC controller, for both LDPE autoclave reactors, was investigated and compared with the performance of conventional LMPC and PID controllers.

1.2   Thesis Organization

- Chapter 2 reviews some recent, relevant, industrial and academic contributions to the *application* of NMPC for the control of continuous polymerization systems, with special emphasis paid to LDPE autoclave reactors.

- Chapter 3 briefly outlines the development of the nonlinear process models used in this work. The relevant reaction mechanism, together with the single and multi-zone LDPE autoclave reactor models are presented.

- Chapter 4 begins with a brief introduction to nonlinear model predictive control, followed by a detailed presentation of the controller formulation (algorithm) used in this work.

- Chapter 5 provides details on the extended Kalman filtering (EKF), and unscented Kalman filtering (UKF) nonlinear state estimation algorithms employed in this study.

- Chapter 6 addresses a number of issues relating to the implementation and closed-loop simulation of the NMPC controller, for e.g. model discretization, simulation structure, controller tuning, etc.

- Chapter 7 presents and discusses simulation results obtained from testing the NMPC control system on both the single and multi-zone LDPE autoclaves. Wherever possible, the closed-loop NMPC results are compared with conventional PID and LMPC controllers.

- Chapter 8 concludes this thesis with a few comments, and presents some recommendations for future work and improvements.

Chapter 2

Literature Review

The two basic requirements of any model predictive control (MPC) formulation are, first, an internal prediction model, also referred to as process, or controller model, and, second, a finite horizon optimal control, or dynamic optimization, problem that must be solved online to determine control input trajectories which minimize a given, usually quadratic, cost functional. The origins of MPC can be traced back to the early 1970s with the development, in industry, of the so called model predictive heuristic control (MPHC), and competing dynamic matrix control (DMC) algorithms [62]. Ever since, MPC has been a 'hot' research area, with published research articles numbering many thousands. The interested reader is referred to the papers of Qin and Badgwell [62, 63] for a historical perspective on the current state of MPC technology. In [63], the authors provide a nice overview of *industrial* applications of commercial NMPC software, which is of relevance to this thesis.

The MPC control methodology is very 'general', resulting in the development of numerous proposed control formulations in the published literature. Furthermore, tremendous progress has been made in understanding theoretical MPC concepts, such as closed-loop stability, optimality, et cetera. Obviously, a comprehensive review of these topics is outside the scope of this work, and the reader is referred to the excellent survey papers of DeNicolao et al. [14], and Mayne et al. [49] for more information. Linear model predictive control (LMPC), i.e. MPC based on linear process models, has enjoyed tremendous commercial success, with reportedly over 2000 industrial applications, especially in industries with 'moderate' degrees of process nonlinearity, such as the refinery and petrochemical

business [63]. The literature dealing with theoretical and practical/implementational LMPC issues is vast, and is not reviewed here. The text of Maciejowski [43], and the MATLAB MPC Toolbox 2 software [4] provide a good introductory treatment of LMPC concepts.

While significant progress, mainly due to academia, has been made in understanding closed-loop NMPC properties (see for example [48, 51, 50, 10, 49, 14, 83]), this has not translated as yet into wide industrial acceptance, as is quite clear from the significantly smaller number of applications compared to LMPC. Furthermore, academic contributions, both experimental and simulation-based, toward the *application* of recent NMPC technology has been somewhat limited. The latter is very surprising, especially in the context of chemical/process and polymer reaction engineering, since these processes exhibit strong nonlinear characteristics, which are quite difficult to handle using conventional control methodologies. However, there have been very good reasons for the reluctance in embracing NMPC despite its potential benefits. For instance, until recently, the online computation burden involved with solving a potentially large nonlinear programming (NLP) problem online was prohibitively expensive. Another practical concern is the presence of nonconvexity and local minima in the underlying optimization problem, which in certain cases can have disastrous consequences, for example reactor light-off.

One can conclude that there still exists a strong need to *demonstrate*, via experiment and simulation, the effectiveness and robustness, or lack thereof of current NMPC formulations for the control of chemical process systems, especially polymerization systems where the potential for benefits from NMPC is large. This is the motivation behind the present research into the NMPC control of LDPE autoclave reactors. In this review, we focus primarily on literature dealing with NMPC applications and simulation-based studies on *continuous* polymerization systems. However, since the amount of published research on NMPC control of continuous polymerization reactors is actually relatively small, we also include in this review a few relevant NMPC studies and applications on other chemical processes. Note that we do not review the growing literature on NMPC control of batch polymerization systems, where the impact NMPC could be just as significant.

2.1   NMPC of Continuous Polymerization Reactors

Ahn, Park, and Rhee [1] compared experimentally the closed-loop performance of NMPC, LMPC, and PID controllers for the control of monomer conversion and polymer weight-averaged molecular weight in a lab-scale continuous methyl methacrylate (MMA) solution polymerization reactor. Their extended Kalman filter (EKF) based NMPC scheme utilized a detailed first-principles nonlinear process model coupled with input/output disturbances to predict future plant behavior. Estimates of conversion and molecular weight were obtained inferentially using online density and viscosity measurements, respectively. The results showed significant improvement in closed-loop performance of the NMPC controller, over the LMPC and PID controllers, for both servo and regulatory control.

The research group of Prof. Bequette at Rensselaer Polytechnic Institute has worked extensively on modeling and control of styrene polymerization systems. In particular, the articles Russo and Bequette [70], Schley, Prasad, Russo, and Bequette [72], and Prasad, Schley, Russo, and Bequette [61] describe the application of an EKF based nonlinear quadratic dynamic matrix control (NL-QDMC) approach, proposed by Lee and Ricker [42], for the control number-averaged molecular weight and other polymer properties, such as polydispersity, in continuously stirred styrene polymerization reactors. They show, through simulations, that NL-QDMC controller performs adequately well in disturbance rejection and setpoint tracking situations.

BenAmor, Doyle III, and McFarlane [5] reports on an industrially-relevant simulation-based study in which the problem of grade transition control in polymerization reactors is considered through the coupling of an industrial real-time optimization (RTO) package–Rigorous Online Modeling and equation-based optimization (ROMeo)–with an NMPC control system. The goal of their work was "to demonstrate that these (control) algorithms can be incorporated into the framework of commercial grade software for online applications". The performance of their RTO-NMPC-based control scheme in polymer grade transition situations was tested using continuously stirred MMA, and gas-phase fluidized bed polyethylene reactor models. The simulation results showed that their receding horizon estimation (RHE) based controller provided good tracking performance, even in the presence of reasonable model mismatch and measurement noise.

Ali, Abasaeed, and Al-Zahrani [2] applied an NL-QDMC control scheme due to Ali and Zafiriou [3]

for the stabilization of gas-phase polyethylene reactors. They showed, using simulations, that multi-loop PI control resulted in unacceptable closed-loop performance, potentially leading to reactor light-off, even for relatively small process disturbances. Furthermore, using PI controllers, it was not possible to utilize all available degrees of freedom due to the nonsquare nature of the reactor model. The designed NL-QDMC scheme was shown to posses excellent closed-loop disturbance rejection and setpoint tracking properties, in addition to being able to take advantage of the nonsquare plant.

2.2 Control of LDPE Autoclave Reactors

While several research papers have been published dealing with advanced control of styrene and MMA polymerization reactors, comparatively very little has been done in the area of high-pressure LDPE autoclave reactors. One of first published works on the control of LDPE autoclaves was that of Marini and Georgakis [45, 46], where they considered the problem of temperature control in imperfectly-mixed single-zone autoclaves. They show that classical PI controllers are incapable of stabilizing the system over a wide operating range, and, from system dynamics considerations, propose a so called 'reaction rate controller', which is able to adequately control the reactor temperature over a wide range. This work, however, did not 'directly' consider molecular or end-use properties of the polymer, which is very important in industrial applications.

Berber and Coskun [6] investigated, via simulations, the control of reactor temperature profile in a three-zone multi-feed autoclave using a linear QDMC controller. The temperatures in each zone were controlled by manipulating initiator feed rates to the respective zones. Again, direct online control of polymer molecular properties was not considered in the study. Their simulations showed that the QDMC control scheme delivered superior closed-loop regulatory and servo performance compared to PI control. It must be noted that the results in their study indicate an unusually slow, damped response under PI control, which might have more to do with over-conservative tuning than poor performance.

Ham and Rhee [25] used a two-compartment four-cell compartmental mixing scheme to model the dynamical behavior of so called slim-type LDPE autoclave reactors. They performed one and two-parameter continuation analyses in order to study the steady state characteristics of the reactor

model. In addition, they developed PID and pole placement controllers for the control of the reactor temperature. The showed, through simulations using the multi-compartment reactor model, that the pole placement controller yielded better closed-loop performance than the PID controller in reactor startup and setpoint tracking situations.

Singstad, Nordhus, Strand, Lien, Lyngmo, and Moen [76] presents details about a collaborative project between SINTEF Automatic Control and STATOIL Petrochemicals and Plastics on the development and commissioning of a multivariable nonlinear control system for STATOILs LDPE autoclave reactors in Bamble, Norway. The multilevel control scheme is designed to control temperature profile and production rates at the basic level, and polymer quality properties at the supervisory level. The control strategy is based on the well known feedback linearization, or internal nonlinear decoupling, approach, whereby the nonlinear model is transformed into an equivalent linear system by appropriate nonlinear transformations. Results from the implementation of this strategy on the actual plant show a considerable reduction in production of off-spec product. Singstad et al. [76] also presents simulation results which show the feedback linearization strategy provides superior control performance compared to multi-loop PID control.

Chapter 3

Model Development

The polymerization of ethylene in a LDPE autoclave reactors follows the well-established free-radical chain growth reaction mechanism. Free-radical polymerization takes place in the presence of one or more initiators, such as benzoyl peroxide (BPO) and dioctanoyl peroxide (DCT), which dissociate into primary radicals in the reaction mixture. Primary radicals react readily with free monomer molecules generating growing (or live) polymer radicals which sequentially add monomeric units to the polymer chain. In this Chapter, we briefly describe the polymerization *reaction mechanism* and the resulting *process model* used in this study. For a more comprehensive discussion of free-radical polymerization, the reader is deferred to the texts of Kumar and Gupta [39], and Rudin [69]. The details presented in this Chapter lean heavily on the work of Dhib, Gao, and Penlidis [16], Dhib and Al-Nidawy [15], and Khazraei and Dhib [37], which deal specifically with the issue of free-radical polymerization in the context of LDPE reactors.

3.1   Reaction Mechanism

The free-radical LDPE production takes place at extremely harsh temperature and pressure conditions when the thermodynamics of the reaction favor the polymerization of ethylene. Commercial autoclave and tubular reactors usually operate in the vicinity of around 150–270°C and 1400–2000bar. In order to develop first-principles, mechanistic process models capable of adequately describing the

dynamic behavior of LDPE autoclave reactors, it is first necessary to postulate an experimentally verified kinetic reaction mechanism. The overall reaction mechanism can be classified into four distinct parts, namely, initiation, propagation, termination, and chain transfer. In this Section, these reactions will be discussed in greater detail.

3.1.1   Initiation

The initiation stage refers to the generation of monomeric radicals R_1 from free monomer molecules in the reaction mixture. In general, initiation can occur in one of two ways, *chemical* and *self* initiation. Though the effect of chemical initiation usually outweighs that of self initiation, both are considered in this reaction mechanism.

Chemical Initiation

Free-radical polymerizations are usually aided through the addition of chemical compounds known as initiators to the reacting mixture. The function of initiators is to supply primary radicals R_{in} to the system, which then combine with monomer molecules to generate monomeric radicals. Primary radicals are usually generated by the homolytic decomposition of initiator molecules as seen in equation (3.1a) below. The most common initiators are azo and peroxide based, though redox initiators are used occasionally [39].

$$I \xrightarrow{\quad K_d \quad} 2R_{in} \tag{3.1a}$$

$$R_{in} + M \xrightarrow{\quad K_1 \quad} R_1 \tag{3.1b}$$
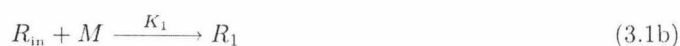
We assume that the peroxide initiator–dioctanoyl peroxide–is used to initiate polymerization in the LDPE autoclave reactors modeled in this study.

Self Initiation

At high temperatures, monomer molecules spontaneously react to form monomeric radicals. This process is called self initiation, and can be represented by equation (3.2) below.

$$3M \xrightarrow{\quad K_{th} \quad} 2R_1 \tag{3.2}$$

3.1.2 Propagation

In the propagation stage, live polymer radicals grow in size through the sequential addition of monomer molecules at the active center of the growing chain. This process can be represented for polymer chains of any length by equation (3.3) below [15, 37]

$$R_n + M \xrightarrow{K_p} R_{n+1} \tag{3.3}$$

3.1.3 Termination

Termination refers to reactions in which two live polymer radicals mutually annihilate each other resulting in the formation of dead polymer. There are two types of termination reactions, *combination* and *disproportionation*. In this work, we assume that chain termination occurs primarily via the combination mechanism.

$$R_r + R_s \xrightarrow{K_t} P_{r+s} \tag{3.4}$$

3.1.4 Chain Transfer

Chain transfer reactions are reactions in which the active center of growing radical chains are transferred to another molecule, or another location on the growing polymer chain.

Transfer to Monomer

The active center of growing polymer chains can be transferred to free monomer molecules, which act as transfer agents, resulting in the formation of dead polymer and monomeric radicals.

$$R_n + M \xrightarrow{K_{fm}} P_n + R_1 \tag{3.5}$$
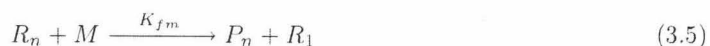
Transfer to Polymer

Dead polymer chains can revert back into growing polymer radicals by transfer of the active center from the growing radical to the dead polymer. Transfer to polymer reactions are responsible for the formation of long chain branching (LCB), which can significantly affect polymer microstructure and molecular weight distribution (MWD).

$$R_n + P_s \xrightarrow{K_{fp}} P_n + R_s \tag{3.6}$$

β–Scission to Secondary Radicals

Beta scission of live polymer radicals essentially results in the formation of dead polymer chains P_n together with monomeric radicals R_1 as seen in equation (3.7) below.

$$R_{n+1} \xrightarrow{K_\beta} P_n + R_1 \tag{3.7}$$

Intramolecular Transfer

Intramolecular transfer, also known as backbiting, refers to the reaction in which the active center at the end of a growing polymer radical is transferred to an internal $-CH_2-$ group in the polymer chain, resulting in the formation of short chain branched (SCB) polymer microstructure.

$$R_n \xrightarrow{K_b} R_{bn} \tag{3.8}$$

3.2   Process Modeling

Depending on the chosen reactor configuration, the reaction mechanism postulated in the previous Section can be utilized to develop kinetic models describing the dynamic behavior of the reaction system. Prior to presenting details on the mathematical modeling of LDPE autoclaves, it is beneficial to discuss some characteristic features of these reactors. The principal feature of the industrial LDPE autoclave is that the reactor operates, to a very good approximation, adiabatically. This can be attributed to the fact that the thick reactor walls required to withstand the high operating pressures prevent heat transfer from the reaction mixture [88]. Consequently, external cooling jackets which are common in other stirred polymerization reactors cannot be used to remove heat from the system. The only cooling source available to the reactor is the cool monomer feed stream(s), which typically enter at about 30–40°C. The author is only aware of one publication, that of Lee, Ham, Chang, Kim, and Rhee [41], which investigated the behavior of compact LDPE autoclaves model with *internal* cooling jackets. However, such configurations are not common in industry, and therefore, not considered in this study.

The decomposition of ethylene into byproducts such as ethane, methane, carbon, and hydrogen becomes significant at temperatures in the range of 300°C. The decomposition reactions are highly

exothermic, occur extremely rapidly, and if initiated, can result in reactor runaway in the order of just a few seconds. The problem of ethylene decomposition is critically important in LDPE autoclave reactors, as opposed to, for example, tubular reactors, due to the adiabatic nature of the reactor. However, ethylene conversion is maximized by operation at higher temperatures, therefore, commercial LDPE autoclaves are usually operated close to the boundary where decomposition dynamics become dominant. Once initiated, ethylene decomposition is essentially impossible to control, and reactor runaway is inevitable, therefore, from a process control perspective, the modeling of decomposition kinetics is of limited usefulness, and was therefore, not attempted in this work. Zhang, Read, and Ray [88], Villa, Dihora, and Ray [85], and Lee, Yeo, and Chang [40], are examples of modeling studies which account for ethylene decomposition kinetics in the reaction mechanism.

The residence time in most LDPE autoclave reactors is normally in the 1–2min range, and is, quite often, lower depending on the particular reaction conditions. The monomer conversion attained is relatively low, often only in the 10–20% range. Higher residence times (and conversions), while desirable, are accompanied by higher operating temperatures (due to the absence of reactor cooling), which is undesirable, since it moves the system closer to instability. In the following subsections, we present, briefly, first-principles based dynamic models developed for two classes of LDPE autoclave reactors, namely, single-zone autoclaves, and multi-zone multi-feed autoclaves.
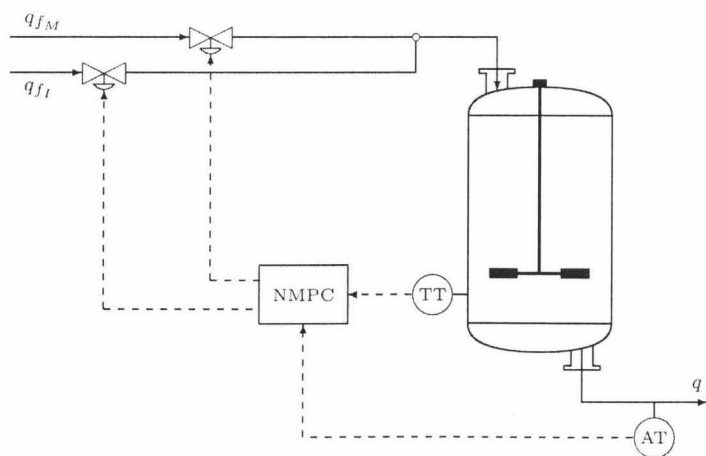

Figure 3.1: Single-zone (compact) LDPE autoclave reactor showing the controller, measurements, and control inputs.

3.2.1 Single-Zone Autoclave Model

Single-zone, or compact, LDPE autoclaves are well-agitated high-pressure vessels with relatively low L/D ratios, usually in the neighborhood of around 2–5m/m [41]. The pressurized monomer and initiator feed streams typically enter from the top of the reactor, while the produced polymer and unconsumed reactants are siphoned off from the bottom. Figure 3.1 shows a simple schematic of a typical single-zone autoclave reactor. In certain situations, chain transfer agents (CTA), such as solvents, are also fed to the reactor in order to modify properties of the polymer obtained, however, we did not consider such cases in the present study. Despite the high agitation power input supplied to the reactor, the compact autoclave cannot be considered completely well-mixed. In fact, experimental results and computational fluid dynamics (CFD) simulation studies [66] point to the existence of concentration and temperature gradients inside the reactor.

Compartmental mixing models, in which the reactor volume is partitioned into two or more well-mixed compartments (or cells), are by far, the most commonly employed practice in the modeling of imperfect mixing in LDPE autoclaves, see for example [45, 85, 87, 41]. The choice of compartment shape and size can be made based on reactor design considerations, experimental evidence, or from CFD studies. In the following, for the sake of simplicity, we present the dynamic model pertaining to the case of the perfectly-mixed reactor. Note that this model can be extended quite easily to include multiple compartments.

The following assumptions were made in the modeling of the LDPE autoclave reactor

- The reaction mixture is perfectly mixed, i.e. there are no concentration or temperature gradients inside the reactor.

- The density of the reaction mixture, while temperature and pressure dependent, does not change appreciably with time, i.e. there is negligible mass accumulation in the reactor [59].

- Heat effects due to mechanical agitation, chemical and thermal initiation, termination, and chain transfer reactions are negligible compared to the heat of polymerization.

- The reaction mixture behaves as a single-phase system, i.e. the contribution of the polymer phase to the overall kinetics is minimal.

- Diffusional effects on the polymerization kinetics are negligible, i.e. the cage and Trommsdorff gel effects are absent.

Using these assumptions, simple molar and energy balances on the reacting species can be performed to yield equations (3.9) to (3.12) for the single-zone reactor. Here, I is the initiator concentration in the reactor, M is the free monomer concentration, M_t is the 'total' monomer concentration, and T is the reactor temperature.

$$\frac{dI}{dt} = r_I + (q_{f_I} I_f - qI)/V \qquad (3.9)$$

$$\frac{dM}{dt} = r_M + (q_{f_M} M_f - qM)/V \qquad (3.10)$$

$$\frac{dM_t}{dt} = r_{M_t} + (q_{f_M} M_f - qM_t)/V \qquad (3.11)$$

$$\frac{dT}{dt} = r_T + (q_f T_f - qT)/V \qquad (3.12)$$

The total monomer concentration M_t refers to the 'combined' concentration of free monomer, and bound monomer in growing and dead polymer chains. The notation q_{f_X} denotes the feed flowrate of component X, and X_f denotes the corresponding feed concentration. The total feed and exit flowrates are given by q_f and q, respectively. The notation r_X refers to the rate of production/consumption (or rate of change) of component X.

$$r_I = -2K_d I \qquad (3.13)$$

$$r_M = -K_p M \lambda_0 \qquad (3.14)$$

$$r_{M_t} = 0 \qquad (3.15)$$

$$r_T = \frac{(-\Delta H_p) K_p M \lambda_0}{\rho C_p} \qquad (3.16)$$

The heat of polymerization $(-\Delta H_p)$ is a function of the reactor temperature and pressure conditions given by the correlation [37]

$$(-\Delta H_p) = 84185 + 0.209(T - 273) + 0.105P \qquad (3.17)$$

The density of the reaction mixture ρ is also a function of the reactor temperature and pressure

given by the correlation [20]

$$\rho = 1995.8 - 261.1 \log\left(\frac{P}{1000}\right) + 257.7 \log\left(\frac{1}{T}\right) - 63.3 \log\left(\frac{P}{1000}\right) \log\left(\frac{1}{T}\right) \tag{3.18}$$

The heat capacity C_p of the reaction mixture is given by the correlation [36]

$$C_p = 0.518(1 - x_M) + (1.041 + 8.3 \times 10^{-4}T)x_M \tag{3.19}$$

Here, x_M denotes the fractional monomer conversion achieved in the reactor defined by

$$x_M = (M_t - M)/M_t \tag{3.20}$$

The temperature and pressure dependence of the reaction rate constants K is given by a modified form of the Arrhenius rate equation.

$$K = A \exp\left(-E_a/RT - \Delta v P/RT\right) \tag{3.21}$$

Here, A is the preexponential factor, E_a is the activation energy, Δv is the activation volume, and R is the universal gas constant. The kinetic rate law parameters for the above equation are given in Table 3.1.

Equations (3.9) to (3.12) obtained from molar and energy balances adequately describe the open-loop dynamics of the reactor temperature, and the initiator, and free and 'total' monomer concentrations. However, molar and energy balances do not provide any information on the properties of the polymer (LDPE) produced. In fact, it is impossible to use molar balance techniques to obtain information about the polymer as at any point in time there exists a *distribution*, known as a chain

Table 3.1: Reaction rate constant data [15]

	A	E_a	Δv
K_d	1.83×10^{14}	3.06×10^{4}	5.9
K_{th}	6.04×10^{3}	3.87×10^{4}	0.0
K_p	5.12×10^{5}	4.21×10^{3}	−5.6
K_{tc}	2.53×10^{9}	3.37×10^{3}	9.2
K_{fm}	1.20×10^{4}	1.44×10^{4}	−20.0
K_{fp}	1.80×10^{5}	9.40×10^{3}	0.0
K_{β}	1.40×10^{9}	1.93×10^{4}	9.9
K_b	3.27×10^{5}	7.47×10^{3}	0.0

length distribution (CLD), of growing and dead polymer chain lengths in the reactor. In general, techniques based on *population balances* on the live and dead polymer chains are required to obtain such information.

In this study, we employed the *method of moments* approach in order to model the dynamics of the LDPE properties. This technique is a powerful, yet compact way to obtain important information on *average* molecular properties of the polymer, such as the number and weight-averaged molecular weights, and the frequencies of short (SCB) and long chain branching (LCB). In the following, the notation λ_i refers to the ith moment of the CLD of the live polymer chains R_n, while μ_i refers to the ith moment of the CLD of the dead polymer chains P_n.

$$\lambda_i = \sum_{n=1}^{\infty} n^i R_n \qquad\qquad \mu_i = \sum_{n=1}^{\infty} n^i P_n \tag{3.22}$$

Using the above definitions, it is possible to develop equations describing the dynamics of the leading moments of the CLDs of the growing and dead polymer chains. Since the lifetime of live polymer radicals are usually much smaller than mean residence times in LDPE autoclave reactors, the CLD of the live polymer chains achieves equilibrium very rapidly relative to the remainder of the system. Therefore, in order to reduce the dimensionality of the resulting process model, we make the assumption that the distribution of live polymer radicals in the reactor reaches steady state *instantaneously* in the reaction mixture, commonly known as the quasi steady state assumption (QSSA). Using the QSSA, the dynamical (differential) equations corresponding to the leading moments of the live polymer CLD can be replaced with algebraic equations for the moments given by [37]

$$\lambda_0 = \sqrt{R_I/K_{tc}} \tag{3.23}$$

$$\lambda_1 = \frac{R_I + (K_p M + K_{fm} M + K_b + 2K_{fp}\mu_2)\lambda_0}{K_{tc}\lambda_0 + K_{fm} M + K_\beta + K_{fp}\mu_1 + K_b} \tag{3.24}$$

$$\lambda_2 = \frac{R_I + K_p M(2\lambda_1 + \lambda_0) + (K_{fm} M + K_\beta + K_{fp}\mu_3)\lambda_0}{K_{tc}\lambda_0 + K_{fm} M + K_\beta + K_{fp}\mu_1 + K_b} \tag{3.25}$$

where the rate of radical initiation R_I is given by

$$R_I = 2fK_d I + 2K_{th} M^3 \tag{3.26}$$

The dynamics of the leading moments of the dead polymer CLD is given, generally, by

$$d\mu_i/dt = r_{\mu_i} - (q_f \mu_{i_f} - q\mu_i)/V \tag{3.27}$$

where

$$r_{\mu_0} = K_{tc}\lambda_0^2/2 + (K_{fm}M + K_b)\lambda_0 \tag{3.28}$$

$$r_{\mu_1} = K_{tc}\lambda_0\lambda_1 + K_{fm}M\lambda_1 + K_b(\lambda_1 - \lambda_0) + K_{fp}(\lambda_1\mu_1 - \lambda_0\mu_2) \tag{3.29}$$

$$r_{\mu_2} = K_{tc}(\lambda_0\lambda_2 + \lambda_1^2) + K_{fm}M\lambda_2 + K_b(\lambda_2 - 2\lambda_1 + \lambda_0) + K_{fp}(\lambda_2\mu_1 - \lambda_0\mu_3) \tag{3.30}$$

When chain transfer to polymer occurs, i.e. equation (3.6), the dead polymer moment equations of order > 1 depend on the next higher moment, for e.g. r_{μ_1} depends on μ_2, making this system of equations open ended. In order to solve this problem, some sort of moment closure technique is required. Here, we make use of the approximation of Hulburt and Katz [28], with which the third moment of the distribution μ_3 is approximated algebraically by lower order moments through the equation

$$\mu_3 = \frac{\mu_2}{\mu_0\mu_1}\left(2\mu_0\mu_2 - \mu_1^2\right) \tag{3.31}$$

The number $\overline{M}_n$, and weight $\overline{M}_w$ averaged molecular weights are related to the moments by equations (3.32) and (3.33), respectively. Usually, the magnitudes of the dead polymer moments greatly exceed the equivalent live polymer moments, leading to the simplifications shown.

$$\overline{M}_n = M_0\frac{\mu_1 + \lambda_1}{\mu_0 + \lambda_0} \approx M_0\frac{\mu_1}{\mu_0} \tag{3.32}$$

$$\overline{M}_w = M_0\frac{\mu_2 + \lambda_2}{\mu_1 + \lambda_1} \approx M_0\frac{\mu_2}{\mu_1} \tag{3.33}$$

3.2.1.1 Notation

In the following Chapters, we will be utilizing, almost exclusively, the notation followed in the control and estimation literature. Therefore, it is useful to introduce some notation that will be used later on in context of the single-zone LDPE autoclave reactor model. The differential equations (3.9 – 3.12, 3.27) of the reactor model can be expressed concisely as

$$\dot{x}(t) = f(x(t), u(t), t) \tag{3.34}$$

where $x(t) \in \mathbb{R}^n$ is the vector of system states, and $u(t) \in \mathbb{R}^m$ is the vector of control inputs. Here, the state and control input vectors are given by

$$
\begin{aligned}
x &= \begin{bmatrix} I & M & M_t & T & \mu_0 & \mu_1 & \mu_2 \end{bmatrix}^T \\
u &= \begin{bmatrix} q_{f_I} & q_{f_M} \end{bmatrix}^T
\end{aligned}
\tag{3.35}
$$

The vector of plant measurements $y_k \in \mathbb{R}^p$ and controlled outputs $z_k \in \mathbb{R}^{n_c}$ are given by

$$
y = z = \begin{bmatrix} T & \overline{M}_w \end{bmatrix}^T = \begin{bmatrix} T & M_0 \mu_2 / \mu_1 \end{bmatrix}^T
\tag{3.36}
$$

3.2.2   Multi-Zone Multi-Feed Autoclave Model

Multi-zone multi-feed LDPE autoclaves are well-agitated high-pressure vessels consisting of multiple reaction zones, separated by disks, in series with one another. In general, each zone possesses a pair of feed initiator and monomer streams, which can be manipulated in order to control the reaction conditions in the particular zone, such that the polymer produced possesses the desired molecular properties [59]. In comparison with single-zone reactors, multi-zone reactors are usually much longer with L/D ratios as high as 20m/m [59]. Figure 3.2 shows a simple schematic of a typical multi-zone multi-feed LDPE autoclave reactor. Each zone in the multi-zone reactor is typically modeled as a single perfectly-mixed compartment (see for example [11]), or as a series of perfectly-mixed compartments (see for example [59]).

In this study, we chose to model each reaction zone in the multi-zone autoclave as a single perfectly-mixed compartment virtually identical to the case of the single-zone reactor model presented in the previous Section. Note that the modeling assumptions outlined in the previous Section for the single-zone reactor still hold for each reaction zone in the multi-zone reactor. Backmixing interaction between adjacent zones are accounted for via the internal upward q_{u_i} and downward q_{d_i}

Table 3.2: Single-zone autoclave model parameters

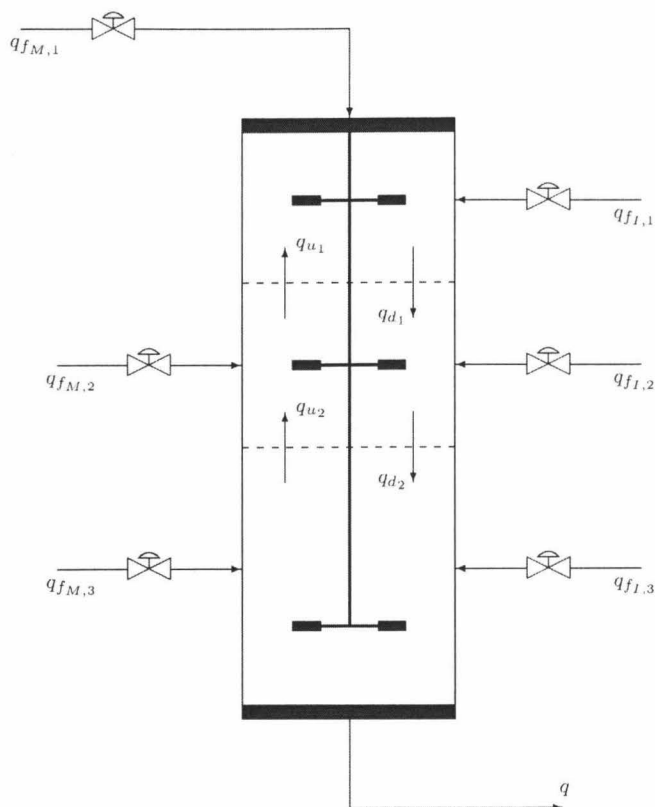|			
P	1700 bar	T_f	313.15 K
f	0.8798	V	1501.9 L
M_0	28.05 g/mol	q_{f_I}	25 cm^3/s
I_f	0.1216 mol/L	q_{f_M}	20 L/s
M_f	20.89 mol/L		

Figure 3.2: Multi-zone multi-feed LDPE autoclave reactor showing the control inputs. The controller and measurement structure (not shown) is analogous to Figure 3.1.

Table 3.3: Multi-zone autoclave model parameters

P	1700 bar	R_1	0.8
f	0.8798	R_2	0.6
M_0	28.05 g/mol	$q_{f_{I,1}}$	10.4 cm^3/s
$I_{f_{1,2,3}}$	0.1216 mol/L	$q_{f_{I,2}}$	11.4 cm^3/s
$M_{f_{1,2,3}}$	20.89 mol/L	$q_{f_{I,3}}$	15.0 cm^3/s
$T_{f_{1,2,3}}$	313.15 K	$q_{f_{M,1}}$	8.658 L/s
V_1	350 L	$q_{f_{M,2}}$	5.661 L/s
V_2	350 L	$q_{f_{M,3}}$	5.661 L/s
V_3	300 L		

flow streams. The notation q_{u_i} denotes the flowrate of the upward stream from the $(i+1)^{\text{th}}$ zone to the ith zone, whereas the notation q_{d_i} denotes the flowrate of the downward stream from the ith zone to the $(i+1)^{\text{th}}$ zone (see Figure 3.2). In order to quantify the effect of backmixing on reactor dynamics, we developed the so called backmixing ratio $\mathcal{R}_i \in [0,1]$ given by

$$\mathcal{R}_i = q_{u_i}/q_{d_i} \tag{3.37}$$

which, for any given reaction zone, is essentially the ratio between the *upward* flowrate *into*, and the *downward* flowrate *away* from the zone. Note that the final zone does not have an associated backmixing ratio, as it neither possesses an upward flowrate into, nor a downward flowrate away from the zone. Other ratios have been proposed to model backmixing in LDPE autoclave vessels, see for example Chien, Kan, and Chen [11], Pladis and Kiparissides [59], and Chan, Gloor, and Hamielec [8], however, the present approach was devised as it possesses a number of interesting properties. Notably, $\mathcal{R}_i = 0$ implies the complete absence of interaction, i.e. basically amounting to physical separation between the ith and $(i+1)^{\text{th}}$ reaction zones, while $\mathcal{R}_i = 1$ implies perfect mixing, i.e. the absence of concentration and temperature gradients between the ith and $(i+1)^{\text{th}}$ zones. The backmixing ratios for the multi-zone reactor can be estimated from reactor operating data, or from experimental studies.

As was done in the case of the single-zone LDPE autoclave reactor, molar, energy, and population balance equations can be developed for each reaction zone in the N–zone multi-zone reactor. The resulting expressions for the first, middle, and final zones can be summarized, respectively, by the

following three equations.

$$\frac{dX_1}{dt} = r_{X_1} + \frac{q_{fX,1}X_{f,1} + q_{u,1}X_2 - q_{d,1}X_1}{V_1} \tag{3.38}$$

$$\frac{dX_i}{dt} = r_{X_i} + \frac{q_{fX,i}X_{f,i} + q_{u,i}X_{i+1} + q_{d,i-1}X_{i-1} - q_{d,i}X_i - q_{u,i-1}X_i}{V_i} \tag{3.39}$$

$$\frac{dX_N}{dt} = r_{X_N} + \frac{q_{fX,N}X_{f,N} + q_{d,N-1}X_{N-1} - q_{u,N-1}X_N - qX_N}{V_N} \tag{3.40}$$

Here, the notation X_i refers to any state variable (concentration, temperature, or moments) in the ith reaction zone, $q_{fX,i}$ is the feed flowrate of component X to the ith reaction zone and $X_{f,i}$ is the corresponding feed concentration, and r_{X_i} is the rate of change (or production, consumption) of component X in the ith zone, for example

$$r_{I_i} = -2K_{d_i}I_i$$

3.2.2.1   Notation

The state and control input vectors for the three-zone LDPE autoclave reactor considered in this study are given by

$$x = \begin{bmatrix} I & M & M_t & T & \mu_0 & \mu_1 & \mu_2 \end{bmatrix}^T$$
$$u = \begin{bmatrix} q_{f_I} & q_{f_M} \end{bmatrix}^T \tag{3.41}$$

where, for example

$$I = \begin{bmatrix} I_1 & I_2 & I_3 \end{bmatrix}$$
$$q_{f_I} = \begin{bmatrix} q_{f_{I,1}} & q_{f_{I,2}} & q_{f_{I,3}} \end{bmatrix}$$

The measurement and controlled output vectors are given by

$$y = z = \begin{bmatrix} T & \overline{M}_w \end{bmatrix}^T = \begin{bmatrix} T & M_0\mu_{2_3}/\mu_{1_3} \end{bmatrix}^T \tag{3.42}$$

Chapter 4

Controller Formulation

Model predictive control (MPC), also known as receding horizon (RH) or moving horizon (MHC) control, refers to a class of control algorithms that make use of an explicit process model to compute future control actions. At any sampling instance, the current measurements are used to initialize an open-loop optimal control problem that is solved over a finite horizon to determine an optimal control input trajectory that minimizes a certain cost function. The cost function is designed so as to achieve some performance criteria, for e.g. maximization of profits, minimization of environmental impact, or as is often the case, minimization of deviations from a desired setpoint. However, only the first control input in the optimal trajectory is applied to the plant. This procedure is then continued repeatedly at all future sampling instants. The MPC methodology is different from 'conventional' approaches in that, in general, off-line computation of the MPC control law is impossible. Instead, the control law is 'derived' online by the periodic solution of the aforementioned optimal control problem.

Prior to proceeding further, it will be helpful to clarify some terminology that will be used frequently in this and subsequent Chapters. The term *plant* is used here to refer to the actual process under control, which in this case, is the LDPE autoclave reactor. The mathematical representation of the plant, in the form of ODEs or DAEs, is referred to as the plant *model*, or equivalently, controller model or internal model. In a simulation-based study such as this, both the plant and plant model are mathematical models. However, as discussed in Chapter 6, the models are different and are handled

'separately' in order to properly maintain this distinction. In general, the MPC formulation places
no restriction on the type of plant models that are acceptable. For example, in conventional linear
MPC implementations, step, finite impulse, and linear state space models have been used to model
the plant behavior. On the other hand, NMPC controllers use nonlinear internal models to represent
the process dynamics. These models can be rigorous mechanistic (i.e. first principles) models, such
as the LDPE autoclave reactor models developed in Chapter 3, or data-driven nonlinear empirical
models, for e.g. second order Volterra [58], and neural network based NARMAX models [82, 24],
among many others in the system identification literature. In the remainder of this Chapter, we
provide some necessary background on NMPC, and present two formulations for the control of the
LDPE autoclave reactors.

The solution of optimal control problems involves finding optimal control policies which lead
to the minimization or maximization of some specified criteria. These criteria are usually lumped
together into a single objective (or *cost*) function, with each criterion weighted according to its
relative importance. This formulation has important implications in the field of control engineering,
as many control problems can be viewed as optimal control problems with the objective being the
minimization of deviations, or errors, between certain quantities and their respective setpoints. In
continuous-time, a general 'MPC-relevant' finite horizon optimal control problem bears the form of
Problem (4.1) shown below.

$$\min_{u(t)} \mathcal{J}\left(x(t), u(t)\right) = \Phi\left(x(t + T_P)\right) + \int_t^{t+T_P} \mathcal{L}\left(x(\tau), u(\tau)\right) d\tau \tag{4.1a}$$

subject to:

$$\dot{x}(t) = f(x(t), u(t), t), \; x(0) = x_0 \tag{4.1b}$$

$$x(t) \in \mathcal{X} \quad u(t) \in \mathcal{U} \tag{4.1c}$$

$$u(t) = u(t + T_M) \quad \forall t \in [t + T_M, t + T_P] \tag{4.1d}$$

Here, $\mathcal{J}\left(x(t), u(t)\right)$ is a scalar-valued finite horizon cost functional in Bolza form, T_P is the length
of the finite horizon commonly referred to as prediction horizon in MPC parlance, and T_M is the
length of the control horizon. The functions $\mathcal{L}\left(x(\tau), u(\tau)\right)$ and $\Phi\left(x(t + T_P)\right)$ are known as the
stage and *terminal* costs (or penalties), respectively. The solution to Problem (4.1) determines

the optimal control input trajectory $u^*(t)$, which minimizes the cost function (4.1a) subject to the constraints (4.1b) to (4.1d). The second constraint (4.1c) forces the states $x(t) \in \mathbb{R}^n$, and control inputs $u(t) \in \mathbb{R}^m$ along the optimal trajectory to lie in the sets $\mathcal{X}$ and $\mathcal{U}$, respectively. In this work, we are interested primarily in simple bound constraints of the form

$$\mathcal{X} = \left\{ x_L \leq x(t) \leq x_U \right\}$$
$$\mathcal{U} = \left\{ u_L \leq u(t) \leq u_U \right\}$$

Constraints of this form are useful in process control, as it allows the engineer to 'inform' the controller of actuator constraints, and process variable ranges, which usually take this form. The final constraint (4.1d) is, perhaps, unique to MPC and is used as a means to limit 'aggressiveness' of the controller. Depending on the situation, additional constraints can be freely introduced, for e.g. inequality path constraints on the outputs y or controlled outputs z, however, this formulation is sufficiently general to handle most cases.

For the case of *unconstrained* linear systems with quadratic objective functions, i.e. the well known linear quadratic regulator (LQR) problem, the optimal control problem can be solved analytically offline via a variety of techniques to obtain the state feedback expression $u_k = K_{LQ}x_k$, which can then be used online to calculate optimal control profiles. However, similar analytic solutions are unavailable for problems with constraints and model nonlinearity. For these cases, the optimal control problem must be solved online to determine the optimal trajectories.

Historically, Problem (4.1) was solved 'indirectly' using principles from the calculus of variations, i.e. by solving the associated Euler-Lagrange equation, and dynamic programming approaches, i.e. by solving the Hamilton-Jacobi-Bellman equation. However, the current online implementations of these methods posses a number of disadvantages [21, 7], and as a result, are seldom used in practice. Instead, an approximate (numerical) solution to Problem (4.1) is usually sought by posing the optimal control problem as a nonlinear programming (NLP) problem through appropriate parameterizations of the control inputs and (optionally) the states. The resulting problem is then solved using conventional NLP methodologies, from which, sequential quadratic programming (SQP) based methods are the most popular in the NMPC literature. This method is sometimes called 'direct' as it involves a direct minimization of the cost function subject to constraints, as opposed to relying on
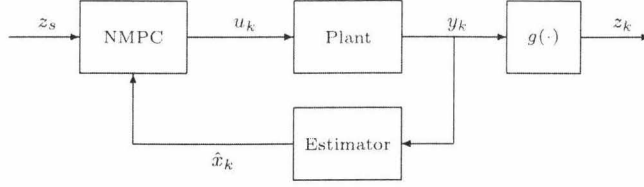
Figure 4.1: Illustration of the control structure

results from optimal control theory. In this study, we use orthogonal collocation on finite elements (OCFE) to discretize both the control inputs and the states, and the resulting system is solved using the commercial SQP package SNOPT. The reader is referred to Chapter 6, which deals more elaborately with issues regarding implementation of the controller formulations.

In digital control, it is standard procedure to regard the control inputs as being constant within each sampling interval, i.e. a zero-order hold (ZOH) is enforced in-between sampling instances. Therefore, it is more convenient to represent the continuous-time nonlinear ODE plant model (4.1b) as a set of nonlinear difference equations, which is common in the MPC literature.

$$x_{k+1} = f(x_k, u_k, t_k) \tag{4.2}$$

with the initial state x_0. Here, $x_k \in \mathbb{R}^n$ and $u_k \in \mathbb{R}^m$ are the plant states and control inputs, respectively, at the kth sampling instant, and t_k is the corresponding time. Now, using the discrete model (4.2), Problem (4.1) can be redefined, so that computer implementation of the formulation is made straightforward. In the following, we assume that both the control inputs and states are discretized.

$$\min_{\mathbf{x}_j, \mathbf{u}_j} \; \mathcal{J}(\mathbf{x}_j, \mathbf{u}_j) = \Phi(x_{j+P}) + \sum_{k=j}^{j+P-1} \mathcal{L}(x_k, u_k) \tag{4.3a}$$

subject to:

$$x_{k+1} = f(x_k, u_k, t_k), \; x_j = x_0 \tag{4.3b}$$

$$x_k \in \mathcal{X} \quad u_k \in \mathcal{U} \tag{4.3c}$$

$$u_k = u_{j+M-1} \quad \forall k = j + M, j + M + 1, \ldots, j + P - 1 \tag{4.3d}$$

Here, $\mathcal{J}(\mathbf{x}_j, \mathbf{u}_j)$ is the finite horizon cost functional for the discrete problem, P is the length of the prediction horizon measured in number of sampling periods, and M is the length of the control horizon. The stage and terminal penalty functions, $\mathcal{L}(x_k, u_k)$ and $\Phi(x_{j+P})$, in Problem (4.3) are now defined in terms of discrete quantities, in contrast to Problem (4.1) where they are functions of continuous variables. Note that the continuous-time objective (4.1a) could very easily have been incorporated into Problem (4.3) instead of (4.3a), by using a suitable numerical quadrature scheme to evaluate the integral. However, in addition to being simpler to compute, when the cost is quadratic, the discrete-time objective is identical to the case of the discrete-time LQR problem, making comparison between the two cases easier. The decision variable vectors $\mathbf{x}_j$ and $\mathbf{u}_j$ are the sequence of states and control inputs at each sampling instance over the P–interval prediction horizon, i.e.

$$\mathbf{x}_j = \begin{bmatrix} x_j^T & x_{j+1}^T & \cdots & x_{j+P-1}^T & x_{j+P}^T \end{bmatrix}^T$$
$$\mathbf{u}_j = \begin{bmatrix} u_j^T & u_{j+1}^T & \cdots & u_{j+P-2}^T & u_{j+P-1}^T \end{bmatrix}^T$$

Figure 4.1 is a simple schematic showing the structure of the feedback loop with the NMPC controller. The Plant block denotes the system we are interested in controlling, which is, in this case, the LDPE autoclave reactor. The NMPC controller accepts as inputs, the setpoints z_s of the *controlled outputs* z_k, and the current estimate $\hat{x}_k$ of the plant state. The setpoints to the controller can be supplied manually by operator intervention, or automatically using an upper real-time optimization (RTO) layer [5]. Using the current estimate as the starting point, the NMPC controller solves a given *open-loop* finite horizon optimal control problem to obtain an optimal control input trajectory $\mathbf{u}_k^*$ which minimizes the associated cost function. Only the first input in this trajectory u_k is sent to the plant.

The main requirement for solving the NMPC problem is the availability of the current plant state. Usually, however, the complete state vector is not measured online, and in general, the available measurements y_k can be some nonlinear function of the state, or some subset of the state. Furthermore, the measurements taken might be distorted by sensor noise. Therefore, the role of the Estimator block (i.e. the state estimator) is to use the available measurements to construct an *estimate* of the plant state $\hat{x}_k$, which is then fed back to the controller. More information on the state estimators used in this study can be found in Chapter 5.

In the following Sections, we will present two NMPC formulations, namely, the nominal, and the offset-free NMPC formulations for the control of the LDPE autoclave reactor.

4.1   Nominal Formulation

The process of modeling most systems of interest involves making simplifying assumptions on, and approximations of the underlying phenomena. This is especially true for polymerization reactors, which display complex phenomena, for e.g. nonideal mixing, multi-phase polymerization, and gel formation, etc. It is an extremely difficult task to properly model these features, and oftentimes, one must resort to empirical correlations to describe complicated behavior. Due to these factors, it is essentially impossible to develop a process model capable of matching the plant dynamics exactly. Fortunately, for process control, it is only essential that the 'most important features' of the plant's dynamic response are modeled. However, in the nominal formulation discussed here, we assume that the plant model matches the plant dynamics *perfectly*, i.e. there is no plant-model mismatch, and that unmeasured disturbances do not enter the system. Obviously, this formulation cannot generally be used in practice, however, it is useful as an introduction to more sophisticated algorithms, such as the offset-free formulation discussed in Section 4.2.

For this formulation, we postulate that the plant dynamics and measurements are described perfectly by the model

$$
\begin{aligned}
x_{k+1} &= f(x_k, u_k, w_k, t_k) \\
y_k &= h(x_k, t_k) + v_k \\
z_k &= g(y_k)
\end{aligned}
\tag{4.4}
$$

Here, $y_k \in \mathbb{R}^p$ is the vector of plant measurements (or *outputs*), which in general, is some nonlinear function $h(\cdot)$ of the state x_k. The vector of controlled outputs $z_k \in \mathbb{R}^{n_c}$ is modeled, somewhat generally, as a nonlinear function $g(\cdot)$ of the measurements, though in many cases they are coincident. The vectors $w_k \in \mathbb{R}^q$ and $v_k \in \mathbb{R}^p$ are the state (or process) and measurement noise, respectively. Both w_k and v_k are assumed to be zero-mean Gaussian white-noise processes with covariance matrices

Q_k and R_k, respectively, i.e.

$$w_k \backsim \mathcal{N}(0, Q_k)$$

$$v_k \backsim \mathcal{N}(0, R_k)$$

The process noise w_k can be viewed as another input to the system. In this case, however, the input is Gaussian random, and we do not posses control over its magnitude. In order to continue using the difference equation notation, we assume that the process noise is 'sampled' at the beginning of the sampling period, and is then held constant over the duration of the interval [32]. The measurement noise v_k is assumed to be additive, though more general nonlinear relationships can be modeled, if necessary.

As mentioned previously, the NMPC objective function is designed by weighting several, some-times competing, performance criteria within a single cost function. In general, we require that the controller maintain a number of controlled outputs (or process variables), for e.g. reactor tempera-ture and liquid level, at some desired setpoints. Furthermore, we desire that the controller do this by employing 'minimal' control effort, and without taking 'very large' control moves. These notions are incorporated into a quadratic cost function which penalizes deviations, or errors, between the controlled output z_k and its setpoint z_s, the control input u_k and its setpoint u_s, as well as the control rate Δu_k over the entire prediction horizon. Therefore, the controller NLP that is solved at each sampling instance is given by

$$\min_{\mathbf{x}_j, \mathbf{u}_j} \quad \|z_{j+P} - z_s\|_{\mathbf{Q}}^2 + \sum_{k=j}^{j+P-1} \|z_k - z_s\|_{\mathbf{Q}}^2 + \|u_k - u_s\|_{\mathbf{R}}^2 + \|\Delta u_k\|_{\mathbf{S}}^2 \tag{4.5a}$$

subject to:

$$x_{k+1} = f(x_k, u_k, 0, t_k), \; y_k = h(x_k, t_k), \; z_k = g(y_k) \tag{4.5b}$$

$$x_L, u_L, \Delta u_L \leq x_k, u_k, \Delta u_k \leq x_U, u_U, \Delta u_U \tag{4.5c}$$

$$u_k = u_{j+M-1} \quad \forall k = j + M, j + M + 1, \ldots, j + P - 1 \tag{4.5d}$$

Here, $\mathbf{Q} \in \mathbb{R}^{n_c \times n_c}$ is the controlled output penalty matrix, $\mathbf{R} \in \mathbb{R}^{m \times m}$ is the control input penalty matrix, and $\mathbf{S} \in \mathbb{R}^{m \times m}$ is the control rate penalty matrix. The norm notation used in the objective function is simply a compact representation of the quadratic form, for e.g.

$$\|z_k - z_s\|_{\mathbf{Q}}^2 = (z_k - z_s)^T \mathbf{Q}(z_k - z_s) \tag{4.6}$$

The control rate Δu_k in formulation (4.5) is simply the difference between the current and past control inputs, i.e.

$$\Delta u_k = u_k - u_{k-1} \tag{4.7}$$

The setpoints z_s and u_s are not independent, and must correspond to a steady state (or equilibrium) of the the plant model, i.e.

$$\begin{aligned} x_s &= f(x_s, u_s, 0, \cdot) \\ y_s &= h(x_s, \cdot) \\ z_s &= g(y_s) \end{aligned} \tag{4.8}$$

The closed-loop response of the NMPC controller is tuned using the quadratic penalty matrices $\mathbf{Q}$, $\mathbf{R}$, and $\mathbf{S}$. Details on the tuning parameters used in this study can be found in Chapter 7.

In the presence of plant-model mismatch and/or unmeasured disturbances, the nominal NMPC formulation is known to cause steady state errors (or *offsets*) in the controlled variables. This feature can be attributed partly due to the structure of the quadratic objective employed in the formulation. For example, when an unmeasured disturbance enters a system at equilibrium, the steady state control input setpoint u_s that is required to maintain the controlled output z_k at its setpoint z_s changes depending on the type and magnitude of the disturbance. The nominal formulation, however, lacks any mechanism to estimate this disturbance, and to accordingly adjust setpoint u_s to the necessary value. Consequently, the NLP solver is forced to compromise by balancing offsets between the controlled output and its setpoint, and the control input and its 'incorrect' setpoint. The extent of the offset will, obviously, depend on the relative weighting between the two in the objective function. Note that, in this example, we have chosen to ignore coupled state estimation issues which also arise due to model mismatch when using this formulation.

4.2   Offset-free Formulation

The nominal NMPC formulation discussed previously does not make any accommodation for modeling inaccuracies or unmeasured disturbances within the controller architecture, leading to steady state offset in the controlled output. In most chemical processes, such behavior is undesirable as it

results in, for e.g. variable product quality and suboptimal operation, depending on the extent of the plant-model mismatch, and/or the type and magnitude of the disturbance. Perhaps, in keeping with the tradition of the popular PID controller, the most intuitive way of achieving offset-free operation is to augment the model state vector with a number integral states x_f corresponding to the controlled outputs, i.e.

$$
\begin{aligned}
x_f &= \int_0^t \left(z(\tau) - z_s(\tau) \right) d\tau = \int_0^t e(\tau) \, d\tau \\
\dot{x}_f &= z(t) - z_s(t) = e(t)
\end{aligned}
\tag{4.9}
$$

However, doing so has several disadvantages, most notably, the increased computational cost incurred due to the inclusion of additional states, which have to be incorporated into the NLP that is solved online, and the requirement for some anti-windup feature for the integral states in order to prevent control performance degradation due to integral windup [52].

The most popular choice, by far, in the MPC literature is to augment the state vector of the plant model with *constant* disturbance states [52, 57]. It is well known that this essentially duplicates the function of integral control [23], while avoiding the need for an anti-windup feature [52]. Due to this property, the disturbance states are occasionally referred to as integrating disturbances. Obviously, since these states are artificially introduced quantities, they are not controllable, however, a suitable disturbance model (i.e. controller model) can be designed such that their magnitudes can be estimated from available plant measurements. The disturbance states essentially function as 'model equalizers' in the sense that they serve to 'equalize' the plant and model dynamics with respect to the plant outputs. The flexibility provided by integrating disturbances permits structural accommodation of the effects of 'moderate' plant-model mismatch and unmeasured disturbances
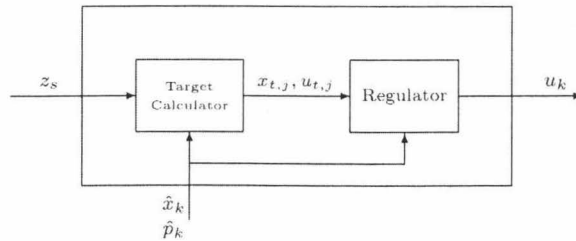

Figure 4.2: Internal view of the NMPC block

from within the framework of the controller model.

In the offset-free NMPC formulation, the actual plant dynamics and measurements are approximated 'internally', i.e. according to the controller, by the model

$$
\begin{aligned}
x_{k+1} &= f(x_k, u_k, p_k, w_k, t_k) \\
y_k &= h(x_k, p_k, t_k) + v_k \\
z_k &= g(y_k)
\end{aligned}
\tag{4.10}
$$

Here, $p_k \in \mathbb{R}^{n_d}$ is the vector of disturbance states, and all other quantities are as previously defined. Disturbance models can be classified into *input* and *output* disturbance models depending on where the disturbance p_k is *modeled as* entering the plant. For example, an input disturbance model approximates the effect of model mismatch and/or unmeasured disturbances as an (artificial) disturbance originating at the plant input. The model (4.10) is general and allows for both input and output disturbances, as well as some combination of the two. Particular details on the design of the disturbance model used in this work can be found in Chapter 7. The dynamics of the integrating disturbance is modeled by

$$
p_{k+1} = p_k + \xi_k
\tag{4.11}
$$

where $\xi_k \in \mathbb{R}^{n_d}$ is assumed to be zero-mean Gaussian white-noise with covariance matrix S_k. In the context of NMPC, this implies that the disturbance remains *constant* over the prediction horizon. The disturbance model (4.10) is very general, and allows for the integrating disturbance states to be introduced into the model dynamics and/or measurement equations in any arbitrary manner. However, in this work, we use the simplified disturbance model (4.12), in which the disturbance states are related linearly to the model dynamics and measurements as shown below.

$$
\begin{aligned}
x_{k+1} &= f(x_k, u_k, t_k) + X_u p_k + w_k \\
y_k &= h(x_k, t_k) + X_y p_k + v_k \\
z_k &= g(y_k)
\end{aligned}
\tag{4.12}
$$

Here, $X_u \in \mathbb{R}^{n \times n_d}$ and $X_y \in \mathbb{R}^{p \times n_d}$ are the user-supplied input and output disturbance matrices, respectively. Figure 4.2 shows the internal structure of the NMPC controller block (see Figure 4.1) for the offset-free formulation. Here, the controller consists of two components, namely, the Target Calculator, and the Regulator subsystems. The target calculator uses the current estimates $\hat{x}_k$ of

the plant state and disturbance $\hat{p}_k$ to calculate steady state (equilibrium) targets for the state $x_{t,j}$ and control input $u_{t,j}$, which is sent to the Regulator. The regulator solves an open-loop finite horizon optimal control problem to obtain the optimal control input profile $\mathbf{u}_k^*$, which minimizes a given (quadratic) objective function. The first control input in this trajectory u_k is sent to the plant. In the following subsections, we will discuss in detail the functions of the target calculator and regulator in the offset-free NMPC formulation.

4.2.1 Target Calculator

As mentioned previously, the principal limitation of the nominal formulation was that it possessed no mechanism to adjust the setpoints z_s, u_s to the controller, which, in the presence of modeling errors, unmeasured disturbances, and/or process constraints, can lead to steady state offsets in the controlled variables. The offset-free formulation overcomes this limitation through the use of the so called target calculator. The role of the target calculator in this formulation is to identify a steady state, or equilibrium, of the controller model (4.10) at which the controlled output z_k achieves its respective setpoint z_s. In this Section, the notation $z_{t,j}$ and $u_{t,j}$ refers to the controlled output and control input setpoints, respectively, at the jth (i.e. current) sampling instance, and p_j is the current disturbance. The target calculation problem is fundamentally an algebraic problem, which can be stated as

$$
\begin{aligned}
x_{t,j} &= f(x_{t,j}, u_{t,j}, p_j, 0, \cdot) \\
y_{t,j} &= h(x_{t,j}, p_j, \cdot) \\
z_{t,j} &= g(y_{t,j}) \\
0 &= z_s - z_{t,j}
\end{aligned}
\tag{4.13}
$$

The first equation in (4.13) is the equilibrium condition for the disturbance model (4.10), given the current disturbance p_j. The final condition ensures that the equilibrium point corresponds to the desired setpoints for the controlled variables. The only unknowns in the above equation are the target states and control inputs, i.e. $x_{t,j} \in \mathbb{R}^n$ and $u_{t,j} \in \mathbb{R}^m$, respectively. Clearly, for square plants (i.e. where $n_c = m$), in the absence of constraints, the algebraic problem (4.13) is well-posed, and any multivariable root-finding algorithm, for e.g. Newton-Raphson, can be used to solve it. Difficulties

arise, however, for 'thin' ($n_c > m$) and 'fat' ($n_c < m$) plants, where the above system is *not* well-posed. For thin plants, there are more equations than free variables, and in general, it is impossible to find equilibrium targets which satisfy the controlled output setpoint. For fat plants, there are fewer equations than free variables, and in general, several equilibrium solutions exist which satisfy the controlled output setpoint. Obtaining a solution to (4.13) is further complicated by the presence of process constraints, which might be critical in determining whether the controlled output setpoint is feasible.

Due to the reasons discussed previously, the problem of identifying steady state targets is resolved in many proposed MPC algorithms by formulating it as an optimization (i.e. QP/NLP) problem. For example, following the approach of Muske and Badgwell [52], and Pannocchia and Rawlings [57] for linear MPC, a quadratic objective NLP such as

$$\min_{x_{t,j}, u_{t,j}} (z_{t,j} - z_s)^T Q(z_{t,j} - z_s) + (u_{t,j} - u_s)^T R(u_{t,j} - u_s) \tag{4.14}$$

can be defined, subject to the steady state controller model (4.13), and any necessary process constraints. Obviously, the last condition in (4.13) is no longer applicable. Here, z_s and u_s are the *desired* setpoints, which may or may not be achievable, and $z_{t,j}$ and $u_{t,j}$ are the feasible (achievable) targets. The matrices Q and R in (4.14) can be chosen to penalize (relatively) deviations of the controlled output target from its desired setpoint, and the control input target from its desired setpoint. In practice, one is usually more concerned with maintaining the controlled output target at or close to its setpoint, therefore, the elements in Q are usually selected to be much higher than the elements in R.

In this work, we adopt the exact penalty approach proposed by Rao and Rawlings [64] for linear MPC, and Tenny, Wright, and Rawlings [83] for NMPC. Here, in order to accommodate situations where achieving the controlled output setpoint is impossible, the requirement that the setpoint be achieved exactly is relaxed by incorporating it into the target calculation NLP by defining the soft constraint

$$z_s - \eta \leq z_{t,j} \leq z_s + \eta \tag{4.15}$$

where $\eta \in \mathbb{R}^{n_c}$ is a nonnegative vector of slack variables. This constraint forces the controlled output target $z_{t,j}$ to lie within some 'radius' η of the desired setpoint z_s. This radius can be made arbitrarily

small by appropriately penalizing η in the objective function, such that, for all intents and purposes, the equality $z_{t,j} = z_s$ holds when achieving the desired setpoint is feasible. In this study, the l_1/l_2^2 penalty approach of Rao and Rawlings [64] is used to penalize η in the target calculation NLP. Therefore, the NLP that is solved at each iteration is given by

$$\min_{x_{t,j}, u_{t,j}, \eta} \quad \frac{1}{2}\|\eta\|_Q^2 + \mathrm{II}^T\eta + \frac{1}{2}\|\Delta u_{t,j}\|_{\mathcal{R}}^2 \tag{4.16a}$$

subject to:

$$x_{t,j} = f(x_{t,j}, u_{t,j}, p_j, 0, t_j), \; y_{t,j} = h(x_{t,j}, p_j, t_j), \; z_{t,j} = g(y_{t,j}) \tag{4.16b}$$

$$z_s - \eta \leq z_{t,j} \leq z_s + \eta \tag{4.16c}$$

$$x_L, u_L \leq x_{t,j}, u_{t,j} \leq x_U, u_U \tag{4.16d}$$

$$\eta \geq 0 \tag{4.16e}$$

In practice, the l_1/l_2^2 penalty matrices $Q \in \mathbb{R}^{n_c \times n_c}$ and $\mathrm{II} \in \mathbb{R}^{n_c}$ are chosen 'sufficiently large', so that the soft constraint is guaranteed to be exact [64]. Here, the notation $\Delta u_{t,j}$ represents the difference between the current and past control input *targets*, i.e.

$$\Delta u_{t,j} = u_{t,j} - u_{t,j-1} \tag{4.17}$$

Penalizing $\Delta u_{t,j}$, via the quadratic penalty matrix $\mathcal{R} \in \mathbb{R}^{m \times m}$, ensures that, if multiple control input targets satisfy the controlled output setpoint, the targets selected are ones that are closest to the previous target [83].

4.2.2 Regulator

The regulator in the offset-free NMPC formulation solves an open-loop optimal control NLP online to calculate optimal control input trajectories which drive the system to, or equivalently, stabilize the system about the current controlled output $z_{t,j}$ and control input $u_{t,j}$ targets. Therefore, given the current estimate of the integrating disturbance state p_j, the resulting quadratic objective based NLP that is solved at each sampling instance is given by

$$\min_{\mathbf{x}_j, \mathbf{u}_j} \quad \|z_{j+P} - z_{t,j}\|_Q^2 + \sum_{k=j}^{j+P-1} \|z_k - z_{t,j}\|_Q^2 + \|u_k - u_{t,j}\|_R^2 + \|\Delta u_k\|_S^2 \tag{4.18a}$$

subject to:

$$x_{k+1} = f(x_k, u_k, p_j, 0, t_k), \; y_k = h(x_k, p_j, t_k), \; z_k = g(y_k) \qquad (4.18b)$$

$$x_L, u_L, \Delta u_L \leq x_k, u_k, \Delta u_k \leq x_U, u_U, \Delta u_U \qquad (4.18c)$$

$$u_k = u_{j+M-1} \quad \forall k = j + M, j + M + 1, \ldots, j + P - 1 \qquad (4.18d)$$

Note that the structure of the regulator NLP is virtually identical to the case of the nominal NMPC formulation. Furthermore, note that the model constraints (4.18b) above implicitly assume that the integrating disturbance state p_j remains constant over the prediction horizon.

Chapter 5

State Estimation

The operation of any state feedback control scheme, such as model predictive control, is dependent on the availability of good state estimates at each sampling instance on which to base future control decisions. However, it is rarely the case that physical measurements of all state variables are available, and those that are available are frequently contaminated with measurement noise. Furthermore, the system dynamics might be subjected to random disturbances (or noises) which can neither be controlled nor modeled deterministically [47]. Therefore, the role of the state estimator in the control system is to reconstruct unmeasured state variables from the available measurements, and also to filter the measurements to account for the effects of noise [12]. In this context, state estimators are oftentimes also referred to as filters.

The state estimation techniques developed for linear systems are based on the highly advanced linear estimation theory [53]. The well known Kalman filter [34, 35], originally proposed by R. E. Kalman in 1960, produces minimum variance and maximum likelihood (optimal) recursive state estimates for unconstrained linear systems [53]. However, the optimal solution to the nonlinear filtering problem is infinite dimensional [33], and there currently exists no truly optimal solution which can reasonably be implemented online. Therefore, a number of suboptimal filtering strategies suitable to online implementation have been suggested in order to solve the nonlinear filtering problem. In the following Sections, we outline two such approaches that were utilized in this work, namely, the extended Kalman filtering (EKF), and unscented Kalman filtering (UKF) state estimation schemes.

Note that in the context of the offset-free NMPC formulation, where the quantities that must be estimated comprise both the state and disturbance vectors, the state vector x_k in the discussions to follow should be thought of as the augmented vector of states and disturbances, i.e.

$$x_k \longleftarrow \begin{bmatrix} x_k^T & p_k^T \end{bmatrix}^T$$

5.1 Extended Kalman Filter

The Kalman filter [34, 35] is the optimal filter for unconstrained linear systems. The *extended* Kalman filter (EKF), as the name suggests, is an extension of the linear Kalman filtering algorithm to nonlinear systems. However, the EKF is *not* an optimal solution to the nonlinear filtering problem, but is essentially a convenient, improvisatory approach to the solution of a highly complicated problem. The foundational principle of the EKF is that the state errors are 'small', i.e. the true state is sufficiently close to the estimated state, such that the error dynamics can be described fairly accurately by a first-order Taylor series expansion [12]. Practically, this amounts to application of the well-known recursive linear Kalman filtering equations to *locally* linear approximations of the nonlinear model.

Despite its *ad hoc* formulation, and absence of strong theoretical justification, the conceptual simplicity of the EKF implementation has made it one of the most widely used algorithms for
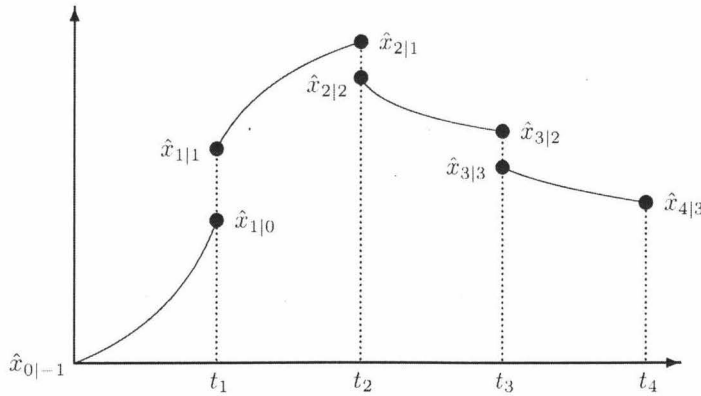

Figure 5.1: Continuous-discrete extended Kalman filter.

nonlinear state estimation. Many published accounts of NMPC applications (see for example [1, 70, 72, 2]) have used EKF based schemes successfully for state estimation. In this Section, we present the continuous-discrete (i.e. continuous model-discrete measurements) extended Kalman filtering algorithm which was used in this work. This configuration is appropriate for most chemical engineering applications, as chemical process models are naturally formulated in continuous-time, and digital computer systems used to monitor most processes are only capable of sampling the plant discretely. For details on other configurations, such as the continuous, and discrete EKF algorithms, the reader is referred to the introductory text of Crassidis and Junkins [12]. Many variations on the underlying EKF methodology have been suggested in order to improve its performance and stability properties, for example, the iterated, and second-order EKF schemes [65], however, only the original EKF scheme is covered here. Here, we shall consider continuous-time ODE plant models with discrete measurements of the form

$$
\begin{aligned}
\dot{x}(t) &= f(x(t), u(t), w(t), t) \\
y_k &= h(x_k, t_k) + v_k
\end{aligned}
\tag{5.1}
$$

where $x(t) \in \mathbb{R}^n$ and $u(t) \in \mathbb{R}^m$ are the plant state and control inputs, respectively. The vector of process measurements $y_k \in \mathbb{R}^p$ is assumed to be some nonlinear function $h(\cdot)$ of the state. The process (or state) noise $w(t) \in \mathbb{R}^q$, and measurement noise $v_k \in \mathbb{R}^p$ are assumed to be zero-mean Gaussian white-noise processes with symmetric covariance matrices $Q(t) \in \mathbb{R}^{n \times n}$ and $R_k \in \mathbb{R}^{p \times p}$, respectively, i.e.

$$
\begin{aligned}
E\left\{w(t)w^T(\tau)\right\} &= Q(t)\delta(t - \tau) \\
E\left\{v_k v_j^T\right\} &= R_k \delta_{kj}
\end{aligned}
\tag{5.2}
$$

Prior to proceeding further, it will be useful to explain some of the terminology and notation that is used throughout the remainder of this Chapter. Here, the *true* state $x(t)$ refers to the plant state, i.e. the state of the actual system which is under observation/control. In reality, one does not have access to the true state. The only accessible information about the plant are the available measurements y_k, from which an *estimate* of the plant state $\hat{x}(t)$ can be inferred. Therefore, from a strict notational point of view, all state and controlled output notation used in Chapter 4 should be thought of as state and controlled output *estimates*, respectively. The state (or estimation) error $\tilde{x}$

is defined as the difference between the true and estimated states, i.e. $\tilde{x}(t) = x(t) - \hat{x}(t)$. The state error covariance matrix $P(t) \in \mathbb{R}^{n \times n}$ is given by the following expectation

$$P(t) = E\left\{\tilde{x}(t)\tilde{x}^T(t)\right\} \tag{5.3}$$

A characteristic feature of discrete Kalman and Kalman-like filters is the recursive predictor-corrector structure of the estimation algorithm. The notation $\hat{x}_{k|k-1}$ refers to the *predicted* state estimate at time t_k given measurements up to time t_{k-1}, while $\hat{x}_{k|k}$ refers to the *corrected* (or updated) estimate at t_k after the latest measurement y_k is available. The covariance matrix notations $P_{k|k-1}$ and $P_{k|k}$ are defined similarly.

Figure 5.1 depicts schematically the prediction and correction stages of the continuous-discrete EKF algorithm. In between sampling instances, the continuous-time nonlinear plant model is numerically integrated forward in time in order to obtain a *prediction* of the plant state estimate $\hat{x}_{k|k-1}$. However, as seen in the figure, whenever a measurement becomes available (i.e. at each t_k), the predicted state estimate is *corrected (updated) instantaneously* to obtain $\hat{x}_{k|k}$, reflecting the effect of the most recent measurement. In the following subsections, we will briefly outline the prediction and correction stages of the continuous-discrete EKF algorithm.

5.1.1 Prediction

In the prediction step, the previous state $\hat{x}_{k-1|k-1}$ and covariance $P_{k-1|k-1}$ updates are propagated over the sampling interval to give predictions of the current state $\hat{x}_{k|k-1}$ and covariance $P_{k|k-1}$, respectively. According to the continuous-discrete EKF algorithm, the predicted state estimate (also known as the predicted, or *a priori* mean) is obtained by directly propagating (i.e. integrating) the nonlinear system over the sampling interval. However, the predicted error covariance is obtained by propagating the matrix Riccati differential equation associated with the continuous-discrete *linear* Kalman filtering algorithm, *together* with the nonlinear system. Therefore, the state and error covariance predictions can be obtained by integrating the following system

$$\begin{bmatrix} \dot{\hat{x}}(t) \\ \dot{P}(t) \end{bmatrix} = \begin{bmatrix} f\left(\hat{x}(t), u(t), 0, t\right) \\ F(\cdot)P(t) + P(t)F^T(\cdot) + G(\cdot)Q(t)G^T(\cdot) \end{bmatrix} \tag{5.4}$$

over the sampling interval $[t_{k-1}, t_k]$. Here, the matrices $F(\cdot) \in \mathbb{R}^{n \times n}$ and $G(\cdot) \in \mathbb{R}^{n \times q}$ are Jacobians of the continuous-time nonlinear model given by

$$
\begin{aligned}
F(\cdot) &\equiv \partial f(\hat{x}(t), u(t), w(t), t) / \partial \hat{x} \\
G(\cdot) &\equiv \partial f(\hat{x}(t), u(t), w(t), t) / \partial w
\end{aligned}
\tag{5.5}
$$

Finally, the predicted state estimate can be used to calculate the predicted output (or measurements) $\hat{y}_k$ using the equation

$$
\hat{y}_k = h(\hat{x}_{k|k-1}, t_k)
\tag{5.6}
$$

For online implementation, it should be noted that since the state error covariance matrix $P(t)$ is symmetrical, integration of the entire matrix differential equation in (5.4) need not be performed. Instead, only the upper or lower triangular matrices of the differential equation (i.e. only $n(n+1)/2$ equations) need be integrated together with the nonlinear plant model. Naive implementations of the EKF prediction algorithm can result in poor performance for large-scale systems. Numerical implementations utilizing the special structure of the EKF equations, such as the ESDIRK scheme proposed by Jørgensen, Kristensen, Thomsen, and Madsen [29], should be preferred in situations where naive implementations are expected to fair poorly.

5.1.2   Correction

In the correction (or update) step, the predicted state and error covariance are corrected using the most recent measurements y_k. The EKF update algorithm is completely identical to the cases of the discrete and continuous-discrete linear Kalman filters, except here, the output matrix of the linear system is replaced with the output Jacobian of the nonlinear system. Therefore, the EKF state and covariance update equations are given by

$$
\begin{aligned}
\hat{x}_{k|k} &= \hat{x}_{k|k-1} + K_k (y_k - \hat{y}_k) \\
P_{k|k} &= \big[I - K_k H(\hat{x}_{k|k-1}, t_k) \big] P_{k|k-1}
\end{aligned}
\tag{5.7}
$$

where $H(\hat{x}_{k|k-1}, t_k) = \partial h(\hat{x}_{k|k-1}, t_k)/\partial \hat{x}$ is the output Jacobian matrix of the nonlinear model, and K_k is the Kalman gain given by

$$
K_k = P_{k|k-1} H^T(\hat{x}_{k|k-1}, t_k) \big[H(\hat{x}_{k|k-1}, t_k) P_{k|k-1} H^T(\hat{x}_{k|k-1}, t_k) + R_k \big]^{-1}
\tag{5.8}
$$

5.2   Unscented Kalman Filter

The EKF algorithm described previously is conceptually simple, relatively easy to implement, and performs reasonably well on several systems of interest. However, the error introduced by linearization in the EKF procedure can occasionally lead the filter to perform poorly, and in certain situations, can cause the filter to diverge completely [32]. For example, Haseltine and Rawlings [27] provide a number of examples showing the failure of the EKF for relatively simple chemical engineering systems. Furthermore, calculation of analytic Jacobian matrices required by the EKF is highly time-consuming and prone to human-error. Finite difference Jacobians are an obvious solution to this problem, however, they are computationally expensive to evaluate and can introduce additional errors. The unscented transform [30, 31, 33, 32] (UT) on which the unscented Kalman filter (UKF) is based was developed to overcome problems associated with linearization in the EKF, while maintaining the computational advantages of the Kalman-like recursive predictor-corrector structure.

The UT is founded on the notion that "it is easier to approximate a probability distribution than it is to approximate an arbitrary nonlinear function or transformation" [33, 32]. Following this approach, a deterministic set of so called *sigma* points about the prior conditional mean are initiated and transformed through the nonlinear process model to yield a cloud of transformed points. The statistics of the transformed points can then be used to develop an estimate of the transformed mean and covariance [32]. Julier, Uhlmann, and Durrant-Whyte [33], and Julier and Uhlmann [32] show that this procedure results in a filter which is more accurate than the EKF, and whose performance, in fact, lies between those of the modified, truncated second-order filter, and the Gaussian second-order filter. Furthermore, the UKF behaves, in every practical sense, as a *black box* filter, requiring only that the nonlinear process model be supplied, making it much easier to implement than the EKF which requires, additionally, that the Jacobian be specified, and the second-order filters which require both the Jacobian and the Hessian.

Despite its many practical advantages, the UKF has received surprisingly relatively very little attention, until very recently, from the chemical engineering and process control community. Romanenko and Castro [67] applied the UKF algorithm of Julier, Uhlmann, and Durrant-Whyte [33]

for state estimation of a highly nonlinear nonisothermal exothermic CSTR. They showed, through simulations, that the UKF greatly outperforms the EKF, especially in high noise situations where the effects of linearization begin to affect quality of EKF state estimates. In a follow-up study, Romanenko, Santos, and Afonso [68] compared EKF and UKF performance on a simulated pH system having a nonlinear measurement model. They showed, using a number of example cases, that the UKF provides better state estimates than the EKF for this application. Recently, Prakash, Deshpande, and Patwardhan [60], and Marafioti, Olaru, and Hovd [44] have applied the UKF for state estimation in context of nonlinear model predictive controllers. Kolås, Foss, and Schei [38] have suggested a number of modifications to the standard UKF algorithm to handle constrained estimation problems. They showed that the modified UKF performs well, even for systems with multimodal probability density functions, using the EKF-failure examples of Haseltine and Rawlings [27].

In this Section, we first present a general UKF algorithm corresponding to the situation where the process and measurement noise vectors appear nonlinearly in the system and measurement models, respectively. When the process and/or measurement noise vectors are assumed additive, as is quite often the case, certain simplifications to this procedure can be made, which shall be discussed towards the end of this Section. Therefore, consider the general discrete-time nonlinear model

$$
\begin{aligned}
x_{k+1} &= f(x_k, u_k, w_k, t_k) \\
y_k &= h(x_k, u_k, v_k, t_k)
\end{aligned}
\tag{5.9}
$$

where $w_k \in \mathbb{R}^q$ is the process noise, and all other quantities are as previously defined. We start by defining a 'new' vector $x^a_{k-1|k-1}$, by augmenting the state vector with the process and measurement noise vectors to give

$$
x^a_{k-1|k-1} = \begin{bmatrix} x^T_{k-1|k-1} & w^T_{k-1} & v^T_{k-1} \end{bmatrix}^T
\tag{5.10}
$$

where $x^a_{k-1|k-1} \in \mathbb{R}^{n+q+p}$ is known as the augmented state vector. The model (5.9) can be easily rewritten in terms of $x^a_{k-1|k-1}$, therefore

$$
\begin{aligned}
x^a_{k+1|k} &= f^a(x^a_{k|k}, u_k, t_k) \\
y_k &= h^a(x^a_{k|k}, u_k, t_k)
\end{aligned}
\tag{5.11}
$$

The covariance matrix $P^a_{k-1|k-1}$ of the augmented state vector can, in the general case, be represented by the matrix

$$P^a_{k-1|k-1} = \begin{bmatrix} P_{k-1|k-1} & P^{xw}_{k-1} & P^{xv}_{k-1} \\ P^{wx}_{k-1} & Q_{k-1} & P^{wv}_{k-1} \\ P^{vx}_{k-1} & P^{vw}_{k-1} & R_{k-1} \end{bmatrix} \tag{5.12}$$

However, in many practical situations, the state error, and process/measurement noise vectors are not correlated among one another, therefore, the above augmented covariance matrix can be simplified, yielding

$$P^a_{k-1|k-1} = \begin{bmatrix} P_{k-1|k-1} & \mathbf{0}^{n \times q} & \mathbf{0}^{n \times p} \\ \mathbf{0}^{q \times n} & Q_{k-1} & \mathbf{0}^{q \times p} \\ \mathbf{0}^{p \times n} & \mathbf{0}^{p \times q} & R_{k-1} \end{bmatrix} \tag{5.13}$$

where, for example, the notation $\mathbf{0}^{n \times q}$ indicates a zero matrix with n rows and q columns.

5.2.1   Prediction

The prediction step in the UKF algorithm consists of two sub-steps, first, the generation of a set of sigma points, second, followed by propagation of the sigma points through the nonlinear model to obtain a set of transformed points, which are then used to develop an *a priori* estimate of the plant state. These sigma points are not generated randomly, unlike for e.g. particle filters, but are chosen carefully such that they satisfy certain criteria, namely, they must have a mean equal to the previous state estimate $\hat{x}^a_{k-1|k-1}$, and a sample covariance equal to the previous covariance $P^a_{k-1|k-1}$. Using the notation of Romanenko and Castro [67], letting $n^a = (n + q + p)$, a set of $(2n^a + 1)$ *zero-mean* sigma points can be computed from the *columns* of the matrix

$$\mathcal{X}^*_{k-1|k-1} = \begin{bmatrix} \mathbf{0}^{(2n^a+1) \times 1} & \sqrt{(n^a + \kappa)P^a_{k-1|k-1}} & -\sqrt{(n^a + \kappa)P^a_{k-1|k-1}} \end{bmatrix} \tag{5.14}$$

Here, $\kappa \in \mathbb{R}$ is a scalar parameter that can be used to 'fine tune' higher order moments of the distribution, and can be used to reduce overall prediction errors [33]. If the distribution of x_k is assumed to be Gaussian, Julier, Uhlmann, and Durrant-Whyte [33] recommend that κ be chosen such that $n^a + \kappa = 3$, however, a different choice of κ might be required if a different distribution of x_k is assumed. Note that in equation (5.14) it is assumed that the structure of the matrix square

root is of the form $P = \sqrt{P}\sqrt{P}^T$. Using this convention, the columns of $\mathcal{X}^*_{k-1|k-1}$ form the set of sigma points. However, if the root is of the form $P = \sqrt{P}^T\sqrt{P}$, the *rows* of $\sqrt{P}$ together with the zero row vector $\mathbf{0}^{1\times(2n^a+1)}$ forms the complete set of sigma points [33, 32]. To evaluate the matrix square root, Julier and Uhlmann [32] recommend numerically efficient and stable methods, such as Cholesky factorization, for which efficient algorithms already exist. The sigma point set in (5.14) is zero-mean, but has the same variance as the augmented state $\hat{x}^a_{k-1|k-1}$. The mean must be corrected by the addition of the previous estimate $\hat{x}^a_{k-1|k-1}$ to all points in the set, i.e. to every column in $\mathcal{X}^*_{k-1|k-1}$. Therefore, using Kronecker product notation, (true mean) this can be represented very nicely by

$$\mathcal{X}_{k-1|k-1} = \mathcal{X}^*_{k-1|k-1} + \mathbf{1}^{1\times(2n^a+1)} \otimes \hat{x}^a_{k-1|k-1} \tag{5.15}$$

where the notation $\mathbf{1}^{1\times(2n^a+1)}$ refers to a matrix of ones with one row and $(2n^a + 1)$ columns. Note that the past estimate (mean) $\hat{x}^a_{k-1|k-1}$ in (5.15) is given by

$$\hat{x}^a_{k-1|k-1} = \begin{bmatrix} \hat{x}^T_{k-1|k-1} & \mathbf{0}^{1\times q} & \mathbf{0}^{1\times p} \end{bmatrix}^T \tag{5.16}$$

Each sigma point in the set $\mathcal{X}_{k-1|k-1}$ is propagated through the nonlinear model, i.e. integrated forward in time, over the sampling interval $[t_{k-1}, t_k]$, to generate a set of transformed points $\mathcal{X}_{k|k-1}$. Therefore, with some abuse of notation, this operation can be represented by

$$\mathcal{X}_{k|k-1} = f^a(\mathcal{X}_{k-1|k-1}, u_{k-1}, t_{k-1}) \tag{5.17}$$

The *a priori* state estimate $\hat{x}_{k|k-1}$ can then be calculated as a weighted average of the transformed points, i.e.

$$\hat{x}_{k|k-1} = \sum_{i=1}^{2n^a+1} W_i \mathcal{X}_{i,k|k-1} \tag{5.18}$$

Here, the notation $\mathcal{X}_{i,k|k-1}$ refers to the ith column of $\mathcal{X}_{k|k-1}$, and W_i is the associated weight. The weights W_i are chosen according to the algorithm

$$W_i = \begin{cases} \kappa/(n^a + \kappa) & \text{if } i = 1 \\ 1/2(n^a + \kappa) & \text{if } i \neq 1 \end{cases} \tag{5.19}$$

In general, the weights can be positive or negative depending on the choice of κ, however, in order to provide unbiased estimates, they must satisfy the condition $\sum_i W_i = 1$, which can readily be

verified from the above equation [32]. The predicted error covariance $P_{k|k-1}$ is given by a weighted outer product of the transformed points, i.e.

$$P_{k|k-1} = \sum_{i=1}^{2n^a+1} W_i \left[\mathcal{X}_{i,k|k-1} - \hat{x}_{k|k-1} \right] \left[\mathcal{X}_{i,k|k-1} - \hat{x}_{k|k-1} \right]^T \tag{5.20}$$

The propagated set of sigma points $\mathcal{X}_{i,k|k-1}$ are then mapped through the nonlinear measurement model $h^a(\cdot)$, yielding a set of outputs $\mathcal{Y}_k$ given by

$$\mathcal{Y}_k = h^a(\mathcal{X}_{k|k-1}, t_k) \tag{5.21}$$

The predicted output $\hat{y}_k$ is calculated in the same way as the predicted state estimate $\hat{x}_{k|k-1}$, i.e. by taking the weighted sum of the outputs $\mathcal{Y}_k$, therefore

$$\hat{y}_k = \sum_{i=1}^{2n^a+1} W_i \mathcal{Y}_{i,k} \tag{5.22}$$

Finally, the innovation covariance P_y and the cross correlation P_{xy} matrices can be calculated from the following expressions

$$P_y = \sum_{i=1}^{2n^a+1} W_i \left[\mathcal{Y}_{i,k} - \hat{y}_k \right] \left[\mathcal{Y}_{i,k} - \hat{y}_k \right]^T \tag{5.23}$$

$$P_{xy} = \sum_{i=1}^{2n^a+1} W_i \left[\mathcal{X}_{i,k|k-1} - \hat{x}_{k|k-1} \right] \left[\mathcal{Y}_{i,k} - \hat{y}_k \right]^T \tag{5.24}$$

If the process and/or measurement noise vectors are additive, take for example, the disturbance model (4.12), the model state vector need *not* be augmented with the appropriate process and/or measurement terms. Instead, for additive process noise, the covariance matrix Q_k can be added directly to equation (5.20), i.e.

$$P_{k|k-1} = Q_k + \sum_{i=1}^{2n^a+1} W_i \left[\mathcal{X}_{i,k|k-1} - \hat{x}_{k|k-1} \right] \left[\mathcal{X}_{i,k|k-1} - \hat{x}_{k|k-1} \right]^T \tag{5.25}$$

Likewise, for additive measurement noise, the covariance matrix R_k can be added directly to equation (5.23), i.e.

$$P_y = R_k + \sum_{i=1}^{2n^a+1} W_i \left[\mathcal{Y}_{i,k} - \hat{y}_k \right] \left[\mathcal{Y}_{i,k} - \hat{y}_k \right]^T \tag{5.26}$$

5.2.2   Correction

The UKF state and covariance updates can be calculated using the following equations

$$\hat{x}_{k|k} = \hat{x}_{k|k-1} + K_k(y_k - \hat{y}_k)$$

$$P_{k|k} = P_{k|k-1} - K_k P_y K_k^T$$

$$(5.27)$$

where the Kalman gain K_k for the unscented filter is given by

$$K_k = P_{xy} P_y^{-1} \qquad (5.28)$$

Chapter 6

Controller Implementation

The heart of the NMPC algorithm is the online solution of a computationally tractable optimal control problem over a finite horizon to determine the control profiles to be implemented. At each sampling instant, the current plant measurements are sent to a state estimator, such as an extended (EKF), or unscented Kalman filter (UKF), which constructs an estimate of the plant state. The estimated state is then supplied to the NMPC controller to initialize the finite horizon optimal control problem. Only the first control input u_0 in the optimal sequence is sent to the plant. This procedure is then performed repeatedly whenever new plant measurements are obtained. In both the nominal and offset-free NMPC formulations discussed in Chapter 4, we assumed implicitly that a discrete-time process model $x_{k+1} = f(x_k, u_k, t_k)$ was readily available. However, the autoclave reactor models outlined in Chapter 3 are defined in continuous-time, and therefore, must be discretized in order to make the NMPC formulations amenable to solution using conventional NLP software. In this study, we employed a 'complete discretization' approach using orthogonal collocation on finite elements (OCFE), i.e. both the control inputs and the state variables were discretized, as opposed to only the control inputs, which is the case in control vector parameterization (CVP) based approaches. In this Chapter, we provide a detailed description the particular OCFE scheme implemented in this study.

Orthogonal collocation belongs to a family of numerical integration schemes collectively known as the method of weighted residuals (MWR). The underlying assumption of MWR methods is that

the solution to any system of differential equations can be approximated by a linear combination of chosen trial (or basis) functions, i.e.

$$\tilde{x}(t) = \sum_{i=1}^{N} a_i \varphi_i(t) \tag{6.1}$$

where $\tilde{x}(t)$ is the solution profile, $\varphi_i(t)$ are appropriate trial functions, and a_i are unknown coefficients. In general, MWR methods can be applied to help solve ODE, DAE, and PDE systems, however, the discussion in this section is focused mainly on ODE systems. For an arbitrary ODE system given by $\dot{x}(t) = f(x(t), u(t), t)$, a residual function $R(t)$ can be defined by substituting the trial solution (6.1) into the ODE model to give

$$R(t) = \dot{\tilde{x}}(t) - f(\tilde{x}(t), u(t), t) \tag{6.2}$$

The residual function is a measure of the accuracy with which the trial solution approximates the true solution. The coefficients a_i in equation (6.1) are determined by forcing the integral of the weighted residual function to be zero over the required domain, i.e.

$$\int_{t_0}^{t_K} w_i R(t) \, dt = 0 \tag{6.3}$$

$\forall i = 1, 2, \ldots, N$. The choice of weighting function w_i in equation (6.3) is characteristic of a particular MWR technique. For example, if $w_i = t^{i-1}$, then the MWR technique is referred to as the method of moments, since the first N moments of the residual function are forced to be zero. A detailed discussion of other MWR techniques can be found in the seminal texts of Finlayson [22], and Villadsen and Michelsen [86].

The collocation method forces the residual to be zero at N distinct points t_i (known as *collocation points*) in the domain, i.e.

$$R(t_i) = 0 \tag{6.4}$$

$\forall i = 1, 2, \ldots, N$. In the language of equation (6.3), the weighting function for the collocation method can be thought of as the shifted Dirac delta function $\delta(t - t_i)$ which has the following property

$$\int_{t_0}^{t_K} \delta(t - t_i) R(t) \, dt = R(t_i) = 0 \tag{6.5}$$

If the collocation points are chosen at locations corresponding to the roots of an orthogonal polynomial, the collocation procedure is referred to as orthogonal collocation. By positioning the collocation points at the roots of an orthogonal polynomial, the collocation method attains a number of

interesting properties. References [50, 22, 86] and citations therein discuss these properties in some detail.

Henceforth, in this Section, particulars of the actual orthogonal collocation method used in the NMPC implementation, along with its extension to finite elements will be discussed. Here, we will make extensive use of the notation found in the work of Cuthrell and Biegler [13]. Consider the system (6.6) modeled by a set of ordinary differential equations over the unit time interval $t \in [0, 1]$ given by

$$\dot{x}(t) = f(x(t), u, t) \tag{6.6}$$

with initial state $x(0) = x_0$, and where $x(t) \in \mathbb{R}^n$ is the vector of system states, and $u \in \mathbb{R}^m$ is the vector of control inputs. Note that, here, the control input u is considered to be constant over the given interval. It will become clear from future discussions that keeping u constant over the interval helps us enforce zero-order hold in between sampling instances. Following the principles of the method of weighted residuals, here, we assume that the solution to ODE system (6.6) can be approximated by a linear combination of Lagrange basis polynomials given below

$$x_{K+1}(t) = \sum_{i=0}^{K} x_i \phi_i(t) \qquad \phi_i(t) = \prod_{\substack{k=0 \\ k \neq i}}^{K} \frac{t - t_k}{t_i - t_k} \tag{6.7}$$

where $(K + 1)$ is the number of collocation points, $x_{K+1}(t)$ is the polynomial approximation to the solution, x_i are unknown coefficients, and t_k is the time corresponding to the $(k + 1)^{\text{th}}$ collocation point. Note that the tilde over the polynomial approximation is dropped for notational convenience. Continuous control inputs $u(t)$, if required, can be handled in a likewise fashion, however, the case with constant control inputs is only considered here.

The interpolating polynomial (6.7) in Lagrange form possesses two unique properties that bear mentioning. First, the interpolating polynomial $x_{K+1}(t)$ evaluated at collocation point t_i reduces to the coefficient x_i, i.e. $x_{K+1}(t_i) = x_i$. This property is advantageous as it implies that evaluation of the coefficients x_i is equivalent to evaluation of the state variables at time t_i, making evaluation of the Lagrange polynomial $x_{K+1}(t)$ unnecessary unless one is interested in determining the evolution of state profiles in between collocation points–which is not the case in the present application. Second, the coefficients x_i are physically meaningful quantities corresponding to the actual state variables

of the ODE system [13], as opposed to some arbitrary constants (see equation (6.1)) depending on the structure of the trial function. This property is somewhat related to the first, and is especially useful in the implementation of the target calculator and regulator NLPs. By virtue of the fact that the coefficients of the Lagrange basis polynomial and state variables (at the collocation points) are equivalent, the definition of bound and path constraints on the states, as well calculation of the respective objective functions is made significantly simpler.

In this case, the residual function $R(t)$ can be expressed as was done previously, i.e. by substitution of the Lagrange basis polynomial (6.7)–the trial function–into the ODE model (6.6) to yield

$$R(t) = \sum_{i=0}^{K} x_i \dot{\phi}_i(t) - f(x_{K+1}(t), u, t) \tag{6.8}$$

According to the principle of collocation, the residual (6.8) is required to be zero at all $(K+1)$ collocation points, therefore

$$R(t_j) = \sum_{i=0}^{K} x_i \dot{\phi}_i(t_j) - f(x_j, u, t_j) = 0 \tag{6.9}$$

$\forall j = 1, 2, \ldots, K$. Furthermore, we also require that the initial value problem be provided with the initial state vector x_0, i.e. the state vector corresponding to t_0. The only remaining issue is to specify the locations of the $(K+1)$ collocation points t_j on the solution element $[0,1]$. In this implementation, two collocation points were positioned at the lower and upper boundaries of the element, i.e. at $t_0 = 0$ and $t_K = 1$, respectively. The remaining $(K-1)$ *interior* collocation points are positioned at locations corresponding to the roots of a $(K-1)^{\text{th}}$ order shifted Legendre (orthogonal) polynomial. Figure 6.1 is a sample schematic showing a single collocation element with interior collocation points corresponding to the roots of a third order shifted Legendre polynomial.

The set of nonlinear algebraic equations (6.9) must be solved simultaneously in order to obtain the Lagrange coefficients x_j, which in this case, are also the system states at times t_j. The derivatives $\dot{\phi}_i(t_j)$ in equation set (6.9) depend only on the ith Lagrange basis polynomial and the location of the collocation point t_j, and can be evaluated beforehand. In this study, the Octave interface to the Villadsen and Michelsen [86] routines was used to evaluate $\dot{\phi}_i(t_j)$, and also to identify roots of the orthogonal shifted Legendre polynomials. With respect to implementation of the NMPC algorithm, the equation set (6.9) can be thought of as nonlinear 'model constraints' for the regulator NLP,
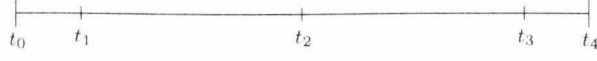
Figure 6.1: Single collocation element with interior collocation points corresponding to the roots of a third order shifted Legendre polynomial.

i.e. these equations represent the process dynamics, which are accommodated as nonlinear algebraic constraints within the framework of the regulator NLP. The notation used in equation set (6.9) is rather cumbersome, however, it can be expressed quite elegantly using the matrix notation of Meadows and Rawlings [50], therefore

$$\dot{\Phi}_0 X - F(X, u) = 0 \qquad (6.10)$$

where

$$\dot{\Phi}_0 = \begin{bmatrix} 1 & 0 & \cdots & 0 \\ \dot{\phi}_1(t_1) & \dot{\phi}_2(t_1) & \cdots & \dot{\phi}_K(t_1) \\ \dot{\phi}_1(t_2) & \dot{\phi}_2(t_2) & \cdots & \dot{\phi}_K(t_2) \\ \vdots & \vdots & \ddots & \vdots \\ \dot{\phi}_1(t_K) & \dot{\phi}_2(t_K) & \cdots & \dot{\phi}_K(t_K) \end{bmatrix}$$

and

$$X = \begin{bmatrix} x_{0,1} & x_{0,2} & \cdots & x_{0,n} \\ x_{1,1} & x_{1,2} & \cdots & x_{1,n} \\ \vdots & \vdots & \ddots & \vdots \\ x_{K,1} & x_{K,2} & \cdots & x_{K,n} \end{bmatrix} \qquad F(X, u) = \begin{bmatrix} x_0^T \\ f^T(x_1^T, u, t_1) \\ \vdots \\ f^T(x_K^T, u, t_K) \end{bmatrix}$$

Here, n is the dimensionality of the system state vector, and $\dot{\Phi}_0$ is the collocation weight matrix. The notation $x_{i,j} \in \mathbb{R}$ used above denotes the jth state variable at the ith collocation point, and $x_i \in \mathbb{R}^n$ denotes the *entire* state vector at the ith collocation point. The collocation procedure described previously is commonly known as global collocation, and was restricted specifically to the $[0, 1]$ interval. Therefore, it is necessary to expand this procedure to an interval $[t_0, t_K]$ of arbitrary
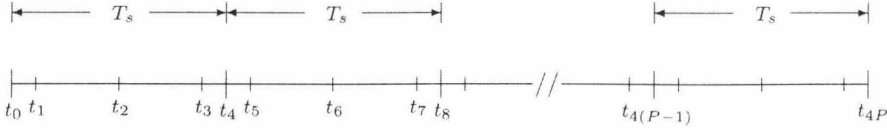
Figure 6.2: Collocation on finite elements with interior collocation points corresponding to the roots of a third order shifted Legendre polynomial.

length. This can be achieved by, first, positioning the collocation points on $[t_0, t_K]$ at locations that correspond proportionally to the points on the $[0, 1]$ interval, and second, by dividing (scaling) all but the first row of the collocation weight matrix $\dot{\Phi}_0$ in (6.10) by the length of the collocation element, i.e. by $(t_K - t_0)$.

In this study, the global collocation approach using a single collocation element is employed to discretize the nonlinear model (6.6) over a *single* sampling period, i.e. over a unit horizon. This strategy can be extended to a horizon of any desired length using orthogonal collocation on finite elements (OCFE). The principal feature of OCFE is that, here, orthogonal collocation is applied consecutively on smaller, possibly unequal, segments called *elements* with the requirement that the state profiles be continuous across the element boundaries. Figure 6.2 is a schematic showing the OCFE methodology applied to a P–interval prediction horizon. In this study, each collocation element in the sequence was required to be of identical length, equivalent to the sampling interval T_s. The primary advantage of using a single collocation element per sampling period is that it readily yields state information at the element boundaries, which is required for evaluating the regulator cost function in the NMPC formulation. However, this approach can become computationally cumbersome for 'long' prediction horizons. In such situations, it is usually beneficial to increase the length of the collocation element with respect to the sampling interval, as this reduces the *total* number of collocation points required, which in turn also reduces the online computational load incurred.

The nonlinear algebraic equations for the OCFE discretized problem, can be expressed analogously to the case of the global collocation approach, therefore

$$\dot{\tilde{\Phi}}\tilde{X} - \tilde{F}(\tilde{X}, \mathbf{u}) = 0 \qquad (6.11)$$

where

$$\dot{\tilde{\Phi}} = \begin{bmatrix} \dot{\Phi}_0 & & & \\ & \dot{\Phi}_1 & & \\ & & \ddots & \\ & & & \dot{\Phi}_{P-1} \end{bmatrix}$$

and

$$\tilde{X} = \begin{bmatrix} x_{0,1} & x_{0,2} & \dots & x_{0,n} \\ x_{1,1} & x_{1,2} & \dots & x_{1,n} \\ \vdots & \vdots & \ddots & \vdots \\ x_{K,1} & x_{K,2} & \dots & x_{K,n} \\ x_{K+1,1} & x_{K+1,2} & \dots & x_{K+1,n} \\ \vdots & \vdots & \ddots & \vdots \\ x_{2K,1} & x_{2K,2} & \dots & x_{2K,n} \\ x_{2K+1,1} & x_{2K+1,2} & \dots & x_{2K+1,n} \\ \vdots & \vdots & \ddots & \vdots \\ x_{PK,1} & x_{PK,2} & \dots & x_{PK,n} \end{bmatrix} \qquad \tilde{F}(\tilde{X}, \mathbf{u}) = \begin{bmatrix} x_0^T \\ f^T(x_1^T, u_0, t_1) \\ \vdots \\ f^T(x_K^T, u_0, t_K) \\ f^T(x_{K+1}^T, u_1, t_{K+1}) \\ \vdots \\ f^T(x_{2K}^T, u_1, t_{2K}) \\ f^T(x_{2K+1}^T, u_2, t_{2K+1}) \\ \vdots \\ f^T(x_{PK}^T, u_{P-1}, t_{PK}) \end{bmatrix}$$

Here, $\dot{\Phi}_0$ is defined identically to the global collocation case (see equation (6.10)), whereas $\dot{\Phi}_{i\neq 0}$ consists of all rows in $\dot{\Phi}_0$ with the exception of the first row, i.e.

$$\dot{\Phi}_{i\neq 0} = \begin{bmatrix} \dot{\phi}_1(t_1) & \dot{\phi}_2(t_1) & \dots & \dot{\phi}_K(t_1) \\ \dot{\phi}_1(t_2) & \dot{\phi}_2(t_2) & \dots & \dot{\phi}_K(t_2) \\ \vdots & \vdots & \ddots & \vdots \\ \dot{\phi}_1(t_K) & \dot{\phi}_2(t_K) & \dots & \dot{\phi}_K(t_K) \end{bmatrix}$$

The vector $\mathbf{u}$ represents the sequence (or profile) of the control inputs over the P–interval prediction horizon, i.e.

$$\mathbf{u} = \begin{bmatrix} u_0^T & u_1^T & \dots & u_{P-2}^T & u_{P-1}^T \end{bmatrix}^T$$

It is important to note the almost block diagonal (ABD) structure of the collocation weight matrix $\dot{\tilde{\Phi}}$ in equation (6.11). This structure arises from the overlap of collocation points at the finite element boundaries. For example, given a prediction horizon $P = 3$, the resulting collocation weight matrix

obtained is given below.

$$
\dot{\Phi} = \begin{bmatrix}
1 & 0 & \ldots & 0 \\
\dot{\phi}_1(t_1) & \dot{\phi}_2(t_1) & \ldots & \dot{\phi}_K(t_1) \\
\vdots & \vdots & \ddots & \vdots \\
\dot{\phi}_1(t_K) & \dot{\phi}_2(t_K) & \ldots & \dot{\phi}_K(t_K) \\
& & & \dot{\phi}_1(t_1) & \dot{\phi}_2(t_1) & \ldots & \dot{\phi}_K(t_1) \\
& & & \vdots & \vdots & \ddots & \vdots \\
& & & \dot{\phi}_1(t_K) & \dot{\phi}_2(t_K) & \ldots & \dot{\phi}_K(t_K) \\
& & & & & & \dot{\phi}_1(t_1) & \dot{\phi}_2(t_1) & \ldots & \dot{\phi}_K(t_1) \\
& & & & & & \vdots & \vdots & \ddots & \vdots \\
& & & & & & \dot{\phi}_1(t_K) & \dot{\phi}_2(t_K) & \ldots & \dot{\phi}_K(t_K)
\end{bmatrix}
$$

Chapter 7

Results and Discussions

Compared to widely-used process control approaches, such as conventional PID and LMPC control, NMPC is significantly more complicated to implement, and requires much higher computational expenditure to solve the resulting NLPs. Therefore, prior to implementation, it is extremely important to justify the selection of NMPC over established approaches. In this Chapter, we evaluate, via simulations, the performance of the NMPC formulation for the control of both single and multi-zone LDPE autoclave reactors. Wherever appropriate, we contrast the NMPC performance directly with that of PID and LMPC algorithms. Before presenting the results, we will briefly outline the PID and LMPC controller algorithms used in this study.

PID Controller Algorithm

The standard proportional–integral–derivative (PID) control algorithm basically involves the superposition of the proportional, integral, and derivative controller modes. Given a single-input single-output (SISO) loop pairing, the basic *analog* PID controller algorithm is given by

$$u(t) = K_c \left(e(t) + \frac{1}{\tau_I} \int_0^t e(t)dt + \tau_D \frac{de(t)}{dt} \right) + u_s \tag{7.1}$$

Here, $e(t)$ is a scalar defined as the error between a particular controlled output and its setpoint, therefore, for the ith controlled output, $e_i(t) = z_{s_i}(t) - z_i(t)$. The closed-loop performance of the PID controller is governed by three (scalar) tuning parameters, namely, the controller gain K_c,

integral time τ_I, and derivative time τ_D. The proportional term in the PID controller algorithm produces a signal proportional to the error in the controlled outputs, while the integral and derivative terms produces signals proportional to the integral and derivative of the error, respectively. The net controller output is the sum of the three signals. The analog PID algorithm (7.1) is not suitable for online implementation on conventional digital computer systems, therefore, the algorithm is usually discretized (zero-order hold) and expressed in the iterative *velocity form* shown below [80, 81]

$$\Delta u_k = K_c \left(1 + \frac{T}{\tau_I} + \frac{\tau_D}{T} \right) e_k - K_c \left(1 + \frac{2\tau_D}{T} \right) e_{k-1} + K_c \frac{\tau_D}{T} e_{k-2} \qquad (7.2)$$

where T is the chosen sampling/control interval. Note that the velocity form requires storage of the past error e_{k-1} for PI, and the past two errors e_{k-1}, e_{k-2} for PID control.

The tuning parameters used in the PID controller simulations were obtained using the simple internal model control (SIMC) tuning rules recommended by Skogestad [77, 78, 79]. Like most published PID tuning rules, for e.g. Ziegler–Nichols, the SIMC tuning rules require that the process dynamics be approximated by a first (FOPDT), or second order plus dead time (SOPDT) transfer function model. The reader is referred to the works of Skogestad [77, 79] for details on the derivation and evaluation of the SIMC rules. For both autoclave reactor models, we found from step tests (not shown) on the linearized model that an FOPDT model provides an adequate approximation of the linearized model dynamics, therefore, the tuning rules in [77, 79] corresponding to the FOPDT model were used. Note that manual detuning of the PID control loops was required in order to obtain good, stable closed-loop responses for the nonlinear plant model.

LMPC Controller Algorithm

The offset-free LMPC formulation used in this work is the exact linear analog of the offset-free NMPC formulation discussed in Section 4.2. The linear disturbance (i.e. internal) model employed by the controller allows for, in general, integrating disturbance inputs on both the states and measurements, as was the case with the nonlinear disturbance model (4.10), therefore

$$x_{k+1} = \Phi x_k + \Gamma u_k + \Gamma_d p_k + w_k$$

$$y_k = C x_k + C_d p_k + v_k \qquad (7.3)$$

$$z_k = H y_k$$

where the discrete-time linear model Jacobian matrices $\Phi \in \mathbb{R}^{n \times n}$ and $\Gamma \in \mathbb{R}^{n \times m}$ are defined by $\Phi = \partial f(x_k, u_k)/\partial x_k|_{(x_s, u_s)}$ and $\Gamma = \partial f(x_k, u_k)/\partial u_k|_{(x_s, u_s)}$, evaluated at the desired equilibrium conditions. Here, the function $f(x_k, u_k)$ represents the discrete-time nonlinear process model. In practice, however, the discrete model Jacobians are derived from continuous model Jacobians using the well-known formulas

$$\Phi = e^{\mathbf{A}T}$$
$$\Gamma = \int_0^T e^{\mathbf{A}\tau} d\tau \mathbf{B} \qquad (7.4)$$

where $\mathbf{A} \in \mathbb{R}^{n \times n}$ and $\mathbf{B} \in \mathbb{R}^{n \times m}$ are the Jacobian matrices of the continuous-time nonlinear model evaluated at the desired steady state conditions, and $e^{\mathbf{A}T}$ is the matrix exponential operator. Software implementations of the matrix exponential operation, such as the c2d function in MATLAB, are available to convert continuous-time linear time invariant (LTI) plant models to discrete-time LTI models. The disturbance matrix $\Gamma_d \in \mathbb{R}^{n \times n_d}$ models the effect of the integrating disturbance input p_k on the system dynamics. The output matrices $C \in \mathbb{R}^{p \times n}$ and $C_d \in \mathbb{R}^{p \times n_d}$ relate the state x_k and disturbance p_k vectors to the measurements y_k, respectively. The controlled output matrix $H \in \mathbb{R}^{n_c \times p}$ relates the measurements to the controlled outputs z_k. The integrating disturbance states are assumed to remain constant over the prediction horizon, therefore

$$p_{k+1} = p_k + \xi_k \qquad (7.5)$$

Similar to the offset-free NMPC algorithm, the offset-free LMPC algorithm consists of target calculator and regulator components. In this case, the role of the target calculator is to identify steady state (equilibrium) targets of the of the linear disturbance model (7.3), which satisfy the controlled output setpoint z_s, and other necessary process constraints. In this study, we implemented a target calculator formulation similar to ones proposed by Muske and Rawlings [54], and Pannocchia and Rawlings [57] for LMPC shown below.

$$\min_{x_{t,j}, u_{t,j}} \quad (u_{t,j} - u_s)^T \mathcal{R}(u_{t,j} - u_s) \qquad (7.6a)$$

subject to:

$$\begin{bmatrix} I - \Phi & -\Gamma \\ HC & 0 \end{bmatrix} \begin{bmatrix} x_{t,j} \\ u_{t,j} \end{bmatrix} = \begin{bmatrix} \Gamma_d \hat{p}_{k|k} \\ -HC_d \hat{p}_{k|k} + z_s \end{bmatrix} \qquad (7.6b)$$

$$x_L, u_L \leq x_{t,j}, u_{t,j} \leq x_U, u_U \tag{7.6c}$$

The first equality in equation (7.6b) is the steady state condition for the disturbance model, while the second equality condition requires that the controlled output z_k achieves its setpoint z_s at the target steady state. The regulator formulation employed in the offset-free LMPC formulation is virtually identical to the case of the offset-free NMPC formulation. By defining the following two deviation variables, $w_k = x_k - x_{t,j}$ and $v_k = u_k - u_{t,j}$, the regulator quadratic program (QP) that is solved at each iteration is given by

$$\min_{\mathbf{w}_j, \mathbf{v}_j} \quad \|w_{j+P}\|^2_{C^T H^T \mathbf{Q} H C} + \sum_{k=j}^{j+P-1} \|w_k\|^2_{C^T H^T \mathbf{Q} H C} + \|v_k\|^2_{\mathbf{R}} + \|\Delta v_k\|^2_{\mathbf{S}} \tag{7.7a}$$

subject to:

$$w_{k+1} = \Phi w_k + \Gamma v_k \tag{7.7b}$$

$$w_L, v_L, \Delta v_L \leq w_k, v_k, \Delta v_k \leq w_U, v_U, \Delta v_U \tag{7.7c}$$

$$v_k = v_{j+M-1} \quad \forall k = j + M, j + M + 1, \ldots, j + P - 1 \tag{7.7d}$$

In order to facilitate comparison between the closed-loop responses of the NMPC, LMPC controllers, wherever appropriate, the two controllers were supplied identical tuning parameters. In the following Sections, we present results of the simulation studies performed in this work in order to observe and compare the performance of the NMPC formulation for the control of the single and multi-zone LDPE autoclave reactors.

7.1   Single-Zone Autoclave

Prior to discussing the closed-loop controller simulation results, it is beneficial to investigate the steady state behavior of the the single-zone LDPE autoclave reactor model. Figures 7.1 and 7.2 are continuation diagrams showing the bifurcation behavior of the well-mixed single-zone LDPE auto-clave reactor model, with the reactor residence time $\theta = V/q$ as the primary bifurcation parameter. The secondary bifurcation parameter is the feed initiator concentration I_f or the feed temperature T_f. The bifurcation analysis of the autoclave reactor was performed by first converting the single-zone reactor model outlined in Chapter 3 into an equivalent dimensionless form. General details on
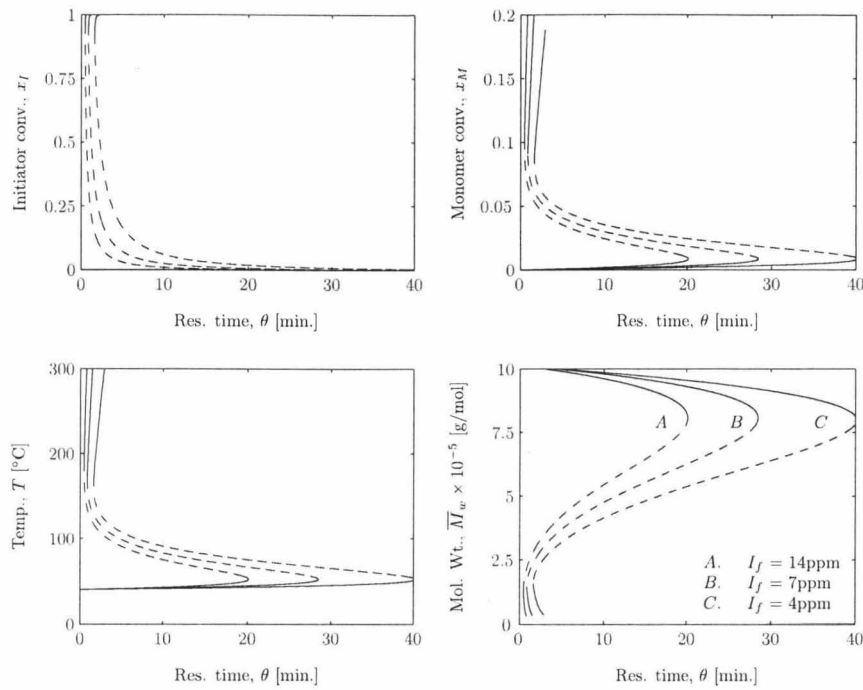
Figure 7.1: Bifurcation diagram showing the effect of feed initiator concentration I_f on steady state model behavior.

how this procedure is carried out can be found in references [73, 26] among others. The MATLAB continuation toolbox MATCONT [18, 17] was then used to perform continuation analyses on the dimensionless reactor model. Note that solid lines (—) in the figures indicate stable equilibrium branches, while dashed lines (− −) indicate unstable branches.

The bifurcation diagrams in both cases display the classical S–shaped curve behavior consistent with the well-known case of the nonisothermal CSTR. A characteristic feature of such curves is the presence of an unstable equilibrium branch sandwiched between two stable branches. This results in the occurrence of three equilibrium points in the normal residence time operating region of the autoclave reactor, which is usually in the 1–2min range. The bottom low-temperature stable branch is associated with extremely low monomer conversions (almost zero), and extremely high weight-averaged molecular weights of polymer (around 1×10^6g/mol). The operating point of the industrial reactor is usually located on the upper high-temperature stable branch, or on the unstable branch in the vicinity of the upper stable branch. In this region, the achievable monomer conversion is in
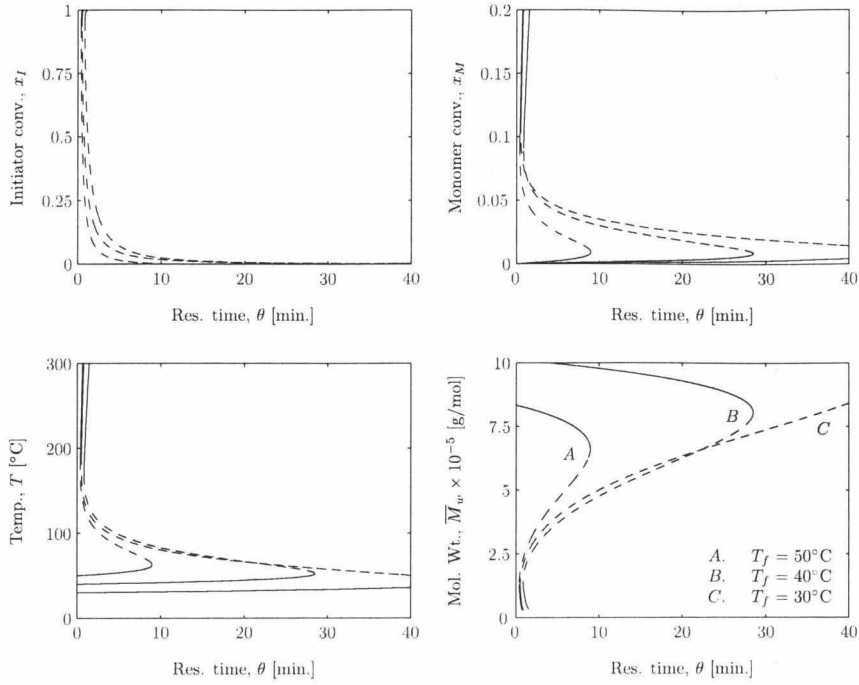
Figure 7.2: Bifurcation diagram showing the effect of feed temperature T_f on steady state model behavior.

the 10–15% range, while the operating temperature is in the 150–275°C range. The weight-averaged molecular weight of the polymer produced in this region is in the range of 0.5×10^5–3×10^5g/mol, which is sufficient for most commercial LDPE products. Note that the bottom low-temperature stable branch is the *upper* branch in the case of the molecular weight curves, while the upper high-temperature stable branch is the *lower* stable molecular weight branch. At reactor temperatures close to 300°C, unmodeled ethylene decomposition dynamics become dominant, leading to reaction runaway. Zhang, Read, and Ray [88], and Villa, Dihora, and Ray [85] present results on the bifur-cation analysis of single-zone LDPE autoclaves, which includes ethylene decomposition kinetics in the process dynamics.

The general offset-free NMPC formulation discussed in Chapter 4 requires that the structure of the disturbance model, as well as the controller tuning parameters (for e.g. the prediction, control horizons, and the quadratic weighting matrices) to be defined. In general, the ability of the controller to achieve offset-free control of the controlled variables, as well as the closed-loop stability and

performance characteristics of the controller are governed by the choices of disturbance model and tuning parameters. In the following subsections, we will discuss some of the major issues encountered in the design of the NMPC/LMPC disturbance models, as well as the design criteria employed in the selection of the NMPC/LMPC tuning parameters for the control of the single-zone LDPE autoclave reactor.

7.1.1   Disturbance Model Design

The ability of the NMPC/LMPC formulations to regulate the controlled outputs at their setpoints depends critically on the structure of the disturbance model employed. The two primary require-ments in the design of any disturbance model are, first, that the integrating disturbance states are observable from the available measurements, and second, that the disturbance states capture the overall effect of unmeasured process disturbances and plant-model mismatch on the controlled out-puts. In context of LMPC control of chemical process systems, many authors, for example, Muske and Badgwell [52], and Faanes and Skogestad [19], recommend the use of input disturbance models in order to achieve offset-free control of the controlled variables. Their recommendations are, in part, due to the fact that, in most practical situations, disturbances to chemical processes are expected to originate at the input, ahead of a dominant time constant, and very often at the control input, as opposed to at the output, which is presupposed by output disturbance models [83]. However, as rec-ommended by Tenny, Wright, and Rawlings [83], a careful study of the steady state plant behavior and expected disturbance dynamics is necessary before choosing an appropriate disturbance model.

The structures of both the linear (7.3) and nonlinear (4.10, 4.12) disturbance models described in this work permit a *combination* of input and output disturbances, which is, as we show later, what was implemented in this study. The general nonlinear disturbance model (4.10) permits the inclusion of disturbance states in any arbitrary fashion, however, in this study, we utilized the simplified disturbance model (4.12) in which the disturbance states are assumed to affect the system dynamics and measurements linearly. This model has the advantage that the matrices X_u and X_y in the NMPC disturbance model coincide exactly with, respectively, the matrices Γ_d and C_d in the LMPC disturbance model, thus allowing for a direct comparison of the two controllers. Unfortunately,

the open literature is essentially silent on the actual design of disturbance models, except in the case of LMPC (see for example, Pannocchia and Rawlings [57], Pannocchia [55], Pannocchia and Bemporad [56], Muske and Badgwell [52]), and a case by case approach assisted by simulation is usually required in order to determine if a particular disturbance model is sufficient.

Since only the two controlled outputs are measured online, namely, the reactor temperature T, and the weight-averaged molecular weight of polymer $\overline{M}_w$, using the results of Pannocchia and Rawlings [57] for LMPC, we can only include up to a maximum of two integrating disturbance states in the controller model. In summary, the NMPC/LMPC disturbance model matrices (see equations (7.3, 4.12)) used in this work are shown below.

$$
X_u^T = \Gamma_d^T = \begin{bmatrix} 0 & 0 & 0 & 1 & 0 & 0 & 0 \\ 0 & 0 & 0 & 0 & 0 & 0 & 0 \end{bmatrix} \qquad X_y = C_d = \begin{bmatrix} 0 & 0 \\ 0 & 100 \end{bmatrix}
$$

Two points must be made clear on the disturbance model matrices selected here. First, the dynamic equation corresponding to the reactor temperature (i.e. the $dT/dt = f_T(x, u, t)$ equation) was augmented with an *input* disturbance state (as is apparent from the X_u, Γ_d matrices). This is in line with the recommendations of [52, 19], albeit for LMPC. Second, the output/measurement equation corresponding to the weight-averaged molecular weight was augmented with an *output* disturbance state (as is apparent from the X_y, C_d matrices). We believe that the output disturbance choice is more appropriate in this situation as the weight-averaged molecular weight $\overline{M}_w = M_0\mu_2/\mu_1$ is a nonlinear function of the states. If an input disturbance approach was adopted, one would have to add input disturbance states to one or more dynamic equations in the nonlinear controller model in order to account for the effects of process disturbances and plant-model mismatch on the molecular weight dynamics. This approach is somewhat awkward, and does not affect the molecular weight dynamics/measurement 'directly', and therefore, was discarded in favor of the output disturbance approach.

7.1.2   Controller Tuning Parameters

The selection of controller tuning parameters greatly affects the closed-loop stability and performance characteristics of the control system. The tuning parameters which must be supplied to the offset-

free NMPC formulation are the prediction P and control M horizons, the regulator quadratic penalty matrices $\mathbf{Q}$, $\mathbf{R}$, and $\mathbf{S}$, and the target calculator penalty matrices $\mathcal{Q}$, Π, and $\mathcal{R}$. Unfortunately, as was the case with the design of the disturbance model, there are no clear guidelines available for the selection of these parameters, and numerical simulations and/or experiments are usually required to judge if the selected parameters are appropriate. In the process of implementing the regulator NLP, we first converted the nonlinear process model into the so called scaled deviation form, by introducing the following transformations for the states, control inputs, and controlled outputs.

$$\overline{x}_i = (x_i - x_{i_s})/x_{i_s}$$

$$\overline{u}_i = (u_i - u_{i_s})/u_{i_s}$$

$$\overline{z}_i = (z_i - z_{i_s})/z_{i_s}$$

Here, for example, the notation $x_i \in \mathbb{R}$ refers to an individual state variable (i.e. not the entire state vector), and $x_{i_s} \in \mathbb{R}$ is a given scaling factor, preferably the equilibrium value of the state variable. In addition to improving the conditioning of the resulting NLP, the above transformations also help simplify selection of the tuning matrices, if the scaling factors chosen are reasonable. In this study,
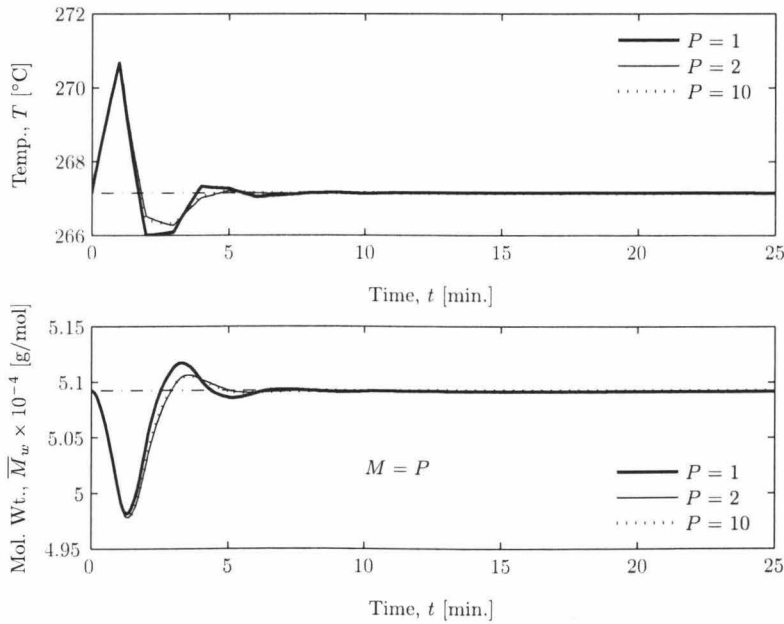

Figure 7.3: Effect of prediction horizon on control performance. Closed-loop response to an unmeasured $+5°C$ step disturbance in feed temperature T_f.

the scaling factors chosen (for all three quantities) correspond to the original steady state (equilibrium) values of the plant. The main advantage, from a tuning perspective, of the scaled deviation transformations is that, if the scaling factors are chosen appropriately, the resulting scaled quantities are all of the same order of magnitude. Therefore, one need not be concerned (as much) with scaling the controlled outputs and control inputs in the regulator and target calculator objective functions via the penalty matrices. The regulator tuning matrices used in all NMPC/LMPC simulations in this study are shown below.

$$\mathbf{Q} = \begin{bmatrix} 2 & 0 \\ 0 & 6 \end{bmatrix} \qquad \mathbf{R} = \begin{bmatrix} 0.5 & 0 \\ 0 & 0.5 \end{bmatrix} \qquad \mathbf{S} = \begin{bmatrix} 1 & 0 \\ 0 & 1 \end{bmatrix}$$

Since we are interested in 'better' control of the polymer weight-averaged molecular weight relative to the reactor temperature, we penalize molecular weight deviations from its setpoint (six) more than reactor temperature deviations from its setpoint (two). The control input penalty matrix $\mathbf{R}$ and the control rate penalty matrix $\mathbf{S}$ above were assigned relatively lower weights, reflecting their lower importance relative to the controlled output. The target calculator parameters employed in this study are shown below.

$$\mathcal{Q} = 1 \times 10^3 I_2 \qquad \amalg = 2 \times 10^3 \begin{bmatrix} 1 & 1 \end{bmatrix}^T \qquad \mathcal{R} = I_2$$

Here, the notation I_2 denotes a two-by-two identity matrix. The matrices $\mathcal{Q}$ and $\amalg$ are supplied with sufficiently high values in order to ensure that the variable η (which is, informally, the discrepancy between the controlled output target and its setpoint) in the target calculation is as small as possible, subject to the process dynamics and constraints. For square plants, as is the case here, the choice of matrix $\mathcal{R}$ is not critical, therefore, here it is assigned the identity matrix.

The remaining NMPC/LMPC tuning parameters which must be specified are the prediction and control horizons. In general, long prediction horizons are desirable, as this allows the controller to 'see' future plant behavior and take appropriate control actions. Furthermore, long prediction horizons might be required in order to stabilize plants operating at unstable operating points. However, increasing the length of the prediction horizon in turn increases the online computational power required to solve the resulting larger NLPs, which is obviously undesirable. Therefore, there is singnificant incentive to keep the prediction horizon as small as possible, while at the same time
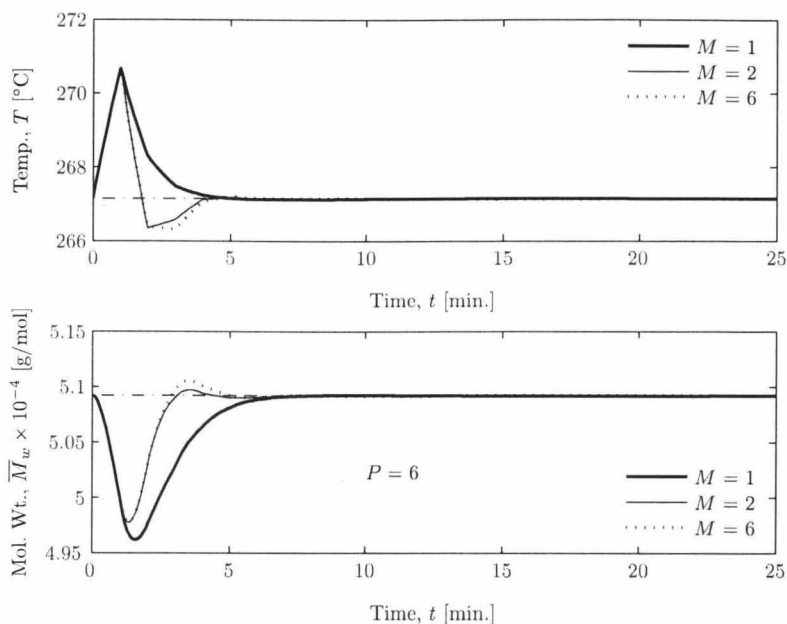
Figure 7.4: Effect of control horizon on control performance. Closed-loop response to an unmeasured $+5°C$ step disturbance in feed temperature T_f.

ensuring adequate closed-loop performance and stability. Figure 7.3 shows the effect of increasing the prediction horizon on the closed-loop response of the controlled outputs. The control horizon in each case is set equal to the prediction horizon to ensure consistency. It is clear from the figure that, while increasing the prediction horizon from one to two yields some improvement in the closed-loop control performance, any further increase in the prediction horizon does not yield any discernible improvement in control performance. In this study, a prediction horizon $P = 6$ was selected for use in all the closed-loop controller simulation cases presented here.

Figure 7.4 shows the effect of varying the control horizon on the closed-loop response of the controlled outputs. In this case, for the sake of comparison, the prediction horizon is kept constant at six. The results obtained from these simulations are consistent with known results from LMPC, specifically, that reducing the control horizon relative to the prediction horizon results in a corresponding decrease in 'controller aggressiveness'. Here, the NMPC controller with a unit control horizon exhibits a relatively slow, gradual response with little, if any, overshoot, while longer control horizons produces more aggressive control response with overshoot. However, much like the

prediction horizon results discussed previously, increasing the control horizon beyond a value of two produces no significant change in closed-loop response, i.e. there is negligible increase in controller aggressiveness. In this work, we selected a control horizon $M = 2$ for use in all closed-loop controller simulations performed.

7.1.3   Simulation Results

Industrial chemical processes are regularly affected by nonzero-mean unmeasured load disturbances during the course of operation. These disturbances generally originate at the process and/or control inputs, and have the ultimate, negative effect of driving the system away from the required operating point, which is obviously undesirable. Disturbances to polymerization reactors can adversely affect the properties, quality of the produced polymer, potentially leading to unmarketable product and/or economic losses. Therefore, a critical requirement of any industrial process control system is its ability to effectively compensate for (or reject) nonzero-mean process disturbances.

Figures 7.5 and 7.6 present simulation results comparing the closed-loop disturbance rejection responses of NMPC, LMPC, and PID controllers for the single-zone LDPE autoclave reactor. We show results of two kinds of process disturbances which can reasonably be expected to affect the reactor during online operation. First, we considered the case of an unmeasured step disturbance in the feed temperature T_f (see Figure 7.5), and second, the case of an unmeasured step disturbance in the feed initiator concentration I_f (see Figure 7.6). In both cases, we assume that NMPC controller model matches the plant dynamics perfectly, i.e. there is no plant-model mismatch, except of course, for the unmeasured disturbance entering the plant. The simulation results show that both linear and nonlinear MPC controllers perform adequately well, and are able to quickly return the controlled outputs to their respective setpoints following the process disturbances. However, the PID control system performs relatively poorly in both cases, providing a very slow, gradual return of the controlled outputs to their setpoints.

It is clear from Figures 7.5 and 7.6 that the 'mixed disturbance' based offset-free LMPC formulation (i.e. one input disturbance on the temperature equation, and one output disturbance on the molecular weight measurement equation) described previously performs reasonably well in the
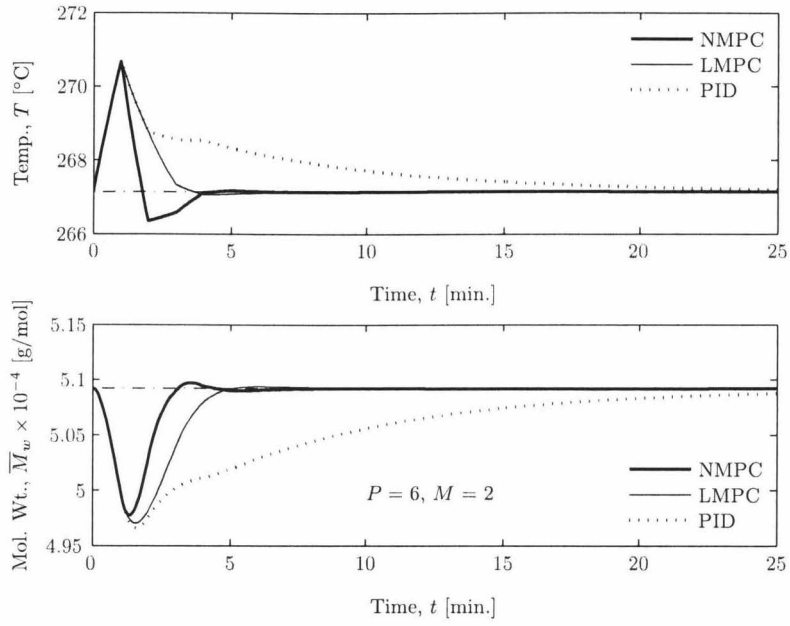
Figure 7.5: Closed-loop response to an unmeasured $+5°C$ step disturbance in feed temperature T_f. Comparison of NMPC, LMPC, and PID controller responses.
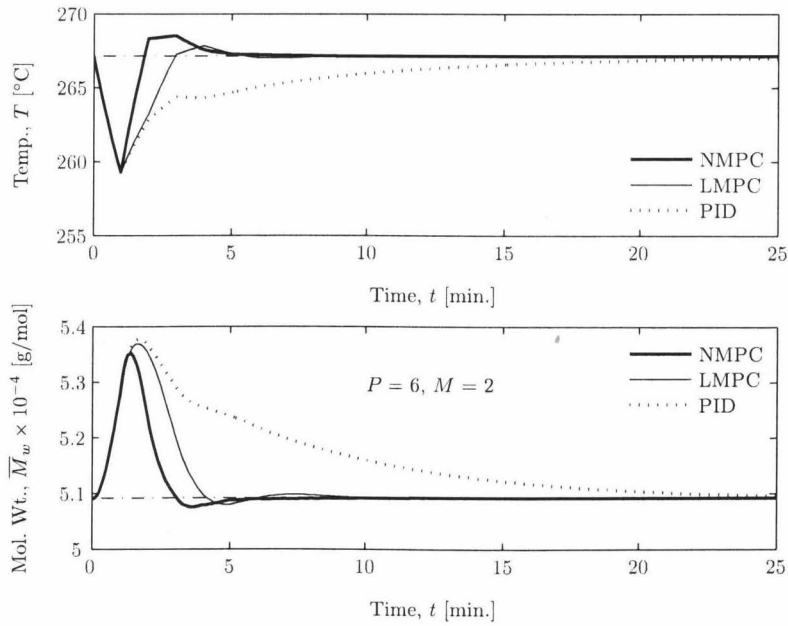

Figure 7.6: Closed-loop response to an unmeasured -10% step disturbance in feed initiator concentration I_f. Comparison of NMPC, LMPC, and PID controller responses.

presence of unmeasured process disturbances. However, our simulations reveal interesting results if an input disturbance model is used instead, as is the recommendation of many researchers for LMPC. The results of this investigation are presented in Figure 7.7, here, we compare the closed-loop controlled output responses of input disturbance based offset-free NMPC, LMPC formulations following injection of a step disturbance in the feed initiator concentration. In this situation, the output disturbance state on the $\overline{M}_w$ measurement equation is eliminated, and instead, the dynamic equation corresponding to the second 'dead polymer' moment μ_2 is augmented with an input disturbance state. The disturbance model matrices corresponding to this particular arrangement of integrating disturbance states are given below.

$$X_u^T = \Gamma_d^T = \begin{bmatrix} 0 & 0 & 0 & 1 & 0 & 0 & 0 \\ 0 & 0 & 0 & 0 & 0 & 0 & 1 \end{bmatrix} \qquad X_y = C_d = \begin{bmatrix} 0 & 0 \\ 0 & 0 \end{bmatrix}$$

The simulation results show that the closed-loop response of the input disturbance based NMPC controller does not differ appreciably from the mixed disturbance based controller (see Figure 7.6). However, the closed-loop response of the input disturbance based LMPC controller response does appears to be sensitive to the disturbance model employed. Although this cannot be observed within the time frame of the presented results, the input disturbance based LMPC controller does *eventually* return the controlled outputs to their respective setpoints, however, in doing so it takes extremely large excursions away from the desired operating point, which is obviously intolerable. Note that there exist other (not shown) arrangements of input disturbance states where such erratic behavior is not observed. However, it is clear, for this particular reactor, that the NMPC controller is more robust (compared to the LMPC controller) with respect to the structure of the disturbance model employed.

The performance of model-based control systems for any given application is impacted directly by the quality of the available process model. This is especially true for NMPC/LMPC control systems—where process models are used *explicitly* in the calculation of future control moves. In general, plant-model mismatch has the ultimate effect of degrading overall controller performance, and can even lead to control system instability depending on the extent of mismatch. Therefore, it is imperative for any practical control system be robust with respect to (at least) moderate
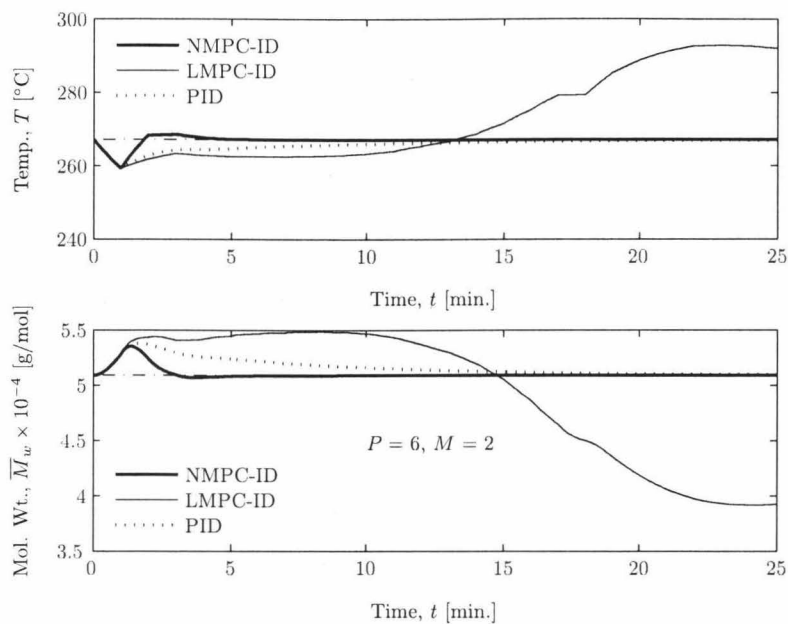
Figure 7.7: Closed-loop response to an unmeasured -10% step disturbance in feed initiator concentration I_f. Both NMPC, LMPC controllers use input disturbance models.
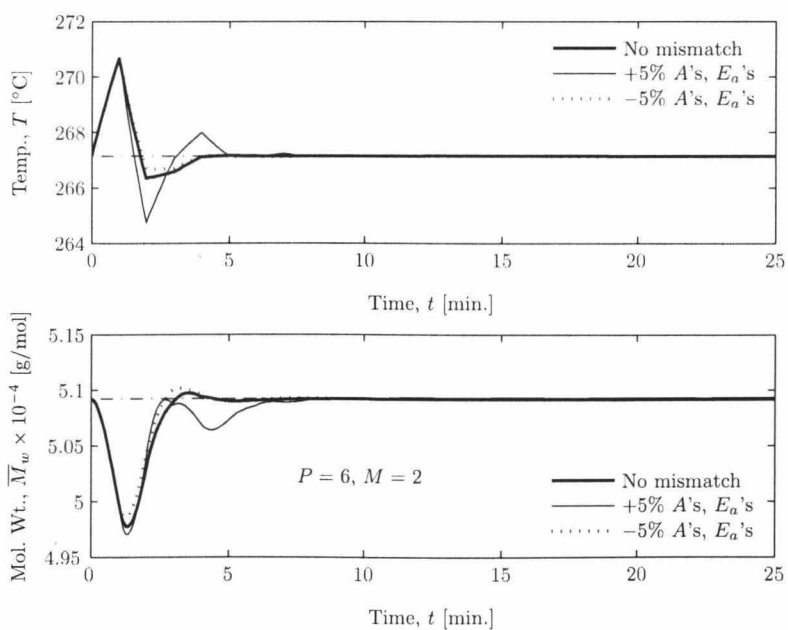

Figure 7.8: Closed-loop response to an unmeasured $+5°C$ step disturbance in feed temperature T_f. Comparison of NMPC controller responses with and without plant-model mismatch.

levels of plant-model mismatch. Mechanistic models of polymerization reactors, such as the one presented in Chapter 3, are usually simplified representations of highly complicated physicochemical reaction phenomena, and therefore, are particularly susceptible to modeling inaccuracies and errors. The most common types of mismatch in polymerization reactor models can be broadly classified into parametric and structural mismatch. Parametric mismatch arises from errors in estimation of model parameters, for e.g. reaction rate parameters, while structural mismatch stems from assumptions based on model structure, for e.g. well-mixed versus compartmental mixing model.

Figures 7.8 and 7.9 show the disturbance rejection response of the closed-loop NMPC control system in the presence of parametric mismatch. Two cases of parametric mismatch were considered here, in the first case, the magnitudes of all preexponential factors (i.e. all the model A's) and activation energies (i.e. all the model E_a's) in the internal NMPC controller model were modified such that they were 5% higher than their 'plant' counterparts, while in the second case, these parameter sets were modified such that they were 5% lesser. The results of our simulations indicate that the 'mixed disturbance' based offset-free NMPC formulation is adequately able to return the
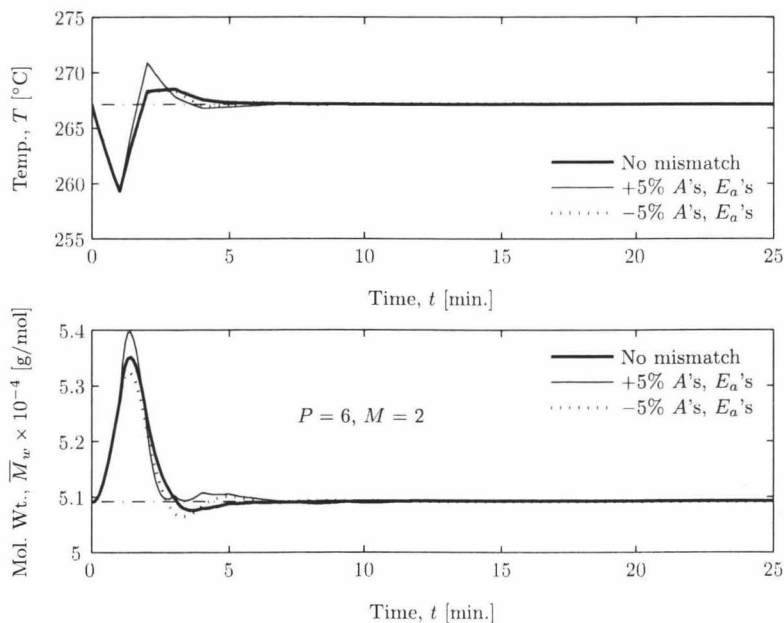

Figure 7.9: Closed-loop response to an unmeasured -10% step disturbance in feed initiator concentration I_f. Comparison of NMPC controller responses with and without plant-model mismatch.
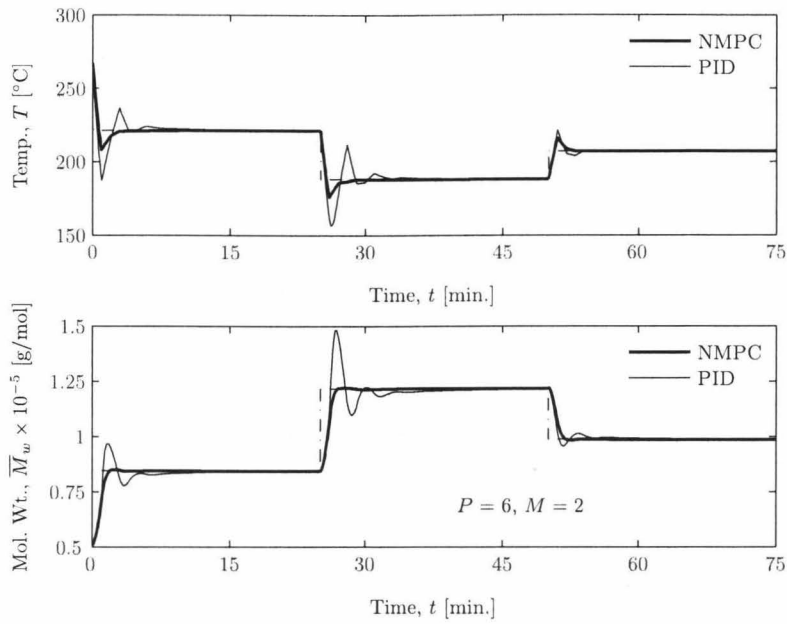
Figure 7.10: Closed-loop tracking response to multiple polymer grade (setpoint) change requests. Comparison of NMPC and PID controller responses.
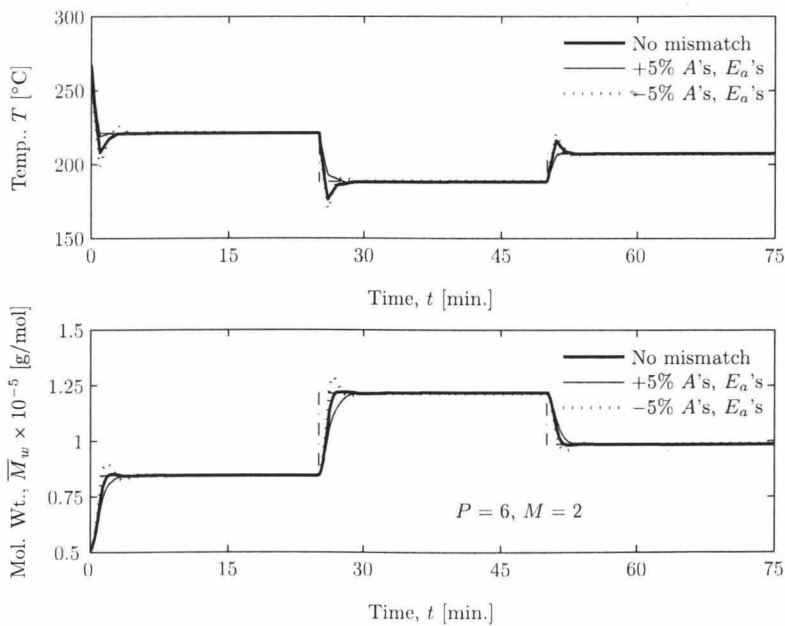

Figure 7.11: Closed-loop tracking response to multiple polymer grade (setpoint) change requests. Comparison of NMPC controller responses with and without plant-model mismatch.
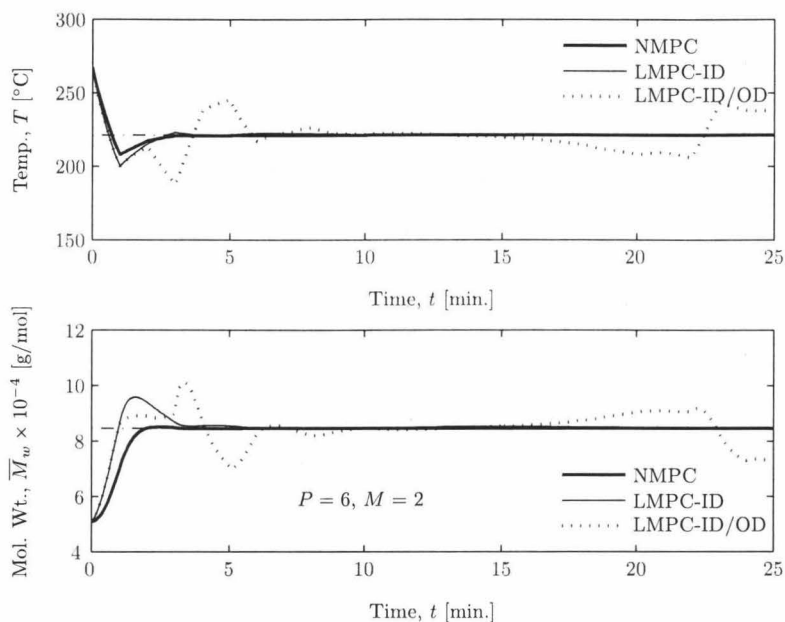
Figure 7.12: Closed-loop tracking response to a single polymer grade (setpoint) change request. Comparison of NMPC response with LMPC using input, input/output disturbance models.

controlled outputs to their setpoints in spite of the mismatch in the model parameters. However, it is clear that this particular type of parameteric mismatch causes a noticable degradation in the closed-loop controller performance, especially in the +5% case, where the mismatch appears to significantly increase overshoots in the temperature response, and introduce oscillations in the molecular weight response.

Continuous polymerization reactors are usually required to produce multiple polymer grades, and are consequently required to operate over a wide range of operating conditions. It is important that the transition between the multiple operating points (or polymer grades) be efficient in order to minimize production of off-spec product. NMPC is ideal for polymer grade change situations as it incorporates a nonlinear process model, which (at least in theory!) describes the reactor behavior over a wide operating region. Figure 7.10 compares the closed-loop tracking behavior of the NMPC and PID controllers in response to multiple polymer grade change requests for the single-zone LDPE autoclave reactor. Note that all three operating points shown are stable equilibriums on the high-temperature stable branch. The simulation results show that the NMPC controller is able drive

the system to the desired operating points extremely quickly with marginal overshoot. The slight overshoot observed in the reactor temperature response is likely due to its lower weight (with respect to the polymer molecular weight) in the NMPC objective function. The PID controller, on the other hand, takes longer to drive the system to the desired operating point, and does so with significant oscillations in the closed-loop response. It should be mentioned that the same set of PID tuning parameters were used for both the disturbance rejection and the tracking simulation tests.

Figure 7.11 compares the (controlled output) closed-loop tracking responses of the offset-free NMPC formulation with and without parametric mismatch. The parametric mismatch used previously in the disturbance rejection simulations was also used in the tracking simulation tests presented here. Note that we experienced numerical difficulties (ill-conditioning) in the target calculator NLP, leading to terminal failure of the controller algorithm in the target calculation step. In order to solve this problem, it was necessary to modify the values of the matrices $\mathcal{Q}$ and Π in the target calculator objective function. The matrices $\mathcal{Q} = I_2$ and $\Pi = [\,2 \quad 2\,]^T$ were used in the 'mismatch' NMPC tracking simulations as they were found to *not* cause the numerical difficulties encountered when using the default values. Naturally, this is an *ad hoc* solution to the problem, and a careful analysis of the source of the numerical instability is required if this algorithm is to be implemented online. Nevertheless, the simulation results show that the closed-loop tracking performance of the NMPC controller is not degraded 'too much' by the parametric mismatch, and in fact, appears to be enhanced slightly in the $+5\%$ case.

The closed-loop tracking simulation results of the LMPC controller were intentionally omitted from Figure 7.10, as the response exhibited a highly erratic and oscillatory character. Figure 7.12 compares the performance of the NMPC controller with that of the input disturbance, and mixed (input-output) disturbance based LMPC controllers in reponse to the first grade change request. The results show that the input disturbance based LMPC controller is successfully able to drive the reactor to the next operating point, albeit with significantly more overshoot in the molecular weight response than the NMPC controller. However, the mixed disturbance based LMPC controller, which was shown to perform extremely well for disturbance rejection, is unable to track even the first setpoint change. In fact, if plotted completely, the closed-loop response exhibits sustained,

erratic oscillations about the setpoint. Note that both LMPC controllers were provided linear models which were obtained by linearizing the nonlinear plant model about the original steady state. Better performance can, perhaps, be attained if nonlinear strategies, such as gain or model scheduling, are used together with LMPC for tracking control.

7.2 Multi-Zone Multi-Feed Autoclave

7.2.1 Disturbance Model Design

In Section 7.1.1, we argued for the use of a mixed disturbance model, i.e. a disturbance model with a combination of input and output disturbances, for the single-zone LDPE autoclave reactor. Following the same line of reasoning, we attest again, that a mixed disturbance model approach is best suited to the multi-zone multi-feed autoclave reactor. In this case, since there are four available online measurements (three temperatures, and one molecular weight), we can add up to a maximum of four integrating disturbance states in the controller model. Here, three input disturbances were added (one each) on the dynamic equations corresponding to the reactor temperatures in each zone, and a single output disturbance was added on the polymer molecular weight measurement equation. Accordingly, the offset-free NMPC/LMPC disturbance model matrices employed here are shown below.

$$
X_u^T = 1_d^{.T} = \begin{bmatrix} \mathbf{0}^{3\times 9} & I_3 & \mathbf{0}^{3\times 9} \\ \mathbf{0}^{1\times 9} & \mathbf{0}^{1\times 3} & \mathbf{0}^{1\times 9} \end{bmatrix} \qquad X_y = C_d = \begin{bmatrix} \mathbf{0}^{3\times 3} & \mathbf{0}^{3\times 1} \\ \mathbf{0}^{1\times 3} & 100 \end{bmatrix}
$$

where the notation $\mathbf{0}^{n\times m}$ denotes a zero matrix with n rows and m columns, and I_n an $n\times n$ identity matrix.

7.2.2 Controller Tuning Parameters

The tuning parameters required by the offset-free NMPC/LMPC formulations for the control of the multi-zone autoclave reactor were selected, in a large part, analogously to the case of the single-zone reactor. The controller prediction ($P = 6$) and control ($M = 2$) horizons were chosen indentically. The regulator tuning matrices used in all NMPC/LMPC simulations in this study are shown below.

$$\mathbf{Q} = \left[\begin{array}{cc} 2I_3 & \mathbf{0}^{3\times1} \\ \mathbf{0}^{1\times3} & 6 \end{array} \right] \qquad \mathbf{R} = 0.5I_6 \qquad \mathbf{S} = \left[\begin{array}{cc} I_3 & \mathbf{0}^{3\times3} \\ \mathbf{0}^{3\times3} & 5I_3 \end{array} \right]$$

The controlled output penalty matrix $\mathbf{Q}$ was, again, chosen to be a diagonal matrix, with 2's corresponding to the reactor temperatures and 6 corresponding to the polymer molecular weight. Likewise, the control input penalty matrix $\mathbf{R}$ is a diagonal matrix with 0.5's along the main diagonal. We wish to discourage the use of large control moves in the feed monomer flowrates q_M relative to the feed initiator flowrates q_I, therefore, the diagonal elements in $\mathbf{S}$ corresponding to the feed monomer flowrates are supplied higher values (five) relative to the feed initiator flowrates (one).

Unlike the single-zone LDPE autoclave reactor, the multi-zone autoclave reactor is nonsquare, possessing more control inputs (six) than controlled outputs (four). In this situation, there exist multiple steady state (equilibrium) targets, or equivalently, multiple combinations of control inputs, which satisfy the controlled output setpoint z_s at steady state. Therefore, it is important that the controller guide the system to a steady state that is 'profitable', i.e. one that makes the most practical sense from an operational perspective. For the multi-zone reactor, a profitable steady state is one at which the *target* feed monomer flowrates q_M are not shifted 'too much' from their design values (in our simulations, the original steady state values), as this has broader production rate implications. Instead, we require that the *target* feed initiator flowrates q_I be manipulated *preferentially* in order to return the controlled outputs to their setpoints. The quadratic penalty matrix $\mathcal{R}$ in the target calculation NLP (see equation (4.16)) is an extremely convenient tool which can be used to achieve this objective. The matrix $\mathcal{R}$ essentially penalizes deviations of the current control input target $u_{t,j}$ from the previous target $u_{t,j-1}$, therefore, the elements of $\mathcal{R}$ can be selected such that 'large' moves in the target feed monomer flowrates are avoided, or equivalently, 'large' moves in the target feed initiator flowrates are favored. The target calculator matrices used in this work are given below.

$$\mathcal{Q} = 1 \times 10^3 I_4 \qquad \Pi = 2 \times 10^3 \left[\begin{array}{cccc} 1 & 1 & 1 & 1 \end{array} \right]^T \qquad \mathcal{R} = \left[\begin{array}{cc} I_3 & \mathbf{0}^{3\times3} \\ \mathbf{0}^{3\times3} & 1 \times 10^4 I_3 \end{array} \right]$$

Notice that the diagonal elements of $\mathcal{R}$ corresponding to the target feed monomer flowrates are supplied relatively large values for reasons previously discussed. The other target calculator parameters

Q and II are also supplied sufficiently high values, similar to what was done in the case of the single zone LDPE autoclave reactor.

7.2.3   Simulation Results

The multi-zone multi-feed autoclave reactor is a nonsquare (fat) plant, having more control inputs (six) than controlled outputs (four). The state space based formulation of the NMPC/LMPC controllers is ideally suited to handling multivariable and nonsquare plants, however, single loop controllers–such as PID–require special consideration, as 'optimal' loop pairings between inputs and outputs must first be identified. Several techniques based on singular value decomposition (SVD) and relative gain array (RGA) analysis among others have been developed to assist in the selection of loop pairings [9, 80]. Chang and Yu [9] shows how RGA analysis can be extended to nonsquare systems using the so called nonsquare relative gain (NRG) array methodology. These techniques can be used to reduce nonsquare fat systems into square subsystems, which can be handled readily by multi-loop PID controllers.

Fortunately, for the multi-zone autoclave reactor, we can rely on engineering judgement instead of such rigourous analysis in order to select appropriate loop pairings. For instance, it is well known that the initiator feed to each reaction zone is extremely effective in regulating the temperature in the zone. In fact, it is current industrial practice to employ the feed initiator flowrates q_{f_I} as control inputs to regulate the temperature profile in the reactor. Therefore, following the same approach, in this study, we paired the initiator flowrates to each reaction zone with the reactor temperature in the zone.

The sole remaining controlled output (i.e. the weight-averaged molecular weight of polymer $\overline{M}_w$) must then be paired with one of the three remaining control inputs (i.e. one of the three feed monomer flowrates q_{f_M}). This is a relatively straightforward problem as there are only three input-output pairing combinations possible. In this study, the best input-output pairing combination among the three remaining options was selected by a simple comparison of the open-loop steady state gains. The combination of the (*input*) feed monomer flowrate to the first zone $q_{f_{M,1}}$ and the (*output*) polymer weight-averaged molecular weight $\overline{M}_w$ was found to possess the highest open-loop gain

$K_{f_{M,1}} = \Delta\overline{M}_w/\Delta q_{f_{M,1}}$, therefore, this was selected as the final pairing.

Figures 7.13 and 7.14 present closed-loop simulation results comparing the disturbance rejection (controlled output) responses of NMPC, LMPC, and PID controllers for the control of the multi-zone multi-feed LDPE autoclave reactor. Figure 7.13 shows the closed-loop controlled output response following the introduction of an unmeasured $-5°C$ step disturbance in the feed temperatures $T_{f_{1,2,3}}$ to all three reaction zones, while Figure 7.14 shows the controlled output response following an unmeasured 10% step disturbance in the feed initiator concentrations $I_{f_{1,2,3}}$ to all three zones. The closed-loop results obtained for the multi-zone autoclave are qualitatively quite similar to the case of the single-zone reactor. Both the NMPC, LMPC controllers appear to perform very well in returning the controlled outputs to their respective setpoints following the process disturbances. However, the closed-loop response of the PID control system is clearly slower than the responses of the other two controllers. Nevertheless, the PID control system appears to fare better in regulating the multi-zone autoclave relative to the single-zone reactor.

The effect of parametric mismatch on the closed-loop disturbance rejection performance of the NMPC formulation is shown in Figures 7.15 and 7.16. Here, the two disturbance rejection simulation cases presented previously were repeated, however, in this case, the rate law parameters (i.e. all the model A's, E_a's) in the internal controller model are perturbed from their nominal (plant) values by +5% and −5%, respectively. The results indicate that this mismatch does not significantly degrade the closed-loop performance. However, the closed-loop system appears to be affected more severely in the +5% case compared to the −5% one.

Figure 7.17 shows the closed-loop tracking responses of the NMPC and PID controllers in response to multiple polymer grade change requests for the multi-zone LDPE autoclave reactor. The LMPC tracking results were, as was the case with the single-zone reactor, omitted since the offset-free LMPC formulation is unable to guide the system to the desired operating points. The closed-loop tracking results show that the NMPC controller is able to drive the plant to the desired operating points relatively quickly, and with marginal overshoot. The closed-loop PID tracking response is surprisingly quite good, although the overshoots in the response can be significant depending on the magnitude of the 'jump' between operating points.
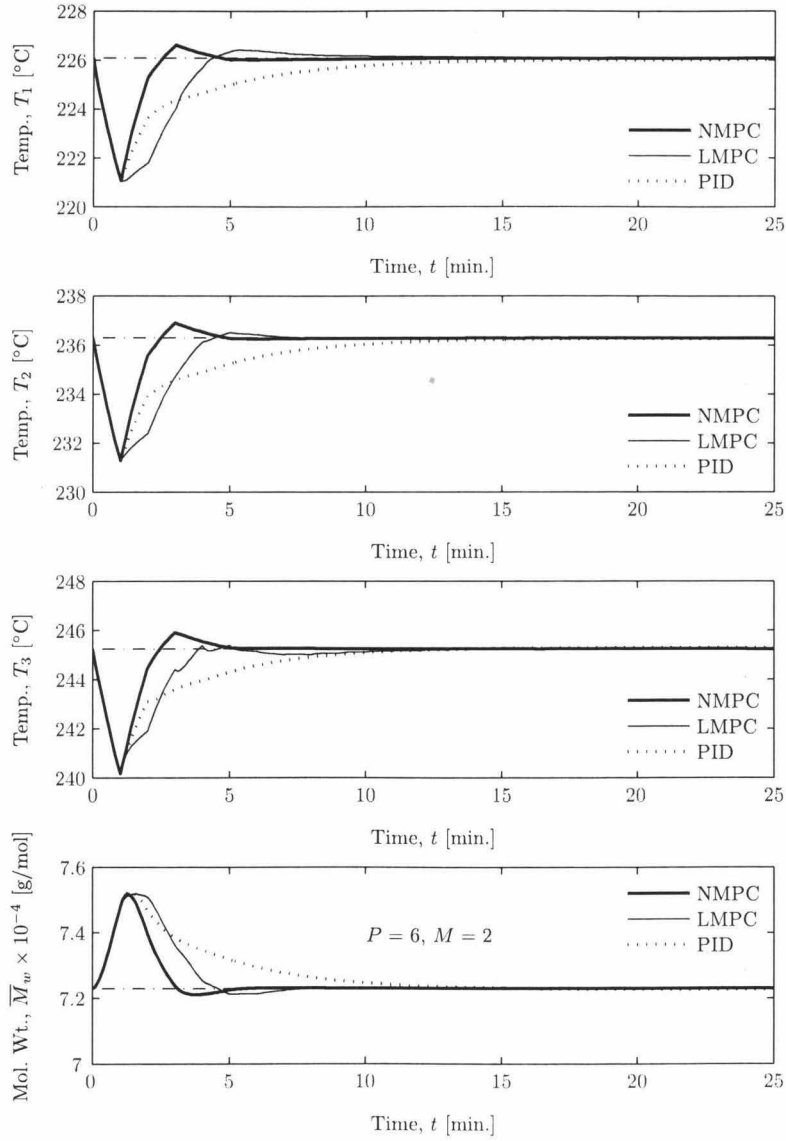
Figure 7.13: Closed-loop response to an unmeasured $-5°C$ step disturbance in feed temperature T_f.
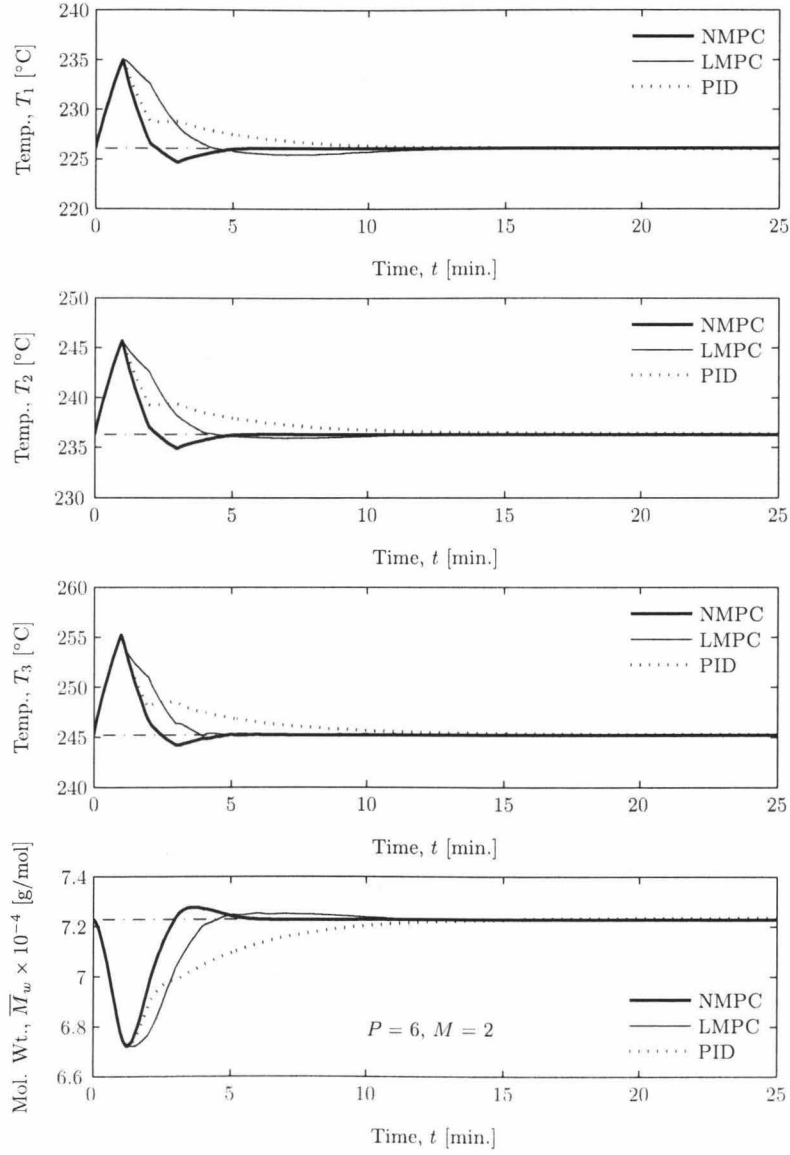Comparison of NMPC, LMPC, and PID controller responses.

Figure 7.14: Closed-loop response to an unmeasured +10% step disturbance in feed initiator concentration I_f. Comparison of NMPC, LMPC, and PID controller responses.
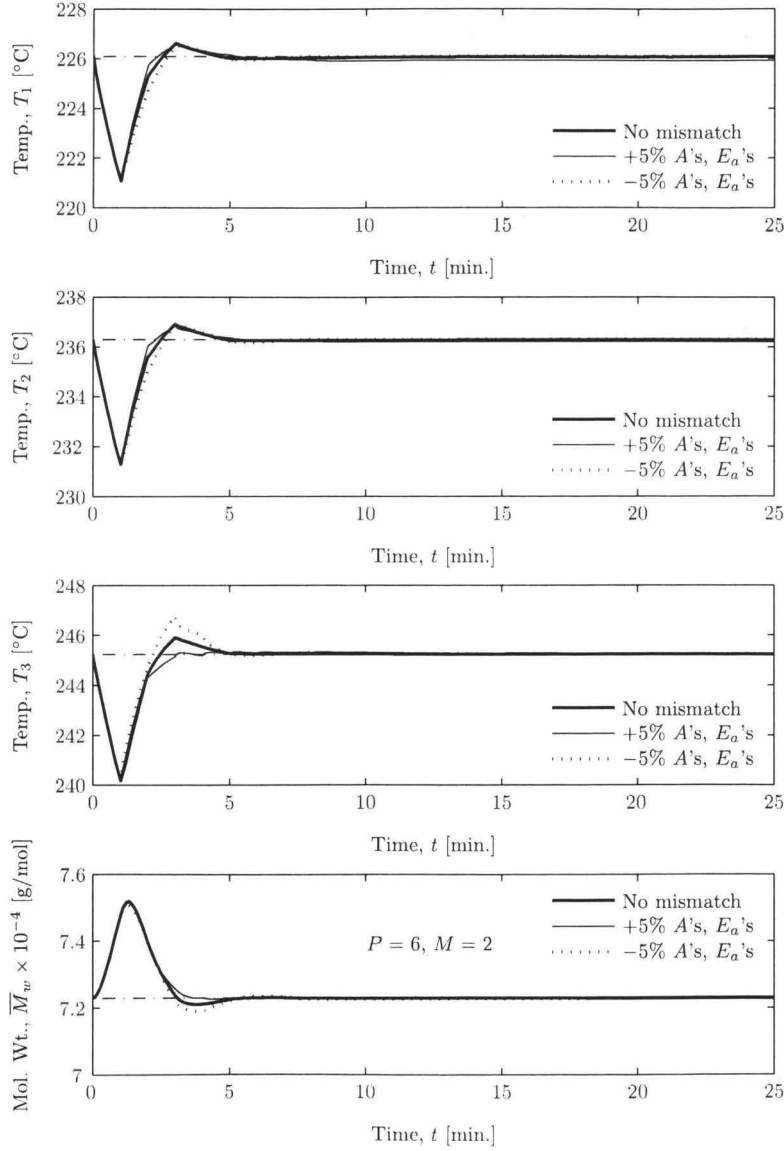
Figure 7.15: Closed-loop response to an unmeasured $-5°C$ step disturbance in feed temperature T_f. Comparison of NMPC controller responses with and without plant-model mismatch.
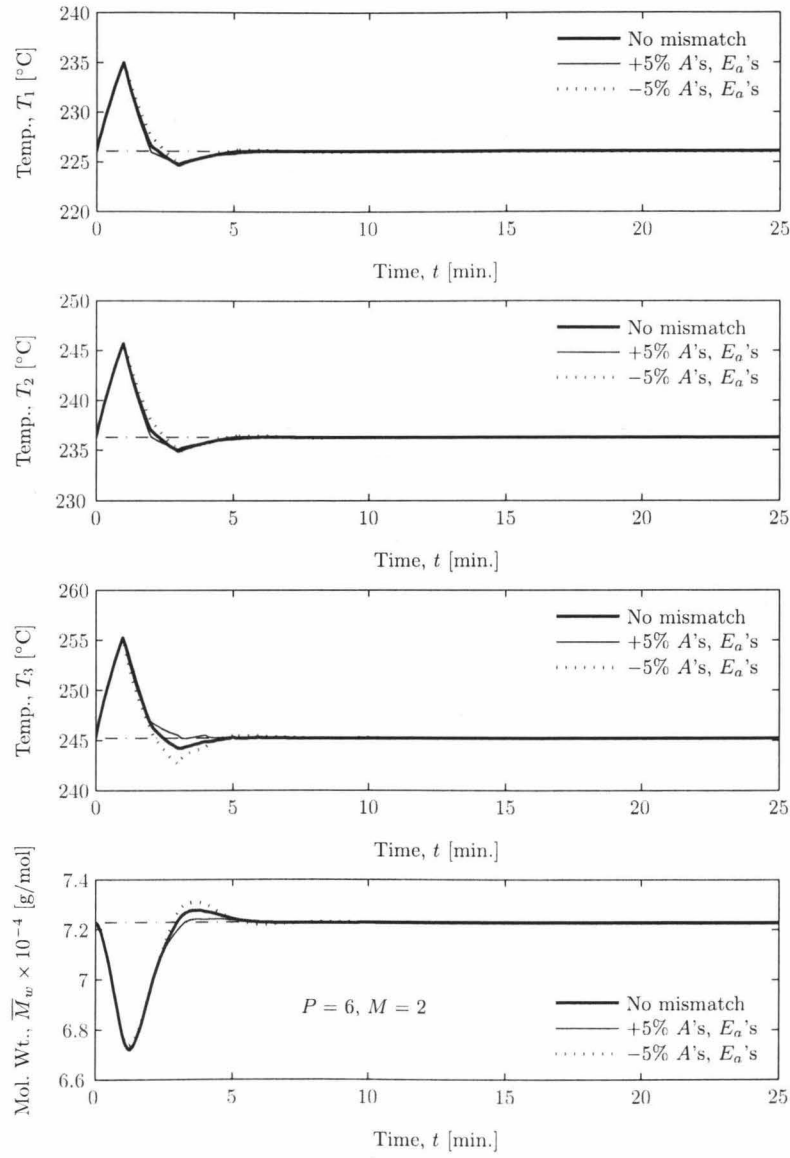
Figure 7.16: Closed-loop response to an unmeasured $+10\%$ step disturbance in feed initiator concentration I_f. Comparison of NMPC controller responses with and without plant-model mismatch.
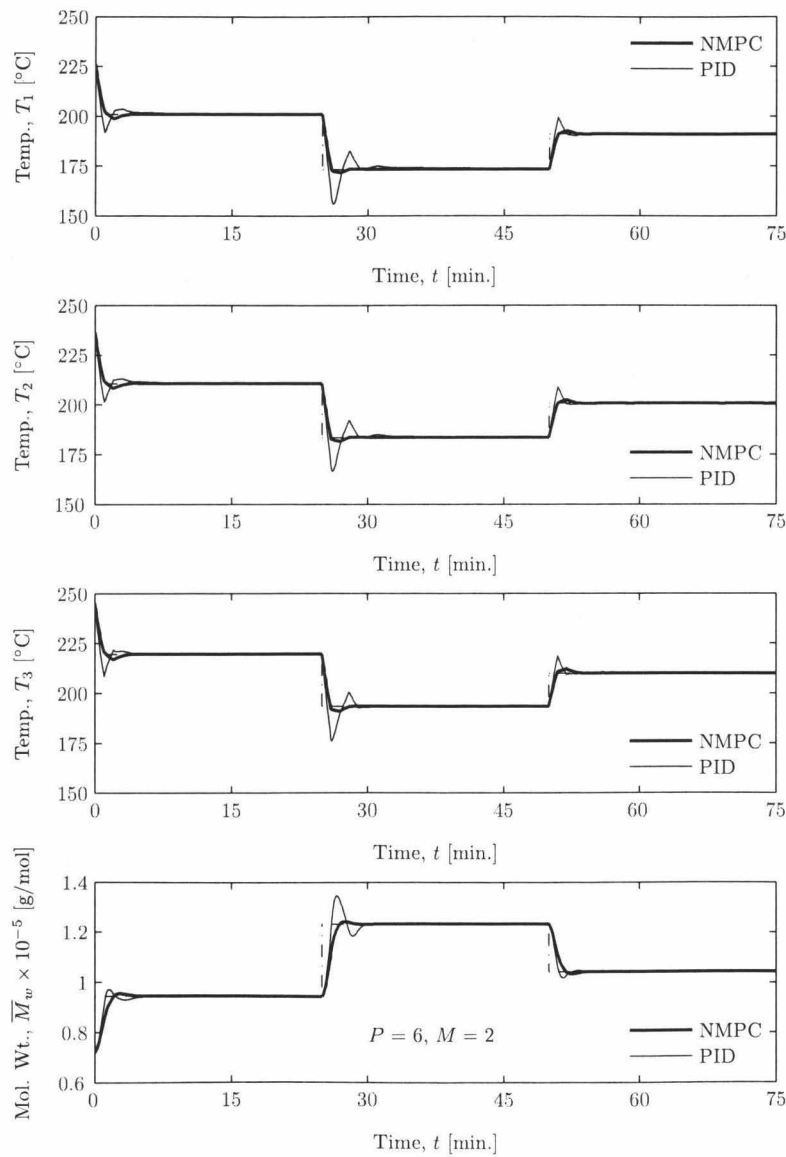
Figure 7.17: Closed-loop tracking response to multiple polymer grade (setpoint) change requests. Comparison of NMPC and PID controller responses.

Chapter 8

Conclusions and Recommendations

EKF and UKF based NMPC formulations were developed and applied for the control of single and multi-zone LDPE autoclave reactors. The closed-loop performance properties of the proposed formulations for disturbance rejection and setpoint tracking were investigated through a number of simulation case studies. The effect of (parametric) plant-model mismatch on closed-loop NMPC performance was also studied. Conventional LMPC and PID controllers were also designed for the control of both LDPE autoclave reactors in order to compare the performance of NMPC with more 'industrially accepted' controllers.

Our results showed that, for both MPC controllers, a mixed disturbance model (input disturbance state(s) on the reactor temperature dynamical equation(s), and a single output disturbance state on the weight-averaged molecular weight measurement equation) was adequately capable of accounting for the effects of unmeasured load disturbances and 'moderate' plant-model mismatch on the plant dynamics. Furthermore, using the single-zone reactor model, we showed that the closed-loop response of the offset-free LMPC formulation is very sensitive to the distribution of disturbance states between inputs and outputs, while the NMPC controller is more 'robust' in this regard.

The simulation results indicate that only marginal performance improvement can be gained from implementing NMPC instead of LMPC for disturbance rejection around any given operating point. In other words, the LMPC controller was shown to perform quite well if the system is operated in a 'small' region around the operating point at which the plant model was linearized. Furthermore,

both MPC controllers provided significantly superior performance relative to conventional multi-loop PID controllers—which was found to reject process disturbances relatively slowly.

We showed that the offset-free LMPC formulation is unfit for setpoint tracking purposes for both LDPE autoclave reactor types, except in certain special situations. The inability of the LMPC controller to adequately track setpoint changes can be attributed directly to the high degree of process nonlinearity. On the other hand, both NMPC and PID controllers were demonstrated to be capable of driving the plant to the desired operating points. However, the PID controller caused significant overshoots and oscillations in the closed-loop tracking response, especially in situations where the 'jump' between operating points was large.

8.1   Recommendations

The offset-free NMPC formulation was demonstrated to perform quite well over a wide operating region and under a variety of operating conditions. However, the computational expenditure required to solve the controller NLPs can be substantial, especially for systems with high dimensionality, such as the multi-zone multi-feed LDPE autoclave reactor. On the other hand, while the offset-free LMPC formulation performs reasonably well in the region close to the operating (linearization) point, its performance was found to deteriorate significantly as the system moved away from the point of linearization. In the case of the LMPC controller, however, relatively marginal computational effort is needed to solve the controller QPs. Using gain, model scheduling techniques, the aforementioned advantages of NMPC, LMPC can be incorporated into a scheduled LMPC controller that is both computationally inexpensive, and also accounts for nonlinearity in the process dynamics. It is recommended that more research be performed to determine if acceptable performance can be obtained using such techniques, especially in setpoint tracking situations.

Nomenclature

λ_i i^{th} moment of the CLD of growing polymer radicals, see eq. (3.22)

μ_i i^{th} moment of the CLD of dead polymer chains, see eq. (3.22)

ρ density of reaction mixture, g/L

ΔH_p heat of polymerization (ethylene), kJ/mol

Δv activation volume, see eq. (3.21), cm^3/mol

$\mathcal{R}_i$ backmixing ratio for the ith reaction zone, see eq. (3.37)

$\overline{M}_n$ number-averaged molecular weight, g/mol

$\overline{M}_w$ weight-averaged molecular weight, g/mol

A preexponential factor, see eq. (3.21)

C_p heat capacity of reaction mixture, J/g–K

E_a activation energy, see eq. (3.21), cal/mol

f initiator efficiency

I initiator concentration, mol/L

I_f initiator feed concentration, mol/L

K reaction rate constant, see eq. (3.21)

K_1 rate constant of reaction (3.1b), L/mol–s

K_b rate constant of back-biting reaction, see eq. (3.8), s^{-1}

K_d rate constant of initiator decomposition reaction, see eq. (3.1a), s^{-1}

K_p rate constant of propagation reaction, see eq. (3.3), L/mol–s

K_t rate constant of termination reaction, see eq. (3.4), L/mol–s

K_β rate constant of β–scission to secondary radical reaction, see eq. (3.7), s^{-1}

K_{fm} rate constant of chain transfer to monomer reaction, see eq. (3.5), L/mol–s

K_{fp} rate constant of chain transfer to polymer reaction, see eq. (3.6), L/mol–s

K_{th} rate constant of thermal self initiation, see eq. (3.2), L^2/mol^2–s

M monomer concentration, mol/L

M_0 molecular weight of a single monomer unit, g/mol

M_f monomer feed concentration, mol/L

M_t total monomer concentration, mol/L

P_n non-growing (dead) polymer chain having n monomeric units, mol/L

q exit volumetric flowrate, L/s

q_f feed volumetric flowrate, L/s

q_{d_i} downward flowrate from the ith to the $(i+1)^{\text{th}}$ reaction zone, L/s

q_{f_I} initiator feed volumetric flowrate, L/s

q_{f_M} monomer feed volumetric flowrate, L/s

q_{u_i} upward flowrate from the $(i+1)^{\text{th}}$ to the ith reaction zone, L/s

R universal gas constant, see eq. (3.21)

R_I rate of radical initiation, see eq. (3.26), mol/L–s

r_I rate of initiator consumption, mol/L–s

r_M rate of monomer consumption, mol/L–s

R_n growing (live) polymer chain having n monomeric units, mol/L

r_T rate of temperature change, K/s

R_{in} primary (initiator) radical concentration, mol/L

R_{bn} growing (live) radical generated in the back-biting reaction, see eq. (3.8), mol/L

r_{M_t} rate of total monomer consumption, mol/L–s

T reactor temperature, K

T_f reactor feed temperature, K

V reactor volume, L

x_M monomer conversion

Bibliography

[1] S.-. Ahn, M.-. Park, and H.-. Rhee. Extended Kalman filter-based nonlinear model predictive control for a continuous MMA polymerization reactor. *Industrial and Engineering Chemistry Research*, 38(10):3942–3949, 1999.

[2] E. Ali, A. Abasaeed, and S. Al-Zahrani. Optimization and control of industrial gas-phase ethylene polymerization reactors. *Industrial and Engineering Chemistry Research*, 37(8):3414–3423, 1998.

[3] E. Ali and E. Zafiriou. Optimization-based tuning of nonlinear model predictive control with state estimation. *Journal of Process Control*, 3(2):97–107, 1993.

[4] A. Bemporad, M. Morari, and N. Ricker. Model predictive control toolbox 2: User's guide. Technical report, The MathWorks, Inc., Natick, MA, USA, 2007.

[5] S. BenAmor, F. Doyle III, and R. McFarlane. Polymer grade transition control using advanced real-time optimization software. *Journal of Process Control*, 14(4):349–364, 2004.

[6] R. Berber and S. Coskun. Dynamic simulation and quadratic dynamic matrix control of an industrial low density polyethylene reactor. *Computers and Chemical Engineering*, 20(Suppl.):S799–S804, 1996.

[7] M. Cannon. Efficient nonlinear model predictive control algorithms. *Annual Reviews in Control*, 28(2):229–237, 2004.

[8] W.-. Chan, P. Gloor, and A. Hamielec. Kinetic model for olefin polymerization in high-pressure autoclave reactors. *AIChE Journal*, 39(1):111–126, 1993.

[9] J.-. Chang and C.-. Yu. The relative gain for non-square multivariable systems. *Chemical Engineering Science*, 45(5):1309–1323, 1990.

[10] H. Chen and F. Allgöwer. A quasi-infinite horizon nonlinear model predictive control scheme with guaranteed stability. *Automatica*, 34(10):1205–1217, 1998.

[11] I.-. Chien, T. Kan, and B.-. Chen. Dynamic simulation and operation of a high pressure ethylene-vinyl acetate (EVA) copolymerization autoclave reactor. *Computers and Chemical Engineering*, 31(3):233–245, 2007.

[12] J. Crassidis and J. Junkins. *Optimal estimation of dynamic systems*. CRC Press, 2004.

[13] J. Cuthrell and L. Biegler. On the optimization of differential-algebraic process systems. *AIChE Journal*, 33(8):1257–1270, 1987.

[14] G. DeNicolao, L. Magni, and R. Scattolini. Stability and robustness of nonlinear receding horizon control. In *Nonlinear model predictive control* (Allgöwer, F. and Zheng, A. editors). Birkhäuser Verlag, 2000.

[15] R. Dhib and N. Al-Nidawy. Modelling of free radical polymerisation of ethylene using difunctional initiators. *Chemical Engineering Science*, 57(14):2735–2746, 2002.

[16] R. Dhib, J. Gao, and A. Penlidis. Simulation of free radical bulk/solution homopolymerization using mono- and bi-functional initiators. *Polymer Reaction Engineering*, 8(4):299–464, 2000.

[17] A. Dhooge, W. Govaerts, and Y. Kuznetsov. MATCONT: A MATLAB package for numerical bifurcation analysis of ODEs. *ACM Transactions on Mathematical Software*, 29(2):141–164, 2003.

[18] A. Dhooge, W. Govaerts, Y. Kuznetsov, W. Mestrom, and A. Riet. CL_MATCONT: A continuation toolbox in MATLAB. pages 161–166, 2003.

[19] A. Faanes and S. Skogestad. Offset-free tracking of model predictive control with model mismatch: Experimental results. *Industrial and Engineering Chemistry Research*, 44(11):3966–3972, 2005.

[20] P. Feucht, B. Tilger, and G. Luft. Prediction of molar mass distribution, number and weight average degree of polymerization and branching of low density polyethylene. *Chemical Engineering Science*, 40(10):1935–1942, 1985.

[21] R. Findeisen and F. Allgöwer. An introduction to nonlinear model predictive control. Technical report, Institute for Systems Theory in Engineering, University of Stuttgart, 2002.

[22] B. Finlayson. *The method of weighted residuals and variational principles*. Academic Press, 1972.

[23] G. Franklin, J. Powell, and M. Workman. *Digital control of dynamic systems*. Addison-Wesley, 3rd edition, 1998.

[24] Y. Gao and M. Er. NARMAX time series model prediction: Feedforward and recurrent fuzzy neural network approaches. *Fuzzy Sets and Systems*, 150(2):331–350, 2005.

[25] J. Ham and H.-. Rhee. Modeling and control of an LDPE autoclave reactor. *Journal of Process Control*, 6(4):241–246, 1996.

[26] J. Hamer, T. Akramov, and W. Ray. The dynamic behavior of continuous polymerization reactors – II. Nonisothermal solution homopolymerization and copolymerization in a CSTR. *Chemical Engineering Science*, 36(12):1897–1914, 1981.

[27] E. Haseltine and J. Rawlings. Critical evaluation of extended Kalman filtering and moving-horizon estimation. *Industrial and Engineering Chemistry Research*, 44(8):2451–2460, 2005.

[28] H. Hulburt and S. Katz. Some problems in particle technology. A statistical mechanical formulation. *Chemical Engineering Science*, 19(8):555–574, 1964.

[29] J. Jørgensen, M. Kristensen, P. Thomsen, and H. Madsen. A computationally efficient and robust implementation of the continuous-discrete extended Kalman filter. *Proceedings of the American Control Conference*, pages 3706–3712, 2007.

[30] S. Julier and J. Uhlmann. A general method for approximating nonlinear transformations of probability distributions. Technical report, The Robotics Research Group, Department of Engineering Science, University of Oxford, 1996.

[31] S. Julier and J. Uhlmann. A new extension of the Kalman filter to nonlinear systems. Technical report, The Robotics Research Group, Department of Engineering Science, University of Oxford, 1997.

[32] S. Julier and J. Uhlmann. Unscented filtering and nonlinear estimation. *Proceedings of the IEEE*, 92(3):401–422, 2004.

[33] S. Julier, J. Uhlmann, and H. Durrant-Whyte. A new method for the nonlinear transformation of means and covariances in filters and estimators. *IEEE Transactions on Automatic Control*, 45(3):477–482, 2000.

[34] R. Kalman. A new approach to linear filtering and prediction problems. *Transactions of the ASME, Journal of Basic Engineering*, 82D:35–45, 1960.

[35] R. Kalman and R. Bucy. New results in linear filtering and prediction theory. *Transactions of the ASME, Journal of Basic Engineering*, 83D:95–108, 1961.

[36] D. Kalyon, Y.-. Chiou, S. Kovenklioglu, and A. Bouaffar. High pressure polymerization of ethylene and rheological behavior of polyethylene product. *Polymer Engineering and Science*, 34(10):804–814, 1994.

[37] P. Khazraei and R. Dhib. Modeling of ethylene polymerization with difunctional initiators in tubular reactors. *Journal of Applied Polymer Science*, 109(6):3908–3922, 2008.

[38] S. Kolås, B. Foss, and T. Schei. Constrained nonlinear state estimation based on the UKF approach. *Computers and Chemical Engineering*, 33(8):1386–1401, 2009.

[39] A. Kumar and R. Gupta. *Fundamentals of polymers*. McGraw-Hill, 1998.

[40] H.-. Lee, Y.-. Yeo, and J. Chang. Modeling of industrial high pressure autoclave polyethylene reactor including decomposition phenomena. *Korean Journal of Chemical Engineering*, 17(2):223–229, 2000.

[41] J. Lee, J. Ham, K. Chang, J. Kim, and H.-. Rhee. Analysis of an LDPE compact autoclave reactor by two-cell model with backflow. *Polymer Engineering and Science*, 39(7):1279–1290, 1999.

[42] J. Lee and N. Ricker. Extended Kalman filter based nonlinear model predictive control. *Industrial and Engineering Chemistry Research*, 33(6):1530–1541, 1994.

[43] J. Maciejowski. *Predictive control with constraints*. Prentice-Hall, 2001.

[44] G. Marafioti, S. Olaru, and M. Hovd. State estimation in nonlinear model predictive control, unscented Kalman filter advantages. In *Nonlinear model predictive control: Towards new challenging applications* (Magni, L., Raimondo, D.M., and Allgöwer, F. editors). Springer Berlin / Heidelberg, 2009.

[45] L. Marini and C. Georgakis. Low-density polyethylene vessel reactors. Part I: Steady state and dynamic modelling. *AIChE Journal*, 30(3):401–408, 1984.

[46] L. Marini and C. Georgakis. Low-density polyethylene vessel reactors. Part II: A novel controller. *AIChE Journal*, 30(3):409–415, 1984.

[47] P. Maybeck. *Stochastic models, estimation, and control*, volume 1. Academic Press, 1979.

[48] D. Mayne and H. Michalska. Receding horizon control of nonlinear systems. *IEEE Transactions on Automatic Control*, 35(7):814–824, 1990.

[49] D. Mayne, J. Rawlings, C. Rao, and P. Scokaert. Constrained model predictive control: Stability and optimality. *Automatica*, 36(6):789–814, 2000.

[50] E. Meadows and J. Rawlings. Model predictive control. In *Nonlinear process control* (Henson, M.A. and Seborg, D.E. editors). Prentice-Hall, 1997.

[51] H. Michalska and D. Mayne. Robust receding horizon control of constrained nonlinear systems. *IEEE Transactions on Automatic Control*, 38(11):1623–1633, 1993.

[52] K. Muske and T. Badgwell. Disturbance modeling for offset-free linear model predictive control. *Journal of Process Control*, 12(5):617–632, 2002.

[53] K. Muske and T. Edgar. Nonlinear state estimation. In *Nonlinear process control* (Henson, M.A. and Seborg, D.E. editors). Prentice-Hall, 1997.

[54] K. Muske and J. Rawlings. Model predictive control with linear models. *AIChE Journal*, 39(2):262–287, 1993.

[55] G. Pannocchia. Robust disturbance modeling for model predictive control with application to multivariable ill-conditioned processes. *Journal of Process Control*, 13(8):693–701, 2003.

[56] G. Pannocchia and A. Bemporad. Combined design of disturbance model and observer for offset-free model predictive control. *IEEE Transactions on Automatic Control*, 52(6):1048–1053, 2007.

[57] G. Pannocchia and J. Rawlings. Disturbance models for offset-free model predictive control. *AIChE Journal*, 49(2):426–437, 2003.

[58] R. Pearson and B. Ogunnaike. Nonlinear process identification. In *Nonlinear process control* (Henson, M.A. and Seborg, D.E. editors). Prentice-Hall, 1997.

[59] P. Pladis and C. Kiparissides. Dynamic modeling of multizone, multifeed high-pressure LDPE autoclaves. *Journal of Applied Polymer Science*, 73(12):2327–2348, 1999.

[60] J. Prakash, A. Deshpande, and S. Patwardhan. State estimation and fault tolerant nonlinear predictive control of an autonomous hybrid system using unscented Kalman filter. In *Nonlinear model predictive control: Towards new challenging applications* (Magni, L., Raimondo, D.M., and Allgöwer, F. editors). Springer Berlin / Heidelberg, 2009.

[61] V. Prasad, M. Schley, L. Russo, and B. Bequette. Product property and production rate control of styrene polymerization. *Journal of Process Control*, 12(3):353–372, 2002.

[62] S. Qin and T. Badgwell. An overview of industrial model predictive control technology. In *Fifth international conference on chemical process control* (Kantor, J.C., Garcia, C.E. and Carnahan, B. editors), pages 232–256, 1997.

[63] S. Qin and T. Badgwell. An overview of nonlinear model predictive control applications. In *Nonlinear model predictive control* (Allgöwer, F. and Zheng, A. editors). Birkhäuser Verlag, 2000.

[64] C. Rao and J. Rawlings. Steady states and constraints in model predictive control. *AIChE Journal*, 45(6):1266–1278, 1999.

[65] J. Rawlings and B. Bakshi. Particle filtering and moving horizon estimation. *Computers and Chemical Engineering*, 30(10–12):1529–1541, 2006.

[66] N. Read, S. Zhang, and W. Ray. Simulations of a LDPE reactor using computational fluid dynamics. *AIChE Journal*, 43(1):104–117, 1997.

[67] A. Romanenko and J. Castro. The unscented filter as an alternative to the EKF for nonlinear state estimation: A simulation case study. *Computers and Chemical Engineering*, 28(3):347–355, 2004.

[68] A. Romanenko, L. Santos, and P. Afonso. Unscented Kalman filtering of a simulated pH system. *Industrial and Engineering Chemistry Research*, 43(23):7531–7538, 2004.

[69] A. Rudin. *The elements of polymer science and engineering*. Academic Press, 2nd edition, 1999.

[70] L. Russo and B. Bequette. Operability analysis and nonlinear model predictive control of a styrene polymerization reactor. *Proceedings of the IEEE Conference on Decision and Control*, 1:443–448, 1998.

[71] L. Russo and B. Bequette. Operability of chemical reactors: Multiplicity behavior of a jacketed styrene polymerization reactor. *Chemical Engineering Science*, 53(1):27–45, 1998.

[72] M. Schley, V. Prasad, L. Russo, and B. Bequette. Nonlinear model predictive control of a styrene polymerization reactor. In *Nonlinear model predictive control* (Allgöwer, F. and Zheng, A. editors). Birkhäuser Verlag, 2000.

[73] A. Schmidt and W. Ray. The dynamic behavior of continuous polymerization reactors – I. Isothermal solution polymerization in a CSTR. *Chemical Engineering Science*, 36(8):1401–1410, 1981.

[74] A. Shenoy and D. Saini. Melt flow index: More than just a quality control rheological parameter. Part I. *Advances in Polymer Technology*, 6(1):1–58, 1986.

[75] A. Shenoy and D. Saini. Melt flow index: More than just a quality control rheological parameter. Part II. *Advances in Polymer Technology*, 6(2):125–145, 1986.

[76] P. Singstad, H. Nordhus, K. Strand, M. Lien, L. Lyngmo, and O. Moen. Multivariable non-linear control of industrial LDPE autoclave reactors. volume 1, pages 615–619, 1992.

[77] S. Skogestad. Probably the best simple PID tuning rules in the world. Technical report, Department of Chemical Engineering, Norwegian University of Science and Technology, 2001.

[78] S. Skogestad. Simple analytic rules for model reduction and PID controller tuning. *Journal of Process Control*, 13(4):291–309, 2003.

[79] S. Skogestad. Simple analytic rules for model reduction and PID controller tuning. *Modeling, Identification and Control*, 25(2):85–120, 2004.

[80] C. Smith and A. Corripio. *Principles and practice of automatic process control*. John Wiley & Sons, Inc, 2nd edition, 1997.

[81] G. Stephanopoulos. *Chemical process control: An introduction to theory and practice*. Prentice-Hall, 1984.

[82] H. Su and T. McAvoy. Artificial neural networks for nonlinear process identification and control. In *Nonlinear process control* (Henson, M.A. and Seborg, D.E. editors). Prentice-Hall, 1997.

[83] M. Tenny, J. Rawlings, and S. Wright. Closed-loop behavior of nonlinear model predictive control. *AIChE Journal*, 50(9):2142–2154, 2004.

[84] J. Valappil and C. Georgakis. Nonlinear model predictive control of end-use properties in batch reactors. *AIChE Journal*, 48(9):2006–2021, 2002.

[85] C. Villa, J. Dihora, and W. Ray. Effects of imperfect mixing on low-density polyethylene reactor dynamics. *AIChE Journal*, 44(7):1646–1656, 1998.

[86] J. Villadsen and M. Michelsen. *Solution of differential equation models by polynomial approximation*. Prentice-Hall, 1978.

[87] S. Zhang and W. Ray. Modeling of imperfect mixing and its effects on polymer properties. *AIChE Journal*, 43(5):1265–1276, 1997.

[88] S. Zhang, N. Read, and W. Ray. Runaway phenomena in low-density polyethylene autoclave reactors. *AIChE Journal*, 42(10):2911–2925, 1996.